Heavy flavor in heavy-ion collisions at RHIC and RHIC II

A. D. Frawley[1], T. Ullrich[2,3] and R. Vogt[4,5]

[1]Physics Department, Florida State University, Tallahassee, FL, USA

E-mail: frawley@fsuhip.physics.fsu.edu
[2]Physics Department, Brookhaven National Laboratory, Upton, NY, USA
[3]Physics Department, Yale University, New Haven, CT, USA

E-mail: thomas.ullrich@bnl.gov
[4]Nuclear Science Division, Lawrence Berkeley National Laboratory, Berkeley, CA, USA
[5]Physics Department, University of California at Davis, Davis, CA, USA

E-mail: vogt@lbl.gov

Abstract. We review the physics opportunities provided by an upgrade to the Relativistic Heavy Ion Collider (RHIC) accelerator offering substantially larger luminosities in conjunction with improved capabilities of the two large RHIC detectors, PHENIX and STAR. We focus on heavy flavor probes. This report is a summary of the results of a series of workshops held by the RHIC II heavy flavor working group.

1. Introduction

During the last 6 years, heavy-ion experiments at the Relativistic Heavy Ion Collider (RHIC) have recorded a wealth of data in Au+Au, d+Au, Cu+Cu, and p+p collisions. Indeed, Au+Au collisions have been studied at energies from s_{NN} = 19.6 GeV to the highest available energy of 200 GeV. It is at these high energies that QCD predictions of new phenomena come into play under conditions where, over nuclear volumes, the relevant degrees of freedom are expected to be those of quarks and gluons rather than of hadrons, the realm of the quark-gluon plasma.

Measurements from the four RHIC experiments, BRAHMS, PHENIX, PHOBOS and STAR, have revealed compelling evidence for the existence of a new form of nuclear matter at extremely high densities and temperatures [1]. Detailed analyses of the data also make it clear that this hot, dense medium has surprising properties.

The properties of the medium are those of a strongly coupled plasma, or sQGP, that behaves like a "perfect liquid" flowing with a near-zero viscosity to entropy ratio [2]. The RHIC observations have spurred significant advances in theory. However, a fundamental understanding of the medium seen in heavy-ion collisions at RHIC does not yet exist. It requires new data that, in turn, necessitate enhanced capabilities of the RHIC detectors and accelerator. A detailed plan is being developed by BNL to implement these upgrades in collaboration with the RHIC scientific community.

The main focus of this report is to outline the scientific opportunities in the heavy flavor sector provided by upgrades of the two large RHIC detectors, PHENIX and STAR, in conjunction with an upgrade of the accelerator/collider facility, referred to as RHIC II. The detector upgrades will improve the acceptance, particle identification and secondary vertex detection capabilities of PHENIX and STAR. The accelerator upgrade is comprised of an order of magnitude increase in luminosity through electron cooling and a new ion injector, EBIS, which will provide high-intensity beams of nuclei as massive as uranium.

This report is the result of the collaboration and research efforts of a RHIC-wide Heavy Flavor Working Group over the last two years. It provides a comprehensive overview of the physics questions than can be addressed by studies of open charm, open bottom and quarkonia at RHIC II. It also includes a detailed assessment of the accelerator and detector capabilities required to carry out these measurements with sufficient precision to resolve many of the outstanding issues by providing detailed results with which to make thorough comparisons to current and future theoretical calculations.

This report is organized as follows. After a general introduction to heavy flavor physics, section 2 discusses the detector upgrade program at RHIC. The projected yields of various heavy flavor measurements that can be achieved utilizing these upgrades and the higher RHIC II luminosities are discussed in section 3. In sections 4 and 5 we present a more detailed discussion of the motivation for studying open heavy flavor and quarkonia in heavy-ion collisions, respectively. These sections also include a review of the current theoretical and experimental status as well as the proposed experimental program. In section 6 we review the relationship between heavy flavor physics at RHIC II and the LHC. We conclude in section 7.

1.1. Motivation

Because of the large masses of the charm and bottom quarks, they are produced almost exclusively in the initial parton-parton interactions in heavy ion collisions at RHIC energies. In the absence of any nuclear effects, the heavy flavor cross sections in $A + A$ collisions at RHIC would simply scale with the number of binary collisions. Thus departures from binary scaling for heavy flavor production in $A + A$ collisions provide information about nuclear effects. These can be divided into two categories: effects due to embedding the colliding partons in a nucleus (cold matter effects) and effects due to the large energy density in the final state. The main focus of the heavy flavor program at RHIC is to investigate the properties of the dense matter produced in $A+A$ collisions by studying its effects on open heavy flavor and quarkonium production. This in turn requires a detailed understanding of cold matter effects so that they can be unfolded from the dense matter effects.

The program thus requires detailed measurements and calculations of pp and $p+A$ heavy flavor cross sections to characterize the cold matter effects, if we are to quantify the differences between QGP and non-QGP effects. Up-to-date benchmark calculations of the total open heavy flavor (charm and bottom hadrons) and quarkonium (J/ψ and Υ families) yields and spectra are imperative. Cold matter effects that need to be included are nuclear shadowing, for both open heavy flavor and quarkonium production, and nuclear absorption of quarkonium. Recent calculations of charm and bottom production to FONLL in pp collisions [3] have been published, along with a discussion of the inherent theoretical uncertainties and reference calculations of heavy quark, heavy flavor meson and decay lepton spectra. Similar calculations have been done for quarkonium production, including studies of shadowing and absorption effects as a function of rapidity and centrality in d+Au [4] and $A + A$ [5] collisions at RHIC.

A number of dense matter effects on heavy flavor production have been predicted. Some of these do not change the total cross section but, instead, modify the p_T spectra of heavy flavor hadrons and their decay products. Heavy quark energy loss [6, 7, 8, 9, 10] by collisional and radiative processes steepens the p_T distribution relative to that in pp collisions. On the other hand, random p_T kicks result in transverse momentum broadening, increasing the average p_T in both cold nuclear matter [11] and in passage through hadron bubbles in the mixed phase of a QGP [12]. If the medium surrounding the heavy quarks after production exhibits collective motion, such as transverse flow [13, 14], the low p_T heavy quarks ($p_T < m$) may be caught in this flow. Strong effects of energy loss [15, 16] on heavy flavor decays to electrons and charm flow [16] have already been seen in Au+Au collisions at RHIC. Studying heavy flavor energy loss using single electrons requires being able to separate electrons from c and b decays, since the large mass difference suggests that bottom energy loss is weaker than charm [6]. Some QGP studies require an accurate baseline for the total heavy flavor cross sections to interpret other effects. For example, if more than one $c\bar{c}$ pair is produced in an $A + A$ event, uncorrelated c and $\bar{c}$ quarks might coalesce to form a J/ψ in a QGP [17, 18, 19, 20]. The total $c\bar{c}$ yield is needed to normalize the J/ψ production rate from this process.

Suppression of J/ψ production was one of the most exciting proposed QGP signatures at the CERN SPS [21]. J/ψ suppression was predicted to occur due to the shielding of the $c\bar{c}$ binding potential by color screening, leading to the break up of the quarkonium states, first the χ_c and ψ', and finally the J/ψ itself as the temperature increases [22, 23]. The QGP suppression may not be so simple, as lattice gauge theory studies of the J/ψ spectral function above the critical temperature for deconfinement, T_c, attest. The J/ψ may exist as a bound state for temperatures considerably larger than T_c [24]. However, the J/ψ may instead be dissociated by hot thermal gluons in medium [25] before it could be suppressed by color screening. Secondary quarkonium production from uncorrelated $Q\overline{Q}$ pairs, either in the plasma phase [18, 20, 26, 27, 28] or in the hadron phase [29, 30], could counter the effects of suppression, ultimately leading to enhanced quarkonium production. Such secondary J/ψ production would lead to different kinematic distributions than the initial production. Because the underlying $c\bar{c}$ distribution falls rapidly with p_T, the p_T distribution produced by coalescence will be softer. If the underlying $c\bar{c}$ distribution peaks at mid rapidity, the J/ψ rapidity distribution from coalescence will be narrower than that produced in the primordial collisions. The coalescence rapidity distribution should be calculated with shadowing effects on the underlying $c\bar{c}$ distribution taken into account since these can cause the $c\bar{c}$ distribution to flatten in more central $A + A$ collisions [5]. Elliptic flow effects are also expected on quarkonium production, in addition to open heavy flavors [13, 14].

With higher luminosity at RHIC, the Υ state yields could also be measured. Since the Υ radius is smaller than that of the J/ψ [23], direct color screening in the QGP would not occur until much higher temperatures. The higher mass bottomonium states, however, would likely be suppressed at RHIC, as are the χ_c and ψ' in the charmonium family. The feed down structure is more complicated for the Υ since there are three S states (Υ, Υ' and Υ'') and two sets of P states (χ_{b1} and χ_{b2}) below the $B\overline{B}$ threshold. The Υ family suppression should be measurable over a large p_T range, with QGP suppression possible on the Υ' and Υ'' up to $p_T \sim 40$ GeV/c [31]. Because of the small number of $b\bar{b}$ pairs produced at RHIC, bottomonium formation by coalescence of unrelated pairs should be negligible.

1.2. Overview of results from the heavy flavor program at RHIC

Heavy flavor measurements capable of discriminating between theoretical models need large integrated luminosity. In RHIC runs so far, useful data sets have been acquired at 200 GeV for pp, d+Au, Cu+Cu and Au+Au collisions. These data sets are not yet fully analyzed for Run 5 (Cu+Cu) and Run 6 pp, but preliminary heavy flavor results, at least, are available for all runs and species through Run 5.

The data collected to date for pp collisions provide an essential reference for the heavy ion program in the form of the underlying heavy flavor production rates as functions of rapidity and p_T. Equally essential, the data from d+Au collisions provide baseline information about cold nuclear matter effects which must also contribute to heavy flavor production in heavy ion collisions. The existing d+Au data provide useful tests of models that include the effects of shadowing on heavy flavor production and of absorption of J/ψ in cold nuclear matter [4].

Two very striking and unexpected results have already been seen for open heavy flavor in heavy ion collisions at RHIC. The first of these is the observation that the nuclear modification factor for electrons from open heavy flavor, R_{AA}, shows very strong suppression in central Au+Au collisions [16, 15], similar to that seen for pions. The second striking result is that the elliptic flow parameter, v_2, of electrons from open heavy flavor decays appears to favor charm quark flow at low p_T [16]. Until recently, it had been expected that heavy quark energy loss would be considerably smaller than that for light quarks due to interference effects [6]. Generating the necessary energy loss for charm and bottom quarks with realistic gluon densities in the material is a major challenge for models [6, 33]. The relatively large v_2 values at low p_T imply at least some degree of charm quark equilibration with the medium. This also implies very strong interactions of charm quarks with the medium at lower p_T [13, 14].

The first high statistics charmonium results for heavy ion collisions at RHIC are now available [34, 35]. These include final Au+Au and preliminary Cu+Cu results for the J/ψ nuclear modification factors, R_{AA}, as a function of the number of participant nucleons, in the rapidity intervals $|y| < 0.35$ and $1.2 < |y| < 2.2$. A striking feature of the final Au+Au J/ψ data is that the suppression is considerably stronger at forward rapidity than at mid rapidity for all $N_{\rm part} > 150$. Comparison with existing models at mid rapidity shows that cold nuclear matter baseline calculations [5] which approximately reproduce the PHENIX d+Au J/ψ rapidity distributions [4] somewhat underpredict the suppression observed in Cu+Cu and Au+Au collisions. On the other hand, several suppression models [20, 37, 38] which were successful in describing J/ψ suppression at the SPS are found to strongly overpredict the suppression at RHIC. Models which incorporate strong suppression combined with J/ψ regeneration from uncorrelated $c\bar{c}$ pairs seem to agree best with the data, although the existing models slightly underpredict the suppression.

In the last few years, theorists have begun exploring the consequences of J/ψ regeneration by coalescence on observables other than the centrality dependence of the nuclear modification factor [17, 40]. This work has led to the prediction that J/ψ formed by coalescence of uncorrelated $c\bar{c}$ pairs will have narrower rapidity and p_T distributions due to the presumed shape of the underlying charm quark distributions. The coalescence contribution to J/ψ production will cause many observables to change with centrality, including the rapidity and p_T dependence of R_{AA}, the shape of the p_T distribution (quantified by the average p_T^2, $\langle p_T^2 \rangle$), and the J/ψ elliptic flow parameter, v_2. Quantitative predictions have been made for $\langle p_T^2 \rangle$ as a function of centrality for Au+Au and Cu+Cu collisions, with and without coalescence [17, 40]. These predictions, compared to the Au+Au and preliminary Cu+Cu data favor the calculations that include coalescence. On the other hand, the large coalescence contributions predicted for central Au+Au (and even central Cu+Cu) collisions in [17] are qualitatively expected to narrow the J/ψ rapidity distributions if the underlying charm distributions are peaked at mid rapidity. The preliminary data presented at Quark Matter 2005 show no evidence of this narrowing in central collisions. There is still work to do to quantify both the theoretical predictions and the experimental observables. The existing data sets will not provide a useful measurement of the J/ψ v_2 due to insufficient yield.

The running schedule for RHIC over the next five years is not settled. Based on the beam use proposal discussions prior to Run 7, it seems likely that more Au+Au data will be collected, providing up to an order of magnitude increase in integrated luminosity (if there are two more Au+Au runs). There will also be a very large increase in the integrated luminosity for *pp* collisions due to the requirements of the Spin program. Such luminosity increases will quantitatively improve the measurements of many heavy flavor observables, especially as a function of centrality. The J/ψ R_{AA} and $\langle p_T^2 \rangle$ as well as R_{AA} and v_2 measurements of charm and bottom semileptonic decays to single electrons will all improve significantly, allowing more definitive tests of models. Measurements of other observables will be qualitatively improved. Examples are: definitive v_2 measurements of semileptonic decays at intermediate to high p_T where we might hope to see the transition from charm to bottom dominance and flow to non-flow; a possible first J/ψ v_2 measurement; definitive measurements of J/ψ R_{AA} with rapidity to quantify the coalescence contribution; and measurements of J/ψ R_{AA} to higher p_T, invaluable for understanding coalescence and formation time effects. Finally, it seems likely that a first, low statistics, Υ suppression measurement would be possible.

However, it is clear that the RHIC heavy flavor program will be limited by the capabilities of the accelerator after about 5 more years. The luminosity increase brought by RHIC II, combined with the detector upgrades in place by that time, will be required for the heavy flavor program at RHIC to move to the next level, as described below.

1.3. Overview of the proposed heavy flavor program at RHIC II

The order of magnitude increase in luminosity, combined with the increased capabilities of the upgraded PHENIX and STAR detectors, will make it possible to add many important new probes to the heavy flavor program at RHIC.

One of the most powerful additions from the luminosity upgrade will be the ability to measure yields of the excited states of charmonium - the ψ' and χ_c states. Lattice calculations predict much smaller melting temperatures for the ψ' and χ_c than for the more tightly bound J/ψ so that these excited states should not be able to exist in the

QGP at RHIC. Therefore comparison of the ψ' and χ_c yields with the J/ψ yield as a function of centrality is considered to be a direct test of deconfinement.

Testing models in which the observed J/ψ yield in heavy ion collisions is due to competition between gluon dissociation of J/ψ and coalescence formation of J/ψ in the QGP requires very high luminosity. Tests of charm coalescence models include measuring J/ψ v_2 as a function of p_T, J/ψ R_{AA} to much higher p_T to follow the trends of suppression as the J/ψ formation time approaches the QGP crossing time, and J/ψ polarization as a function of collision centrality. The rapidity and p_T dependence of R_{AA} as functions of $\sqrt{s_{_{NN}}}$ and centrality, requiring sufficient luminosity for precision measurements at multiple energies, is not possible on a reasonable time scale at the present RHIC luminosity.

The study of bottomonium states, the Υ family, is only possible at RHIC II luminosities. Like the charmonium states, the dissociation temperatures of the bottomonium states depend on the binding energies. There are, however, two important differences from charmonium. First, the bottomonium binding energies, particularly that of the $\Upsilon(1S)$, are higher so that they should dissociate at higher temperatures. Only the higher-lying bottomonium states are thus likely to break up at RHIC energies. Second, the $b\bar{b}$ production rate in central Au+Au collisions is only $\sim$ 0.05 pairs per collision, making coalescence production of bottomonium much less likely. Thus bottomonium production at RHIC II will provide a very different window on color screening effects than charmonium production. The bottomonium yields at RHIC II should be sufficient for measurements of R_{AA} as a function of centrality in heavy ion collisions for the three Υ S states. The Υ yields at RHIC II and at the LHC will not be sufficient for measurements of v_2 or polarization.

As mentioned earlier, lepton measurements of semileptonic open heavy flavor decays at RHIC have already produced strikingly different results than expected. The strong suppression in R_{AA} coupled with the large v_2 suggest very large heavy quark energy loss in the medium. However, these semileptonic decay spectra contain both charm and bottom contributions, a significant complication. The separation of open charm and bottom can be done in several ways. Charm can be observed via $D^0 \to K\pi$ and $D \to K\pi\pi$ hadronic decays, as done by STAR. Precise R_{AA} and v_2 measurements are difficult in this channel. Since these events cannot be triggered, they must be extracted from a minimum bias data set that samples only a small fraction of the available luminosity. The combinatorial background is also very large, making statistical precision difficult. The addition of a displaced vertex measurement in STAR will dramatically reduce the combinatorial background but there is still no trigger for these decays. At RHIC II luminosity, bottom can be observed very cleanly in both PHENIX and STAR via $B \to J/\psi$ decays using displaced vertices, providing good measurements of the $b\bar{b}$ cross section and R_{AA}. However those yields will certainly be too small for v_2 measurements at RHIC II or the LHC. Finally, the combination of RHIC II luminosity with a displaced vertex measurement should allow statistical separation of the charm and bottom contributions to the semileptonic decay spectra, taking advantage of the different c and b quark decay lengths. Such semileptonic decay measurements, while less clean than the direct D and B decay measurements, have the advantage of much larger yields so that separate v_2 measurements for charm and bottom should be possible.

Independent measurements of open charm and bottom R_{AA} and v_2 to high p_T will be a very important capabaility at RHIC II. At low p_T, these measurements reflect the degree of heavy quark thermalization in the medium. At high p_T, they probe the energy loss of heavy quarks in the medium, providing an independent measurement of the initial energy density relative to the light quark energy loss measurements. The thermalization and energy loss mechanisms at low and high p_T respectively may be quite different due to the possible resonance scattering at low p_T.

1.4. Overview of the relationship of RHIC II to the LHC program

The heavy flavor production cross sections are significantly higher at the LHC than at RHIC since the per nucleon Pb+Pb energy at the LHC is a factor of 27.5 higher than the maximum per nucleon Au+Au energy at RHIC. The $c\overline{c}$ and $b\overline{b}$ cross sections increase by factors of 15 and 100 respectively [11] while the J/ψ and Υ cross sections increase by factors of 13 and 55 respectively [41]. But, because of the higher luminosity and the longer heavy ion runs, the Au+Au integrated luminosity at RHIC II is projected to be 36 times higher than for Pb+Pb at LHC. Therefore the heavy flavor yields per year are expected to be similar at the two facilities.

At $\sqrt{s} = 200$ GeV, bottom decays to leptons begin to dominate the single electron spectrum at $p_T \sim 4$ GeV/c. As the collision energy increases, the lepton spectra from B and D decays move closer together rather than further apart [11]. Thus, the large increase in the $b\overline{b}$ cross section relative to $c\overline{c}$ does not make single leptons from B and D decays easier to separate. Preliminary calculations show that the $B \to e$ decay does become larger than that of $D \to e$, but at $p_T > 10$ GeV/c. The two lepton sources differ by less than a factor of two up to $p_T \sim 50$ GeV/c in the range $|y| \leq 1$. Thus interpretation of single lepton results on heavy flavors will be more difficult at the LHC. Other means of separating charm and bottom must be found. ALICE can reconstruct hadronic D^0 decays from $p_T \sim 0$ to $p_T \sim 25$ GeV/c [42] but, like STAR, will have to rely on minimum bias data for these measurements because of the lack of a trigger. While it is not yet clear what CMS and ATLAS will do to reconstruct charm, they should be able to make b jet measurements, similar to the Tevatron. One way that B mesons can be measured at the LHC is through their decays to J/ψ, as discussed further below. It has also been suggested that the $B\overline{B}$ contribution to the dimuon continuum, the dominant contribution above the Υ mass, can be used to measure energy loss [43]. That channel would be fairly clean at the LHC but more difficult at RHIC.

The RHIC II upgrades and the high LHC energies make detailed studies of Υ production and suppression possible. At the LHC, higher initial temperatures make Υ suppression more likely than at RHIC II. But the higher $b\overline{b}$ production rate ($\sim$ 5 per central Pb+Pb collision) means that, unlike RHIC, significant coalescence contributions to Υ production may be expected at the LHC. Thus measurements at the two energies complement each other. At RHIC II, it is likely that PHENIX will be able to measure and resolve the three Υ S states. STAR will see Υ yields similar to those in ALICE but the mass resolution will require fitting to extract yields. At the LHC, all three S states will also be measurable, and CMS has the mass resolution to separate all three. The Υ states can be measured to $p_T \sim 0$ at all LHC detectors. Only ALICE will be able to measure J/ψ production to $p_T \sim 0$ without a special trigger [41] since CMS and ATLAS require high single muon p_T so that typically only J/ψ with $p_T > 5$ GeV/c are accepted. (However, CMS is working on a higher-level trigger to measure lower p_T J/ψ [44].) The larger $b\bar{b}$ cross section at the LHC means that J/ψ production from $B \to J/\psi X$ cannot be neglected. These decay J/ψ should be separable from the initial production using displaced vertices [41].

2. Detector upgrade program at RHIC

Both PHENIX and STAR have extensive upgrade programs underway that are extremely important for the heavy flavor program. The upgrades that are most relevant to heavy flavor measurements are described here. The impact on the heavy flavor program of these detector upgrades, in combination with the RHIC II luminosity increase, will be discussed in sections 4 and 5.

2.1. PHENIX upgrades

Several PHENIX detector upgrades that greatly enhance the heavy flavor capability of the experiment are expected to be available in the RHIC II time frame. The most important upgrades for the heavy flavor program will be the barrel and endcap Silicon Vertex Detectors, the Nose Cone Calorimeter, and the Muon Trigger Upgrade. The central region of the PHENIX detector, after installation of the silicon trackers and the Nose Cone Calorimeter, is shown in Fig. 1. The pseudorapidity and azimuthal angle coverages of the new detectors are illustrated in Fig. 2.

The Silicon Vertex Detector (SVTX) consists of a central arm barrel and two endcap detectors, as shown in Fig. 1. The SVTX barrel will provide a displaced vertex resolution of ~ 50 μm. The SVTX endcaps will provide a displaced vertex resolution of ~ 90 - 115 μm. Together, they will provide inner tracking with full azimuthal coverage for $|\eta| < 2.4$. By connecting to tracks in both the central and muon arms, the SVTX will tag heavy flavor decays by displaced vertices, improve the quarkonium invariant mass resolution and reduce backgrounds for heavy flavor measurements. In the muon arms, a loose displaced vertex cut will eliminate most muon tracks from light hadron decays and a very tight cut, $\sim 2\sigma$, will eliminate punch-through hadrons. The displaced vertex measurement will greatly help $D \to K\pi$ measurements in the central arms, presently very difficult in PHENIX, by reducing the contribution to the combinatorial background

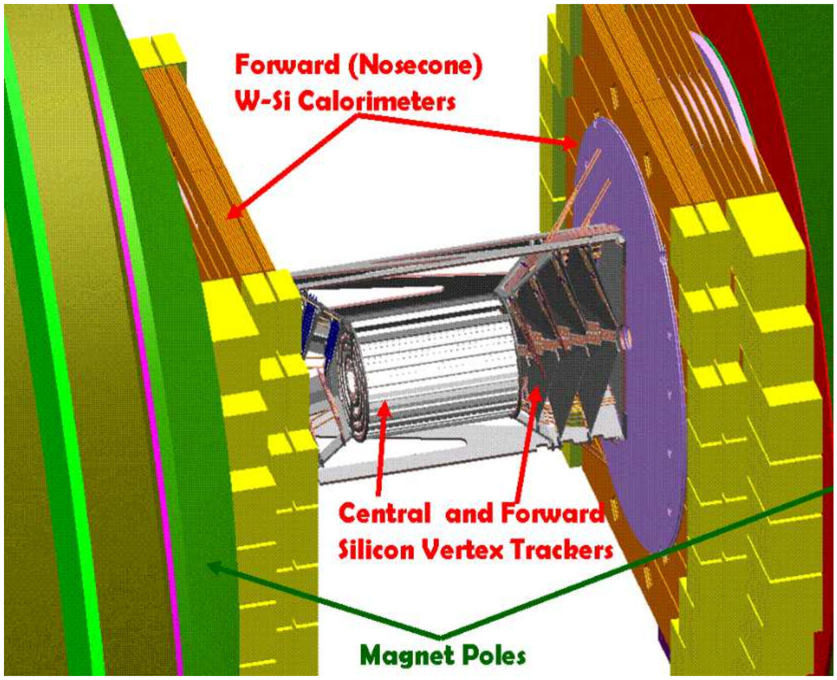

Figure 1. The central region of the PHENIX detector after the addition of the barrel and endcap silicon vertex detectors and the Nose Cone Calorimeter.

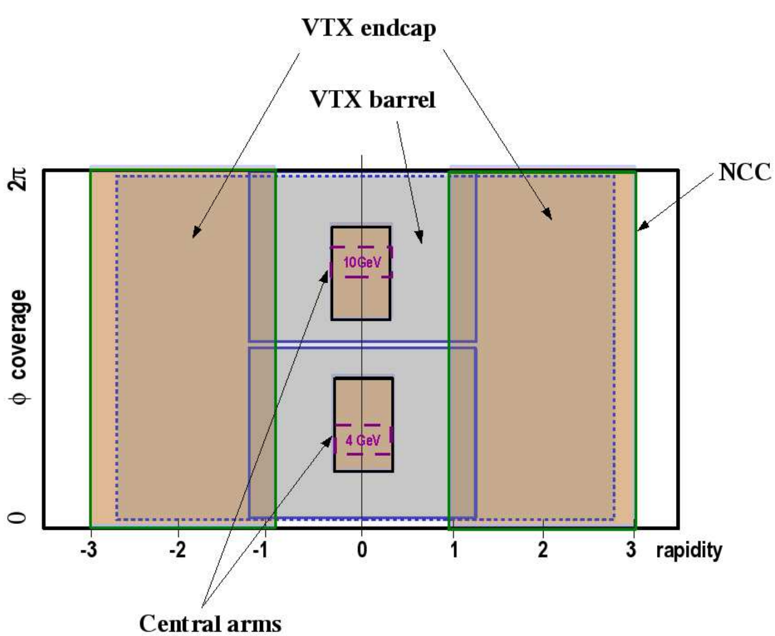

Figure 2. The pseudorapidity and azimuthal angle coverage of the PHENIX barrel and endcap silicon vertex detectors, and of the Nose Cone Calorimeter.

both from prompt tracks (by using a tight vertex cut) and light meson decay tracks (by using a loose cut of $\sim$ 1 cm). A loose displaced vertex cut will also reduce high p_T background tracks in the central arms due to misidentified light hadron decays. In addition to identifying semileptonic heavy flavor decays, displaced vertex measurements can help identify J/ψ's from B meson decays, since all other J/ψ's are prompt.

The SVTX barrel is presently under construction. It will consist of four concentric silicon layers. The two inner layers, at radii of 2.5 and 5.0 cm, consist of pixel detectors with a segmentation of 50 μm by 425 μm. The outer two layers, with radii of 10 and 14 cm, consist of 80 μm by 3 cm strips. The occupancy of the inner layer will be about 4.5% in central Au+Au collisions. The SVTX barrel produces a dramatic improvement in resolution of high p_T tracks in the central arms. The PHENIX Drift Chamber is outside the magnetic field so that, in the present momentum measurement, there is no information about the initial ϕ angle of the track. The momentum is calculated from the difference between the ϕ angle of the track after passing through the magnetic field and the ϕ angle from the vertex position to the Drift Chamber. This difference is only $\sim$ 40% of the total deflection in the field. By adding a precise measurement of the initial ϕ direction, the SVTX barrel directly measures the full deflection, improving the momentum resolution by a factor of $\sim$ 2.5, greatly improving the Υ invariant mass resolution. Installation of the barrel is expected in 2009.

The forward silicon detector endcaps will consist of four silicon mini-strip planes. The mini-strips have 50 μm pitch in the radial direction and lengths in the ϕ direction varying from 1.9 mm to 13.5 mm, depending on the polar angle. The maximum occupancy per strip is estimated to be less than 1.5% in central Au+Au collisions. The displaced vertex resolution of 90 - 115 μm, depending on the number of layers of silicon traversed by the track, should be compared to a mean vertex displacement of 785 μm for the boosted open charm muons. A prototype covering about 1/4 of one muon arm is presently under construction.

The PHENIX Nose Cone Calorimeters, tungsten-silicon calorimeters that will replace the two central arm magnet nosecones, will provide coverage for $0.9 < |\eta| < 3.5$. The simulated energy resolution for photons is $\sim 27\%/\sqrt{E}$ where E is in GeV. The Nose Cone Calorimeters will contain both electromagnetic and hadronic calorimeter sections. The electromagnetic calorimeter will contain a pre-shower detector and a shower-max detector designed to discriminate between individual electromagnetic showers and overlapping photons from high momentum π^0 decays. The pre-shower and shower-max detectors are expected to resolve showers with separations down to 2 mm and 4 mm, respectively. The Nose Cone Calorimeters should thus provide good acceptance for $\chi_c \rightarrow J/\psi + \gamma$ decays with the nJ/ψ detected in the muon arms.

The muon trigger upgrade is required for PHENIX to be able to take complete advantage of the RHIC II luminosity upgrade for muon arm measurements. The existing muon arm level-1 heavy vector meson triggers have enough rejection power to handle Au+Au collision rates of up to $\sim$ 20 KHz and pp collision rates of up to $\sim$ 0.5 MHz. The muon trigger upgrade adds three layers of Resistive Plate Chamber (RPC) detectors, with two dimensional (θ, ϕ) readout, in each muon arm. These layers follow the design of the CMS muon trigger at the LHC with the cathode pad segmentation optimized for PHENIX. The front end electronics and trigger processors will be developed within PHENIX. The muon trigger upgrade will provide an online momentum measurement to improve the level-1 trigger rejection for both single muons (with a p_T cut) and muon pairs (with an invariant mass cut). It will also provide improved high multiplicity background rejection during the final analysis. The muon trigger upgrade is presently under construction.

2.2. STAR upgrades

While work on answering the questions discussed in this document are underway in STAR, to complete many of the challenging measurements, upgrades to the STAR detector are needed. The collaboration has planned a series of upgrades for the near and intermediate term to overcome the current shortcomings and enhance its heavy flavor capabilities. Implementation of these upgrades will also allow optimum utilization of the increased luminosity expected from RHIC II.

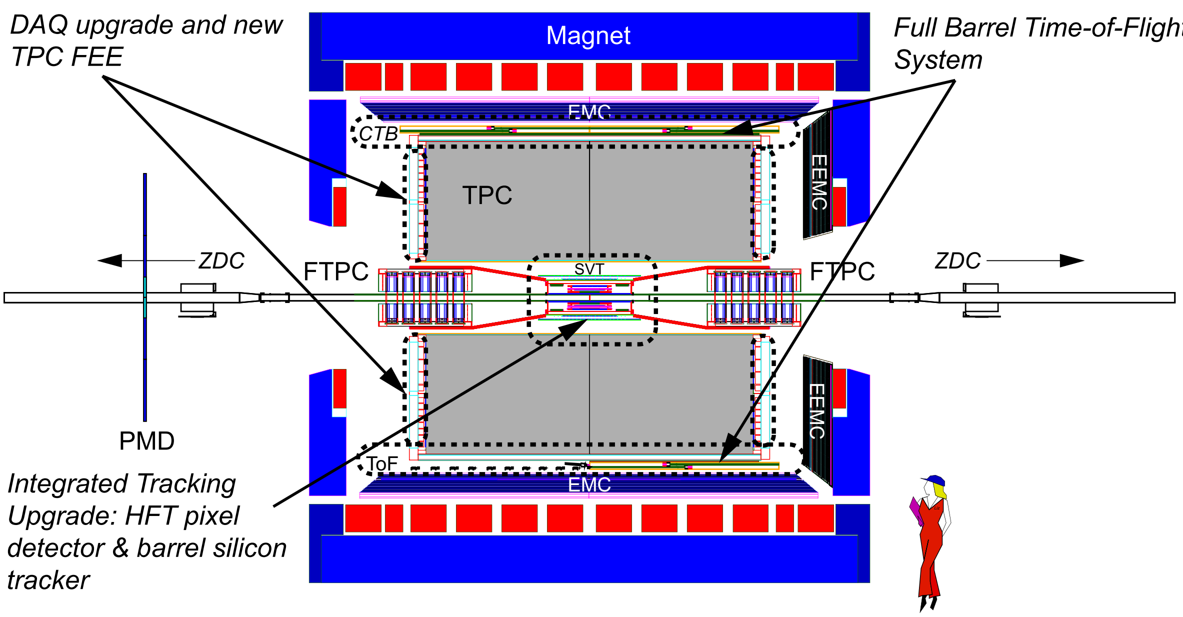

Figure 3. Layout of the STAR experiment 2005/2006 [45]. The locations of the planned upgrades are enclosed by dashed lines. See text for details.

The current layout of the STAR detector is depicted in Fig. 3. The medium term upgrades to the detector relevant for heavy flavor physics include: a full barrel Time of Flight detector (TOF) replacing the current TOF patch and the Central Trigger Barrel (CTB); new front end electronics for the large Time Projection Chamber (TPC); an upgrade to the data acquisition system (DAQ-1000), and a tracking upgrade including a barrel section with two inner layers of silicon pixel sensors (HFT) and three layers of silicon strip detectors (IST).

The new time of flight system covering the full outer barrel of the TPC is planned for construction and installation in STAR over the next three years. The system uses the Multi-gap Resistive Plate Chamber (MRPC) technology developed at CERN and will consist of 3840 MRPC modules with 23,000 channels of readout. The modules will cover the TPC outer barrel ($-1 < \eta < 1$, $0 < \phi < 2\pi$) and will be mounted in 120 trays which will replace the existing CTB (Central Trigger Barrel scintillation counter) trays.

The TOF doubles the current momentum range over which π, K, and p can be identified and thus considerably improves the reconstruction of charm mesons and baryons. When the TOF measurement is combined with the TPC dE/dx measurement, electrons can be cleanly identified from the lowest momentum measured ($\sim$ 200 MeV/c) up to a few GeV/c. This capability complements the electromagnetic calorimeter which works well for momenta above $\sim$ 2 GeV/c. STAR will then be able to reconstruct soft to medium momentum electrons with high efficiency and purity, providing the capability to make a comprehensive J/ψ measurement. The TOF, in conjunction with the EMC, also allows STAR to implement a level-2 trigger scheme to select $J/\psi \rightarrow e^+e^-$decays in $A + A$ collisions.

A series of improvements to the STAR data acquisition system over the past several years has brought the capability from the original design rate of 1 Hz recorded events to 50-100 Hz. To acquire the very large data samples and high data rates needed for heavy flavor measurements, an upgrade has been initiated with the goal of achieving a recorded event rate of at least 1 kHz. This rate could produce data volumes which would significantly exceed the capacity for analysis and storage. The rare-trigger data sets will especially benefit from the upgrade since the pipelined architecture being implemented will virtually eliminate the front end dead time, allowing to make full use of rare event triggers such as the one for the Υ.

The increase in readout speed can be achieved by replacing the TPC front end electronics, making use of circuits developed for the ALICE experiment at CERN, in conjunction with an upgrade of the STAR DAQ. In addition to the increased physics capabilities from the DAQ upgrade, the replacement of the TPC front end electronics, specifically the RDO boards that collect data from the FEE boards, will make space for a future precision tracking chamber between the TPC end planes and the endcap calorimeter. Replacing the TPC front end electronics also assures that this system will be maintainable for the next decade or more. The readout for the other existing detectors, which will remain in place for the RHIC II era, can be adapted to the new high speed DAQ with minor changes.

In order to address heavy quark energy loss and thermalization, it will be necessary to cleanly identify open charm. The recent results from both STAR and PHENIX on the suppression and flow of non-photonic electrons are intriguing. However, without an identified charm sample, the contributions from semileptonic bottom decays and systematic errors on background subtraction make a clear interpretation of these results difficult. Measurement of the yields of various charm species will also allow a study of the charm hadrochemistry.

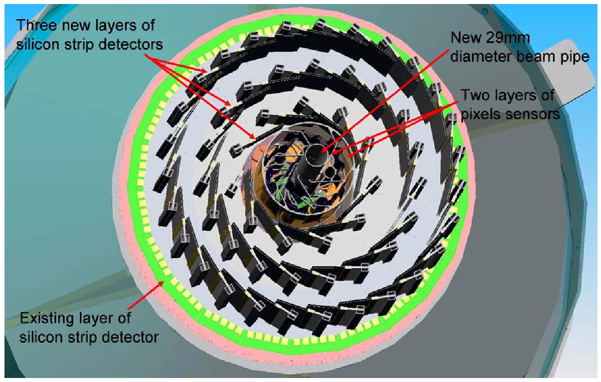

Figure 4. Layout of the new inner tracker for STAR. End view of small radius beam pipe (1.4 cm radius), two layers of pixel sensor, three new layers of silicon strip sensors, and the existing layer of silicon strip sensor.

Efficient topological reconstruction of open charm decays requires tracking "point-back" resolution to the primary collision vertex of ~ 50 μm or less. Further, the beam pipe and innermost detector layers must be very thin to measure the low p_T particles which comprise the bulk of the cross section and thus minimize the systematic errors in extrapolating the measured yield to the total yield. A thin beam pipe and inner detector layers are also key elements in efficiently vetoing photon conversion electrons which, along with the electron identification from the TPC, TOF and electromagnetic calorimeter, will measure the soft lepton and dilepton spectra. STAR is thus developing a tracking upgrade for the central rapidity region ($-1 < \eta < 1, 0 < \phi < 2\pi$). The essential elements under consideration for this upgrade are a new thin, small-radius beam pipe (0.5 mm thick, 14 mm radius), two layers of thinned (50 μm) CMOS pixel detectors at average radii of 1.5 and 4.5 cm (HFT) and three layers of conventional silicon strip detectors at average radii of 10, 15 and 20 cm (IST), see Fig. 4. The existing layer of double-sided silicon strip sensors at a radius of 25 cm (SSD) will be kept. The three new layers of conventional silicon strip sensors (IST) will connect tracks from the TPC and SSD to hits in the pixel layers. These layers will replace the existing three layers of silicon drift detector (SVT). It will be necessary to replace the SVT since, when RHIC II becomes operational, the SVT will be over 10 years old with a readout too slow to be compatible with the upgraded DAQ. It also has a large amount of infrastructure (cables and cooling) that adds undesirable mass in the region $1 < \eta < 2$.

3. Projected RHIC II yields

In this section we present some estimates of the quality of the heavy flavor measurements that can be achieved at RHIC II luminosities with the upgraded detectors.

Table 1 is a summary of the weekly integrated delivered luminosity estimates for RHIC and RHIC II. The weekly luminosity expectations are based on RHIC Collider Accelerator Division guidance. The projected weekly luminosities for RHIC II and for

Table 1. The anticipated luminosity per week delivered by RHIC. This delivered luminosity has to be reduced by a factor that accounts for detector up time and collision vertex cuts imposed by the detectors when estimating rates. The RHIC projected luminosities are 2008 maximum values taken from the RHIC Collider Accelerator Division projections. They represent the performance of a mature RHIC accelerator. Because the length of the collision diamond is smaller for RHIC II, the gain in usable luminosity is larger than the ratio of delivered luminosities when going to RHIC II. There are no d+Au and Cu+Cu RHIC projections available. The numbers in the "obtained" column are the best weekly luminosities from previous runs.

Species	Energy	Units	RHIC I Obtained	RHIC I Projected	RHIC II Projected
Au+Au	200	μb^{-1}	160	327	2500
Cu+Cu	200	nb^{-1}	2.4	–	25
d+Au	200	nb^{-1}	4.5	–	62
pp	200	pb^{-1}	0.9	26	33
pp	500	pb^{-1}	-	50	166

RHIC in 2008 and beyond (projected RHIC) are used to estimate the tabulated yields.

Table 2 summarizes the projected PHENIX yields for critical heavy flavor signals for the mature RHIC accelerator (in 2008 and beyond) and for a 12 week RHIC II physics run. Table 2 also includes the yields observed in recent RHIC runs. The yields are based on a number of criteria. The quarkonium cross sections are taken from Ref. [46] with an assumed ψ' to J/ψ ratio of 0.14. The charmonia cross sections are reduced by a factor of 0.43 in Au+Au interactions, approximately accounting for the suppression measured by PHENIX. No Υ suppression is assumed.

We assume that 80% of the RHIC beam is in the central bucket and thus usable by experiments. The root-mean square (RMS) of the collision diamond is assumed to be 20 cm at RHIC and 10 cm at RHIC II.

The detector acceptances are from PHENIX simulations. The minimum bias trigger efficiency for hard processes is assumed to be 0.75 for *pp* and 0.92 for Au+Au interactions. Where appropriate, an additional, realistic, level-1 trigger efficiency of 0.8 is used.

Realistic lepton pair reconstruction efficiencies of 0.8 in *pp* and 0.4 in Au+Au collisions are used. An additional efficiency factor of 0.4 is assumed when using a 1 mm displaced vertex cut to identify $B \to J/\psi$ decays. The PHENIX vertex detector is assumed for the projected yields, requiring a collision vertex cut of ± 10 cm.

Table 3 is a summary of the STAR projected yields for various critical heavy flavor signals for RHIC and RHIC II. The detector acceptances are from STAR simulations. Otherwise, the assumptions are identical to those used for the PHENIX yields presented in Table 2.

Table 4 summarizes the expected PHENIX and STAR heavy flavor yields in *pp* collisions at $\sqrt{s} = 500$ GeV. Although not directly comparable with heavy ion yields

Table 2. The projected yields of several heavy flavor signals in PHENIX for 12 week physics runs at RHIC II and a mature RHIC. The approximate yields obtained at RHIC to date are also shown. These reflect the fact that RHIC had not yet achieved the full luminosity development for Au+Au by Run 4, or for *pp* by Run 5. The Run 6 data have not yet been fully analyzed. The yields are shown for both *pp* and Au+Au collisions at $\sqrt{s_{_{NN}}} = 200$ GeV. The projected RHIC and RHIC II values assume that the PHENIX SVTX detector is in place, limiting the usable collision vertex range to ± 10 cm. The SVTX detector has a much larger impact at RHIC, where the collision diamond RMS is 20 cm, than at RHIC II where the collision diamond RMS is 10 cm.

Species	signal	$\|\eta\|$	To Date	RHIC	RHIC II
pp	$J/\psi \to e^+e^-$	< 0.35	$\sim 1{,}500$	25,000	55,000
	$J/\psi \to \mu^+\mu^-$	$1.2 - 2.4$	$\sim 8{,}000$	208,000	470,000
	$\psi' \to e^+e^-$	< 0.35	–	440	990
	$\psi' \to \mu^+\mu^-$	$1.2 - 2.4$	–	3,700	8,500
	$\chi_c \to e^+e^-\gamma$	< 0.35	–	1,600	3,600
	$\chi_c \to \mu^+\mu^-\gamma$	$1.2 - 2.4$	–	62,000	139,000
	$\Upsilon \to e^+e^-$	< 0.35	–	90	200
	$\Upsilon \to \mu^+\mu^-$	$1.2 - 2.4$	~ 27	230	500
	$B \to J/\psi \to e^+e^-$	< 0.35	–	130	300
	$B \to J/\psi \to \mu^+\mu^-$	$1.2 - 2.4$	–	1,300	3,000
Au+Au	$J/\psi \to e^+e^-$	< 0.35	~ 800	3,300	45,00
	$J/\psi \to \mu^+\mu^-$	$1.2 - 2.4$	$\sim 7{,}000$	29,000	395,00
	$\psi' \to e^+e^-$	< 0.35	–	60	800
	$\psi' \to \mu^+\mu^-$	$1.2 - 2.4$	–	520	7,100
	$\chi_c \to e^+e^-\gamma$	< 0.35	–	220	2,900
	$\chi_c \to \mu^+\mu^-\gamma$	$1.2 - 2.4$	–	8,600	117,000
	$\Upsilon \to e^+e^-$	< 0.35	–	30	400
	$\Upsilon \to \mu^+\mu^-$	$1.2 - 2.4$	–	80	1,040
	$B \to J/\psi \to e^+e^-$	< 0.35	–	40	570
	$B \to J/\psi \to \mu^+\mu^-$	$1.2 - 2.4$	–	420	5,700

from collisions at $\sqrt{s_{_{NN}}} = 200$ GeV, the order of magnitude larger heavy flavor yields at 500 GeV should help understand the reaction mechanisms in *pp* collisions.

Table 5 contains a summary of the projected yields from the LHC detector collaborations for various critical heavy flavor signals in a 10^6 s $\sqrt{s_{_{NN}}} = 5.5$ TeV Pb+Pb run, the standard planning number for a year of running [47, 48, 49]. Note that the estimates by the LHC collaborations generally assume more optimistic reconstruction efficiencies than those used for the RHIC detectors.

Comparison of Tables 2, 3 and 5 reveal that the projected heavy flavor yields for one year of running are similar at the LHC and at RHIC II. The much larger heavy flavor cross sections at the higher LHC energy are largely compensated at RHIC II

Table 3. The projected yields of several heavy flavor signals in STAR for 12 week physics runs at RHIC II and a mature RHIC. The approximate yields obtained at RHIC to date are also shown. The projected RHIC and RHIC II values assume that the STAR Heavy Flavor Tracker is in place, limiting the usable collision vertex range to ±10 cm. The $D \to K\pi$ yields assume 100 Hz recorded minimum bias data.

Species	signal	$\|\eta\|$	To Date	RHIC	RHIC II
pp	$J/\psi \to e^+e^-$	< 1.0	–	1,260,000	1,600,000
	$\psi' \to e^+e^-$		–	23,000	29,000
	$\Upsilon \to e^+e^-$		–	6,600	8,300
	$B \to J/\psi \to e^+e^-$		–	15,000	19,000
Au+Au	$J/\psi \to e^+e^-$	< 1.0	?	16,000	220,000
	$\psi' \to e^+e^-$		–	300	4,000
	$\Upsilon \to e^+e^-$		?	830	11,200
	$B \to J/\psi \to e^+e^-$		–	190	2,500
	$D \to K\pi$		–	30,000	30,000

Table 4. Projected heavy flavor yields in PHENIX and STAR for 12 weeks of $\sqrt{s_{NN}} = 500$ GeV pp running at RHIC II and a mature RHIC. The projected RHIC and RHIC II values assume that both the the PHENIX SVTX detector and STAR HF tracker are in place, limiting the usable collision vertex range to ±10 cm. These detectors have a much larger impact at RHIC , where the collision diamond RMS is 20 cm, than at RHIC II where the collision diamond RMS is 10 cm.

Experiment	signal	$\|\eta\|$	RHIC	RHIC II
PHENIX	$J/\psi \to e^+e^-$	< 0.35	183,000	600,000
	$J/\psi \to \mu^+\mu^-$	$1.2 - 2.4$	1,650,000	5,500,000
	$\psi' \to e^+e^-$	< 0.35	3,300	11,000
	$\psi' \to \mu^+\mu^-$	$1.2 - 2.4$	30,000	100,000
	$\chi_c \to e^+e^-\gamma$	< 0.35	31,000	100,000
	$\chi_c \to \mu^+\mu^-\gamma$	$1.2 - 2.4$	1,200,000	4,800,000
	$\Upsilon \to e^+e^-$	< 0.35	900	3000
	$\Upsilon \to \mu^+\mu^-$	$1.2 - 2.4$	2,300	7,700
	$B \to J/\psi \to e^+e^-$	< 0.35	2,300	7,700
	$B \to J/\psi \to \mu^+\mu^-$	$1.2 - 2.4$	23,000	77,000
STAR	$J/\psi \to e^+e^-$	< 1.0	3,700,000	12,000,000
	$\psi' \to e^+e^-$		76,000	220,000
	$\Upsilon \to e^+e^-$		25,000	84,000
	$B \to J/\psi \to e^+e^-$		346,000	1,100,000

Table 5. The estimated LHC heavy flavor yields for a 10^6 s Pb+Pb run with 500 μb^{-1} integrated luminosity (one year), reported by the LHC experiments. As for the RHIC tables, the Υ rates include all three states. The ATLAS J/ψ range corresponds to different assumed trigger thresholds.

Species	signal	ALICE	$\lvert\eta\rvert$	CMS	$\lvert\eta\rvert$	ATLAS	$\lvert\eta\rvert$
Pb+Pb	$J/\psi \to \mu^+\mu^-$	740,000	$2.5 - 4$	180,000	< 2.4	8K-100K	< 2.5
	$J/\psi \to e^+e^-$	9,500	< 0.9				
	$\psi' \to \mu^+\mu^-$	14,000	$2.5 - 4$	3,300	< 2.4	1,400-1,800	< 2.5
	$\psi' \to e^+e^-$	190	< 0.9				
	$\Upsilon \to \mu^+\mu^-$	8,400	$2.5 - 4$	36,700	< 2.4	15,000	< 2.5
	$\Upsilon \to e^+e^-$	2,600	< 0.9				
	$D \to K\pi$	8,000	< 0.9				

by integrated luminosities that result from three times longer runs and an order of magnitude higher luminosity.

4. Open heavy flavor

In this section we present a more detailed discussion of the theoretical motivation for studying open heavy flavor in heavy ion collisions, of the present experimental and theoretical status, and of the proposed experimental program of open heavy flavor measurements at RHIC II.

As described in the Introduction, dense matter effects in nuclear collisions may change the kinematic distributions and the total cross sections of open heavy flavor production. Effects such as energy loss and flow can significantly modify the heavy flavor p_T distributions but do not, in fact, change the total yields. In a finite acceptance detector, however, the measured yields may appear to be enhanced or suppressed, depending on the acceptance. Energy loss steepens the slope of the heavy flavor p_T distribution because the heavy quark p_T is reduced. If the momentum is reduced sufficiently for the quarks to be stopped within the medium, the heavy quarks can take the same velocity as the surrounding medium and 'go with the flow'. The present RHIC results on R_{AA} and v_2 for heavy flavor decays to leptons show that these effects are indeed important for charm quarks. However, higher p_T measurements and reconstructed charm hadrons are needed to solidify and quantify the results. In addition, clean separation of leptons from charm and bottom is necessary to determine the bottom quark's importance in the measured electron R_{AA}.

Effects that may modify the total heavy flavor yields are the initial parton distributions in the nuclei and secondary charm production in the medium. The parton distribution functions needed for perturbative QCD calculations of heavy flavor production are modified in the nucleus, as was observed in nuclear deep-inelastic scattering [50]. At very small momentum fractions, x, the gluon fields may be treated as classical color fields. The modifications of the parton distributions in nuclei relative to free protons would affect the total yields. The effect is expected to be small at mid rapidity and moderate p_T at RHIC but is likely to be more important at large rapidity, where lower x values are probed. Although thermal charm production from the medium is likely to be small at RHIC energies, it could moderately enhance the total yields.

Since the J/ψ yields may be enhanced in nuclear collisions by coalescence of uncorrelated c and $\overline{c}$ quarks in the medium, it is important for charmonium production in heavy ion collisions to be properly normalized. The ratio of J/ψ to open charm production in pp collisions is not a strong function of energy. Thus the total charm yield sets the scale against which J/ψ suppression relative to enhancement can be quantified, as discussed in more detail in Section 5.

4.1. Open Heavy Flavor Theoretical Results

4.1.1. Theoretical Baseline Results We now discuss the most recent theoretical baseline calculations of the transverse momentum distributions of charm and bottom quarks, the charm and bottom hadron distributions resulting from fragmentation and, finally, the electrons produced in semileptonic decays of the hadrons [3].

The theoretical prediction of the electron spectrum includes three main components: the p_T and rapidity distributions of the heavy quark Q in pp collisions at $\sqrt{s} = 200$ GeV, calculated in perturbative QCD; fragmentation of the heavy quarks into heavy hadrons, H_Q, described by phenomenological input extracted from e^+e^- data; and the decay of H_Q into electrons according to spectra available from other measurements. This cross section is schematically written as

$$\frac{Ed^3\sigma(e)}{dp^3} = \frac{E_Q d^3\sigma(Q)}{dp_Q^3} \otimes D(Q \to H_Q) \otimes f(H_Q \to e) \tag{1}$$

where the symbol $\otimes$ denotes a generic convolution. The electron decay spectrum, $f(H_Q \to e)$, accounts for the branching ratios.

The distribution $Ed^3\sigma(Q)/dp_Q^3$ is evaluated at Fixed-Order plus Next-to-Leading-Log (FONLL) level [51]. In addition to including the full fixed-order NLO result [52, 53], the FONLL calculation also resums [56] large perturbative terms proportional to $\alpha_s^n \log^k(p_T/m)$ to all orders with next-to-leading logarithmic (NLL) accuracy (i.e. $k = n,\ n-1$) where m is the heavy quark mass. The perturbative parameters are m and the value of the strong coupling, α_s. The central heavy quark masses are $m_c = 1.5$ GeV/c^2 and $m_b = 4.75$ GeV/c^2. The masses are varied in the range $1.3 < m_c < 1.7$ GeV/c^2 for charm and $4.5 < m_b < 5$ GeV/c^2 for bottom to estimate the mass uncertainties. The five-flavor QCD scale is the CTEQ6M value, $\Lambda^{(5)} = 0.226$ GeV. The perturbative calculation also depends on the factorization (μ_F) and renormalization (μ_R) scales. The scale sensitivity, a measure of the perturbative uncertainty, is calculated using $\mu_{R,F}^2 = \mu_0^2 = p_T^2 + m^2$ as the central value while varying μ_F and μ_R independently within a 'fiducial' region defined by $\mu_{R,F} = \xi_{R,F}\mu_0$ with $0.5 \leq \xi_{R,F} \leq 2$ and $0.5 \leq \xi_R/\xi_F \leq 2$

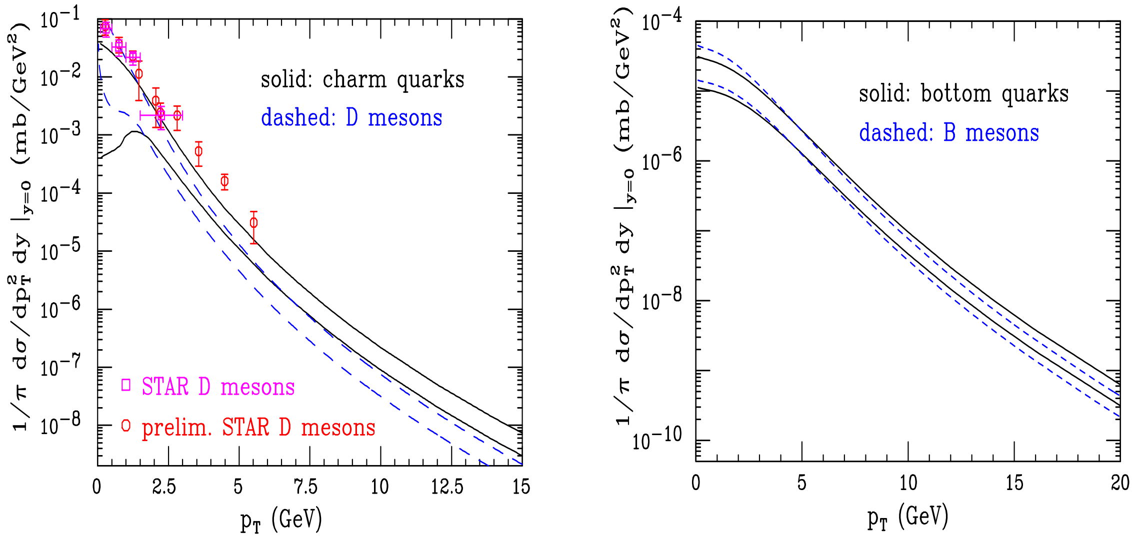

Figure 5. Left-hand side: The theoretical uncertainty bands for c quark and D meson p_T distributions in pp collisions at $\sqrt{s} = 200$ GeV, using $\mathrm{BR}(c \to D) = 1$. The final [54] and preliminary [55] STAR d+Au data (scaled to pp using $N_{\rm coll} = 7.5$) are also shown. Right-hand side: The same for b quarks and B mesons.

so that $\{(\xi_R, \xi_F)\} = \{(1,1), (2,2), (0.5,0.5), (1,0.5), (2,1), (0.5,1), (1,2)\}$. The envelope containing the resulting curves defines the uncertainty. The mass and scale uncertainties are added in quadrature.

These inputs lead to a FONLL total $c\bar{c}$ cross section in pp collisions of $\sigma_{c\bar{c}}^{\rm FONLL} = 256^{+400}_{-146}$ μb at $\sqrt{s} = 200$ GeV. The theoretical uncertainty is evaluated as described above. The corresponding NLO prediction is 244^{+381}_{-134} μb. The predictions in Ref. [11], using $m_c = 1.2$ GeV/c^2 and $\mu_R = \mu_F = 2\mu_0$ gives $\sigma_{c\bar{c}}^{\rm NLO} = 427$ μb, within the uncertainties. Since the FONLL and NLO calculations tend to coincide at small p_T, which dominates the total cross section, the two results are very similar. Thus the two calculations are equivalent at the total cross section level, within the large perturbative uncertainties. The total cross section for bottom production is $\sigma_{b\bar{b}}^{\rm FONLL} = 1.87^{+0.99}_{-0.67}$ μb.

The fragmentation functions, $D(c \to D)$ and $D(b \to B)$, where D and B indicate a generic admixture of charm and bottom hadrons, are consistently extracted from e^+e^- data in the FONLL context [57].

The measured spectra for primary $B \to e$ and $D \to e$ decays are assumed to be equal for all bottom and charm hadrons, respectively. The contribution of electrons from secondary B decays, $B \to D \to e$, was obtained by convoluting the $D \to e$ spectrum with a parton-model prediction of $b \to c$ decay. The resulting electron spectrum is very soft, giving a negligible contribution to the total. The decay spectra are normalized using the branching ratios for bottom and charm hadron mixtures [58]: $\mathrm{BR}(B \to e) = 10.86 \pm 0.35\%$, $\mathrm{BR}(D \to e) = 10.3 \pm 1.2\%$, and $\mathrm{BR}(B \to D \to e) = 9.6 \pm 0.6\%$.

The left-hand side of Fig. 5 shows the theoretical uncertainty bands for c quarks and D mesons, obtained by summing the mass and scale uncertainties in quadrature. The band is broader at low p_T due to the large value of α_s and the behavior of the CTEQ6M

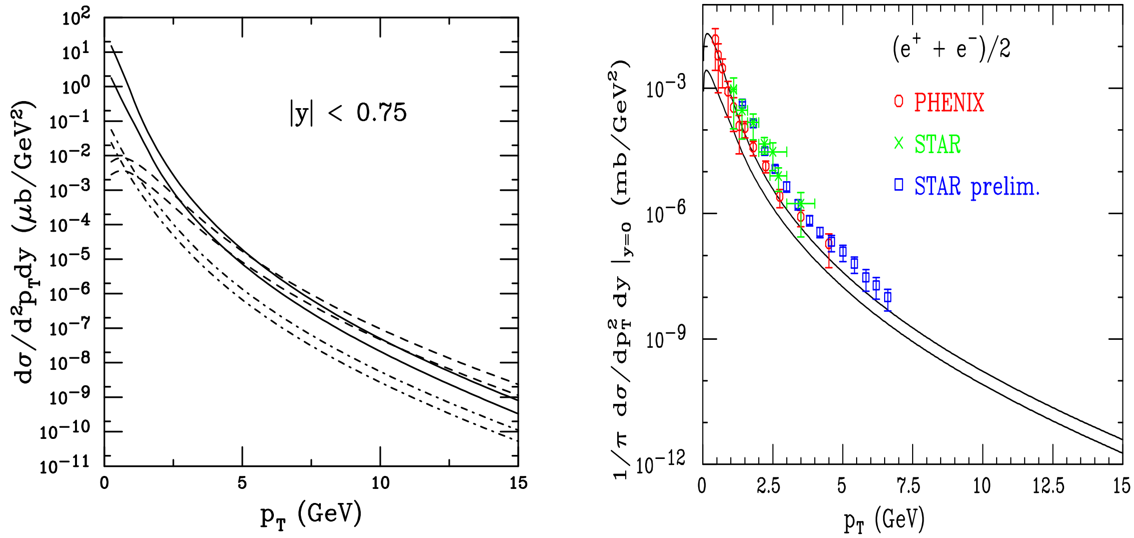

Figure 6. Left-hand side: The theoretical uncertainty bands for $D \to e$ (solid), $B \to e$ (dashed) and $B \to D \to e$ (dot-dashed) as a function of p_T in $\sqrt{s} = 200$ GeV pp collisions for $|y| < 0.75$. Right-hand side: The final electron uncertainty band in pp collisions is compared to the PHENIX [59] and STAR (final [54] and preliminary [55]) data.

parton densities at low scales as well as the increased sensitivity of the cross section to the charm quark mass. The rather hard fragmentation function causes the D meson and c quark bands to separate only at $p_T > 9$ GeV/c. The right-hand side of Fig. 5 shows the same results for b quarks and B mesons. The harder $b \to B$ fragmentation function causes the two bands to partially overlap until $p_T \simeq 20$ GeV/c.

Figure 6 shows the individual uncertainty bands for the $D \to e$, $B \to e$ and $B \to D \to e$ decays to electrons on the left-hand side and compares the RHIC data to the total band on the right-hand side. The upper and lower limits of the total band are obtained by summing the upper and lower limits for each component. The secondary $B \to D \to e$ spectrum is extremely soft, only exceeding the primary $B \to e$ decays at $p_T < 1$ GeV/c. It is always negligible with respect to the total yield. While, for the central parameter sets, the $B \to e$ decays begin to dominate the $D \to e$ decays at $p_T \simeq 4$ GeV/c, a comparison of the bands shows that the crossover may occur over a rather broad range of electron p_T, assuming that the two bands are uncorrelated.

4.2. Models of Heavy Quark Energy Loss

While the heavy quarks are in the medium, they can undergo energy loss by two means: elastic collisions with light partons in the system (collisional) and gluon bremsstrahlung (radiative). We will briefly review some of the predicted results for $-dE/dx$ of heavy quarks for both collisional and radiative loss. We then show the predicted effect on the charm and bottom contributions to single electrons at RHIC [6].

The collisional energy loss of heavy quarks through processes such as $Qg \to Qg$

and $Qq \to Qq$ depends logarithmically on the heavy quark momentum, $-dE/dx \propto \ln(q_{\rm max}/q_{\rm min})$. Treatments of the collisional loss vary with the values assumed or calculated for the cutoffs. These cutoffs are sensitive to the energy of the heavy quark and the temperature and strong coupling constant in the medium. Thus the quoted value of the energy loss is usually for a certain energy and temperature. The calculation was first done by Bjorken [60] who found $-dE/dx \approx 0.2$ GeV/fm for a 20 GeV quark at $T = 250$ MeV. Further work refined the calculations of the cutoffs [61, 62, 63], with similar results. Braaten and Thoma calculated the collisional loss in the limits $E \ll m_Q^2/T$ and $E \gg m_Q^2/T$ in the hard thermal loop approximation, removing the cutoff ambiguities. They obtained $-dE/dx \approx 0.3$ GeV/fm for a 20 GeV charm quark and 0.15 GeV/fm for a 20 GeV bottom quark at $T = 250$ MeV [64].

Other models of heavy quark energy loss were presented in the context of J/ψ suppression: Could a produced $c\overline{c}$ pair stay together in the medium long enough to form a J/ψ? Svetitsky [65] calculated the effects of diffusion and drag on the $c\overline{c}$ pair in the Boltzmann approach and found a strong effect. The drag stopped the $c\overline{c}$ pair after traveling about 1 fm but Brownian diffusion drove them apart quickly. The diffusion effect increased at later times. Svetitsky essentially predicted that the heavy quarks would be stopped and then go with the flow. His later calculations of D meson breakup and rehadronization [12] while moving through plasma droplets reached a similar conclusion. Koike and Matsui calculated energy loss of a color dipole moving through a plasma using kinetic theory and found $-dE/dx \sim 0.4 - 1.0$ GeV/fm for a 10 GeV $Q\overline{Q}$ [66]. The collisional loss was thus predicted to be small, less than 1 GeV/fm for reasonable assumptions of the temperature. The loss increases with energy and temperature. Using the hard thermal loop approach, Mustafa *et al.* found $-dE/dx \approx 1 - 2$ GeV/fm for a 20 GeV quark at $T = 500$ MeV [67].

The first application of radiative loss to heavy quarks was perhaps by Mustafa *et al.* [67]. They included the effects of only a single scattering/gluon emission, $Qq \to Qqg$ or $Qg \to Qgg$. In this case, the loss grows as the square of the momentum logarithm, $\ln^2(q_{\rm max}/q_{\rm min})$, one power more than the collisional loss, but is of the same order in the strong coupling constant [64]. Thus the radiative loss is guaranteed to be larger than the collisional in this approximation. The heavy quark mass enters their expressions only in the definition of $q_{\rm max}$ so that the mass dependence of the energy loss is rather weak. They found, for a 20 GeV quark at $T = 500$ MeV, $-dE/dx \approx 12$ GeV/fm for charm and 10 GeV/fm for bottom.

These large values suggested that energy loss could be quite important for heavy quarks. If true, there would be a strong effect on the $Q\overline{Q}$ contribution to the dilepton continuum. Shuryak [68] was the first to consider this possibility for $A + A$ collisions. He assumed that low mass $Q\overline{Q}$ pairs would be stopped in the medium, substantially suppressing the dilepton contribution from these decays. Heavy quarks are piled up at low p_T and midrapidity if stopped completely. However, stopped heavy quarks

† His drag coefficient $A(p^2)$ is related to the energy loss per unit length through $A(p^2) = (-dE/dx)/p^2$.

should at least expand with the medium rather than coming to rest, as discussed by Svetitsky [65]. Lin *et al.* then calculated the effects of energy loss at RHIC, including thermal fluctuations, for constant $-dE/dx = 0.5 - 2$ GeV/fm [10]. These results showed that heavy quark contributions to the dilepton continuum would be reduced but not completely suppressed. In any case, the energy loss does not affect the total cross section.

Dokshitzer and Kharzeev pointed out that soft gluon radiation from heavy quarks is suppressed at angles smaller than $\theta_0 = m_Q/E$ [9]. Thus bremsstrahlung is suppressed for heavy quarks relative to light quarks by the factor $(1 + \theta_0^2/\theta^2)^{-2}$, the 'dead cone' phenomenon. The radiative energy loss of heavy quarks could then be quite small. However, Armesto *et al.* [8] later showed that medium-induced gluon radiation could 'fill the dead cone', leading to non-negligible energy loss for heavy flavors. They also found that the energy loss would be larger for charm than bottom quarks.

So far the RHIC heavy ion measurements are not for heavy flavored hadrons but for the electrons from their semileptonic decays. If the effects of energy loss are substantially different for charm and bottom quarks, then the results in Fig. 6 which show that, at high p_T, the single electron spectrum is dominated by b decays, would suggest that, if charm quarks lose more energy than bottom quarks, b-quark dominance of the electron spectra would begin at smaller values of electron p_T in $A + A$ collisions. This would, in turn, limit the electron suppression factor, R_{AA}, at moderate p_T since the large bottom contribution would make R_{AA} larger than expected if the spectrum arose primarily from charm quark decays. Recent calculations [69] have revisited the importance of elastic energy loss and have shown that this component may make a larger contribution to the suppression factor than previously expected.

The left-hand side of Fig. 7 compares the c and b distributions at mid rapidity, as well as their contributions to single electrons. Single electrons from bottom dominate the single electron spectra at $p_T \sim 5$ GeV/c for all gluon rapidity densities. This conclusion is further supported by the right-hand side of Fig. 7, where the ratio of charm relative to bottom decays to electrons is shown. The crossover region here is rather narrow because μ_F and μ_R are correlated for c and b. In all cases, the bottom contribution to single electrons is large and cannot be neglected in the computation of single electron suppression, shown in Fig. 8. Since bottom energy loss is greatly reduced relative to charm [6], the possible effect on the electron spectrum is reduced, leading to $R_{AA}(p_T < 6$ GeV/c; $e) > 0.5 \pm 0.1$. A calculation by Armesto *et al.*, with a somewhat different model of energy loss, showed similar results to those in Fig. 8.

Recently two groups, Moore and Teaney [70] and Rapp *et al.* [71, 72] have calculated R_{AA} and the non-photonic electron elliptic flow, v_2, in a Langevin model of the time evolution of heavy quarks in the medium. Both these groups emphasize that elastic (collisional) energy loss should be important at low p_T relative to radiative loss since the boost for heavy flavor hadrons in the medium should not be large. Both also find a strong correlation between R_{AA} and v_2. The approaches differ somewhat but the trends are similar in the two calculations.

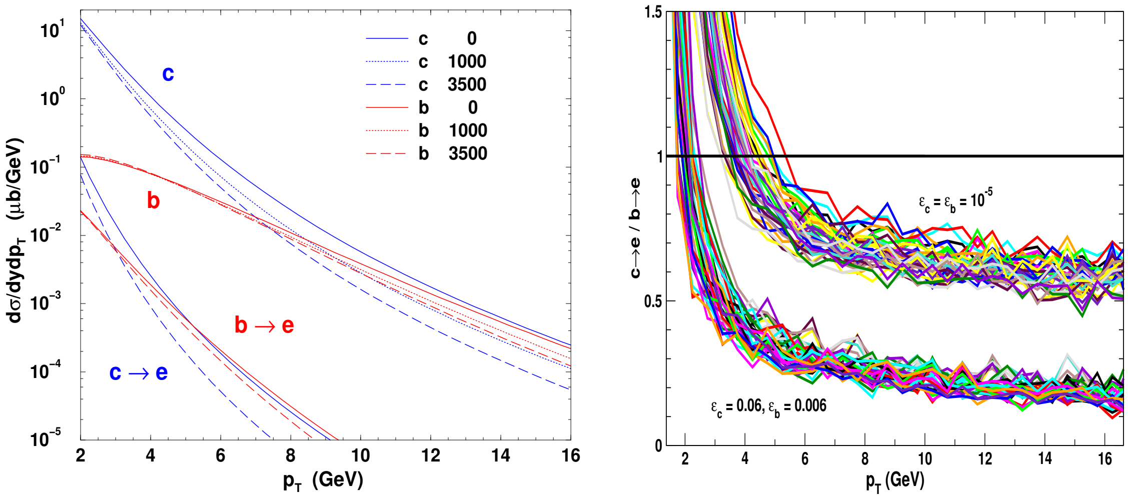

Figure 7. Left-hand side: The differential cross section (per nucleon pair) of charm and bottom quarks calculated to NLO in QCD [3] compared to single electron distributions calculated with the fragmentation and decay scheme of Ref. [3]. The solid, dotted and long dashed curves show the effects of heavy quark energy loss with initial gluon rapidity densities of $dN_g/dy = 0, 1000,$ and 3500, respectively. Right-hand side: The ratio of charm to bottom decays to electrons obtained by varying the quark masses and scale factors. The effect of changing the Peterson function parameters from $\epsilon_c = 0.06$, $\epsilon_b = 0.006$ (lower band) to $\epsilon_c = \epsilon_b = 10^{-5}$ (upper band) is also illustrated for correlated b and c scales. From Ref. [6].

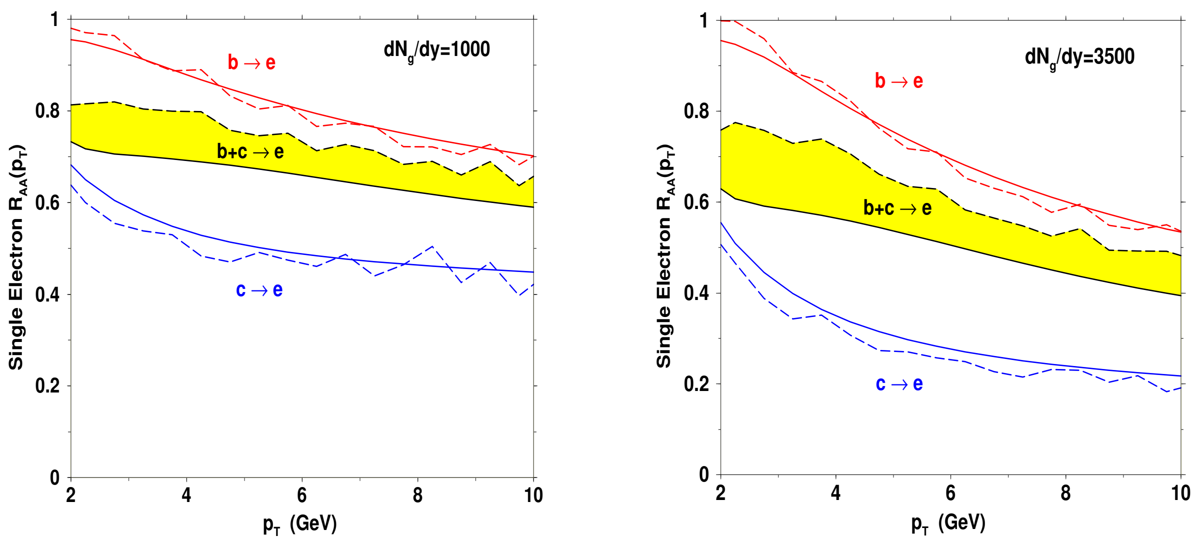

Figure 8. Single electron attenuation pattern for $dN_g/dy = 1000$, left, and $dN_g/dy = 3500$, right. The solid curves employ the fragmentation scheme and lepton decay parameterizations of Ref. [3] while the dashed curves use the Peterson function with $\epsilon_c = 0.06$ and $\epsilon_b = 0.006$ and the decay to leptons employed by the PYTHIA Monte Carlo. Even for the extreme case on the right, the less quenched b quarks dilute R_{AA} so much that the modification of the combined electron yield from both c and b decays does not fall below $\sim 0.5 - 0.6$ near $p_T \sim 5$ GeV/c. From Ref. [6].

Moore and Teaney [70] calculate the diffusion and drag coefficients for charm quarks in perturbative QCD. The diffusion coefficient is proportional to the inverse square of the strong coupling constant, α_s, *e.g.* $D(2\pi T) \propto \alpha_s^{-2}$. They present the effects of a range of values for $D(2\pi T)$ on R_{AA} and v_2, finding the largest effects at high p_T for small $D(2\pi T)$, corresponding to large α_s or strong coupling in the plasma.

Rapp *et al.* [71, 72] calculated the diffusion and drag coefficients assuming that resonant D and B states in the QGP elastically scatter in the medium. Resonance scattering reduces the thermalization times for heavy flavors relative to those calculated with perturbative QCD matrix elements for fixed $\alpha_s = 0.4$. The effect is larger for charm than for the more massive bottom quarks. Including these states thus reduces the electron R_{AA} at high p_T relative to the results in Ref. [6] while increasing the electron v_2 to $\sim 10\%$ at $p_T \sim 2$ GeV/c, in relative agreement with the data.

Thus, given sufficiently strong coupling and/or resonant states, both R_{AA} and v_2 can be described within transport approaches using elastic scattering. More and better data is necessary to distinguish the two approaches.

4.3. RHIC open heavy flavor measurements to date

Open heavy flavor production cross sections can be measured by reconstructing the invariant mass of the heavy quark hadron from its hadronic decay products or by detecting leptons from semileptonic decays of those hadrons. While both PHENIX and STAR can measure heavy flavor cross sections by either technique, PHENIX has some advantages for semileptonic decay measurements and STAR has advantages for the hadronic decay measurements.

In both cases, the signal to background rate can be greatly improved if a precise measurement of the decay vertex position is available, since hadrons containing c or b quarks typically travel several hundred microns from the collision point before decaying. Both PHENIX and STAR have plans to add secondary vertex detectors capable of the necessary precision but they will not be implemented for several years. In addition to reducing the background rates for open heavy flavor decays to leptons and hadrons, the secondary vertex detectors open up the possibility of a clean bottom cross section measurement using displaced vertex J/ψ decays, given sufficient luminosity.

Open heavy flavor cross section measurements based on semileptonic decays of charm and bottom mesons are feasible because a small lepton signal can be identified in a very large hadron background. The background lepton sources are both small and well enough understood that they can be subtracted to get the open heavy flavor signal. However, the loss of information about the decaying heavy meson due to the recoil kinematics is a disadvantage of semileptonic decay measurements. Thus charm and bottom decays cannot easily be distinguished. Open charm measurements using hadronic decay products have two advantages: the D meson kinematic properties are reconstructed and separation of charm from bottom is far easier because only a small fraction of D mesons arise from bottom decays [3]. A disadvantage of hadronic decay measurements is the huge combinatorial background in heavy ion collisions.

PHENIX has measured open heavy flavor yields via semileptonic decays to electrons at mid rapidity ($|\eta| < 0.35$) using the Ring Imaging Cerenkov detector and electromagnetic calorimeter for electron identification. At forward and backward rapidity ($1.2 < |\eta| < 2.2$) the two muon spectrometers are used. PHENIX results are available for pp at mid rapidity [73] and forward rapidity [74] as well as for d+Au [75] and Au+Au at mid rapidity [16]. No open charm results from hadronic decays have yet been reported by PHENIX since the small central arm acceptance is a disadvantage for such measurements.

STAR has measured open heavy flavor yields at mid rapidity ($|\eta| < 1.0$) via semileptonic decays using either a combination of the time projection chamber (TPC) and time of flight (TOF) for electron identification or a combination of the TPC and the electromagnetic calorimeter. The backgrounds that must be subtracted are much larger than they are for PHENIX because of the larger photon conversion rates in STAR and the lack of of a hadron blind electron identifier, but this is compensated somewhat by the larger acceptance. STAR electron results are available for pp d+Au and Au+Au collisions [15]. STAR has also measured open charm yields in the range $|\eta| < 1.0$ through hadronic D meson decays [54] for d+Au collisions.

Because the charm cross section is much larger than the bottom cross section at RHIC and dominates the semileptonic decay spectrum for $p_T < 2.5$ GeV/c, the integrated non-photonic lepton spectrum is usually assumed to be equal to the charm cross section.

4.3.1. Baseline measurements Before any conclusions can be drawn about the hot, dense final state from the results for heavy ion collisions, some baseline information is required. Data from pp collisions are needed to establish the underlying cross sections and kinematic distributions for open heavy flavor, and $p + A$ data are needed to isolate effects due to gluon saturation and the intrinsic k_T distributions in the colliding nuclei.

Both PHENIX and STAR have measured charm production at mid rapidity. These measurements have been extrapolated to all rapidities to yield total cross sections. These total cross sections are compared to results at other energies and to pQCD calculations in Fig. 9. Results for d+Au and Au+Au collisions are scaled by the number of binary collisions ($N_{\rm coll}$) for direct comparison to the pp results. The STAR data are from combined fits to hadronic and semileptonic decay data. The PHENIX data are from semileptonic decay measurements only.

Although the STAR values are somewhat higher than those for PHENIX, the total charm cross sections are in acceptable agreement within the fairly large systematic uncertainties.*Is this still true?*

Since charm and bottom quarks are expected to be produced only in the initial nucleon-nucleon interactions, their yield should scale as the number of binary collisions, $N_{\rm coll}$. Figure 10 shows the PHENIX measurement of the charm invariant yield in Au+Au collisions, scaled by $N_{\rm coll}$, at mid rapidity as a function of $N_{\rm part}$ [16]. The PHENIX data integrated over all $p_T > 0.3$ GeV/c are consistent with no $N_{\rm part}$ dependence, as expected. But the effect of the final state medium can be seen when the distributions are integrated only above 3 GeV/c. These p_T-dependent effects are discussed in the following section.

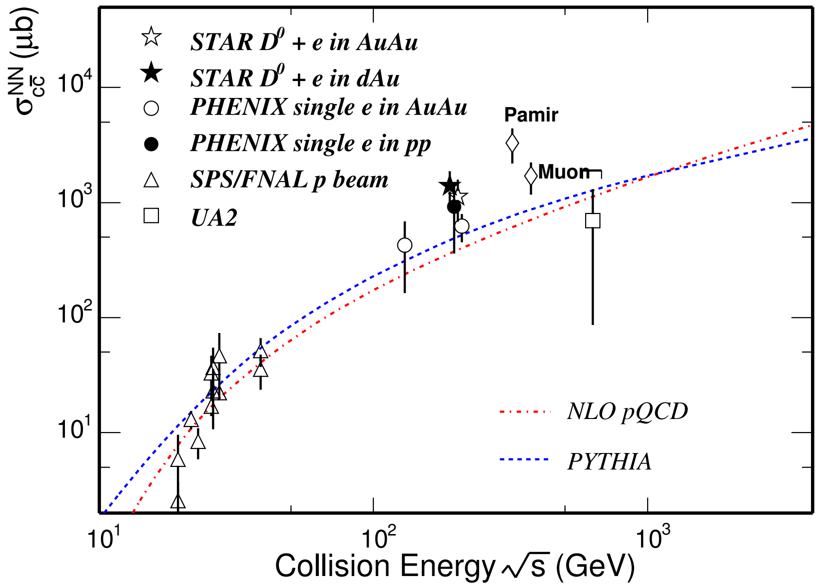

Figure 9. Comparison of total cross section measurements. The STAR and PHENIX results are given as cross section per binary collisions [76]. The theory curves are from Ref. [54]. The NLO pQCD parameters are optimized using low energy data [11].

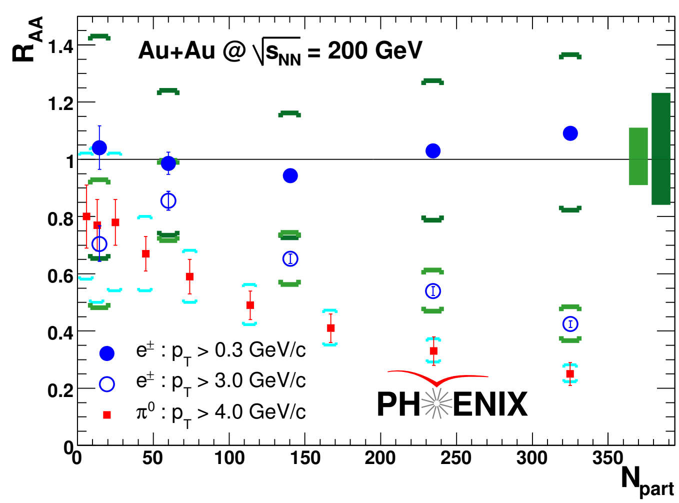

Figure 10. Left: PHENIX measurements of the mid rapidity invariant charm yields scaled by N_{coll} as a function of N_{part} [16]. More than half of the heavy flavor decay electrons are included in the integral above 0.3 GeV/c.

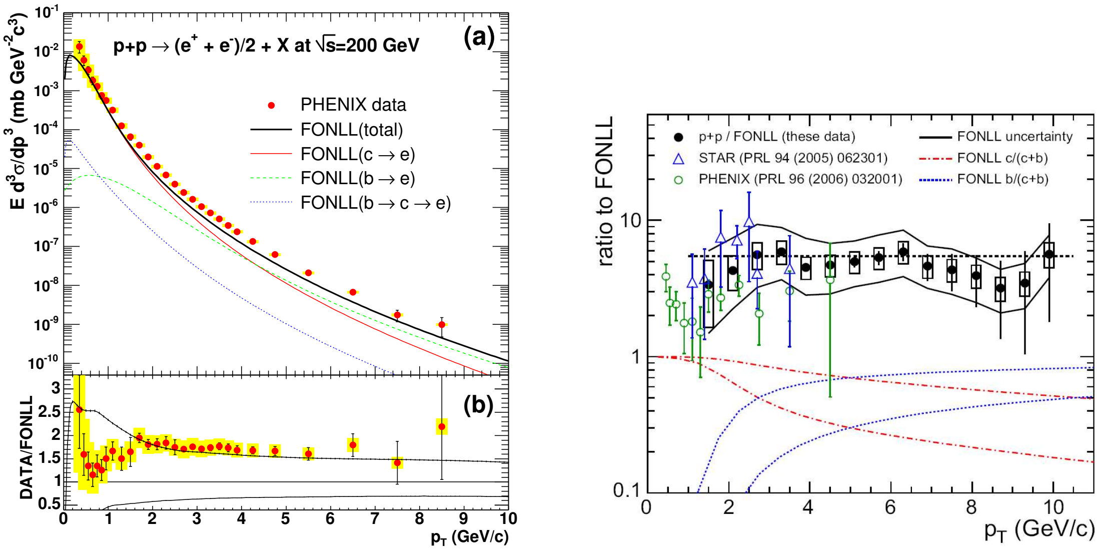

Figure 11. Upper left: PHENIX measurements of the p_T dependence of the semileptonic decay open heavy flavor cross section from 200 GeV pp collisions, compared with FONNL calculations [73]. Lower left: ratio of the data to the FONNL calculation. The dashed lines show the theoretical uncertainty of the calculation. Right: Ratio of STAR open heavy flavor electron cross sections to the same FONNL calculation. The PHENIX data in the right panel are superseded by the more recent, higher statistics data in the left panel.

Fig. 11 shows measurements of the p_T dependence of the cross section for open heavy flavor decays to electrons from 200 GeV pp collisions by PHENIX [73] and STAR [15]. In both cases the ratio of the measured cross sections to a FONNL calculation [77] is shown. The FONNL calculation reproduces the p_T slope of the data in both cases. The magnitude of the calculated cross section is 1.5 times smaller than that of the PHENIX data, just at the limit of the theoretical uncertainty band. But the magnitude of the calculated cross section is smaller than that of the STAR data by a factor of 5.5, which is well outside the theoretical uncertainties of the calculation. The discrepancy of a factor of typically ~ 3.5 between PHENIX and STAR heavy flavor electron cross sections in Fig. 11 is not yet explained.

Unlike J/ψ measurements, the current d+Au and pp open heavy flavor results are not precise enough for any conclusions to be drawn about either shadowing or k_T broadening. Obtaining more precise open heavy flavor baseline results is an important priority for the RHIC program over the next few years.

4.3.2. Heavy ion measurements Both PHENIX and STAR have released striking results on suppression of single electrons from open heavy flavor decays in central Au+Au collisions. PHENIX also has results for the v_2 (elliptic flow parameter) of electrons from open heavy flavor decays

Nuclear modification factors and elliptic flow parameters for electrons from semileptonic decays of open heavy flavor in Au+Au central collisions from PHENIX [16] are shown in Fig. 12. Fig. 13 [15] shows the R_{AA} measurement from STAR for Au+Au and d+Au collisions. The R_{AA} data for Au+Au collisions from the two experiments are in reasonable agreement, and both show very strong suppression in central collisions at high p_T. The suppression factor, R_{AA}, is 0.2-0.3, similar to that seen for light quark hadrons [78].

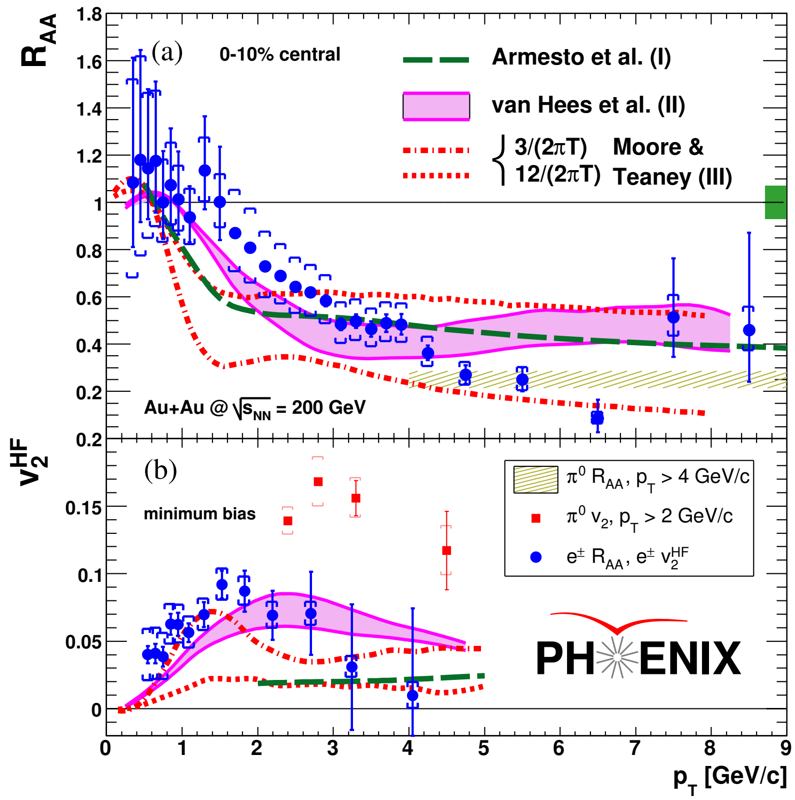

Figure 12. Measurement of non-photonic electron R_{AA} (upper panel) and non-photonic electron v_2 (lower panel) in central Au+Au collisions by PHENIX [16]. The theory curves are discussed in the text.

When comparing the non-photonic electron R_{AA} data to theory, recall that while the electron data contain contributions from both charm and bottom decays, the bottom contribution is expected to dominate for $p_T \sim 4$ GeV/c [3].

The STAR R_{AA} data are compared in Fig. 13 with model calculations. The theory curves are from calculations that were described earlier. Curves I-IV are calculations of the electron spectra from both D and B meson decays incorporating final state energy loss of charm and bottom quarks. Curve I [6] uses DLGV radiative energy loss only, and curve II [33] uses BDMPS radiative energy loss. Both calculations predict much less suppression than observed. Curve III is from a DLGV based calculation including

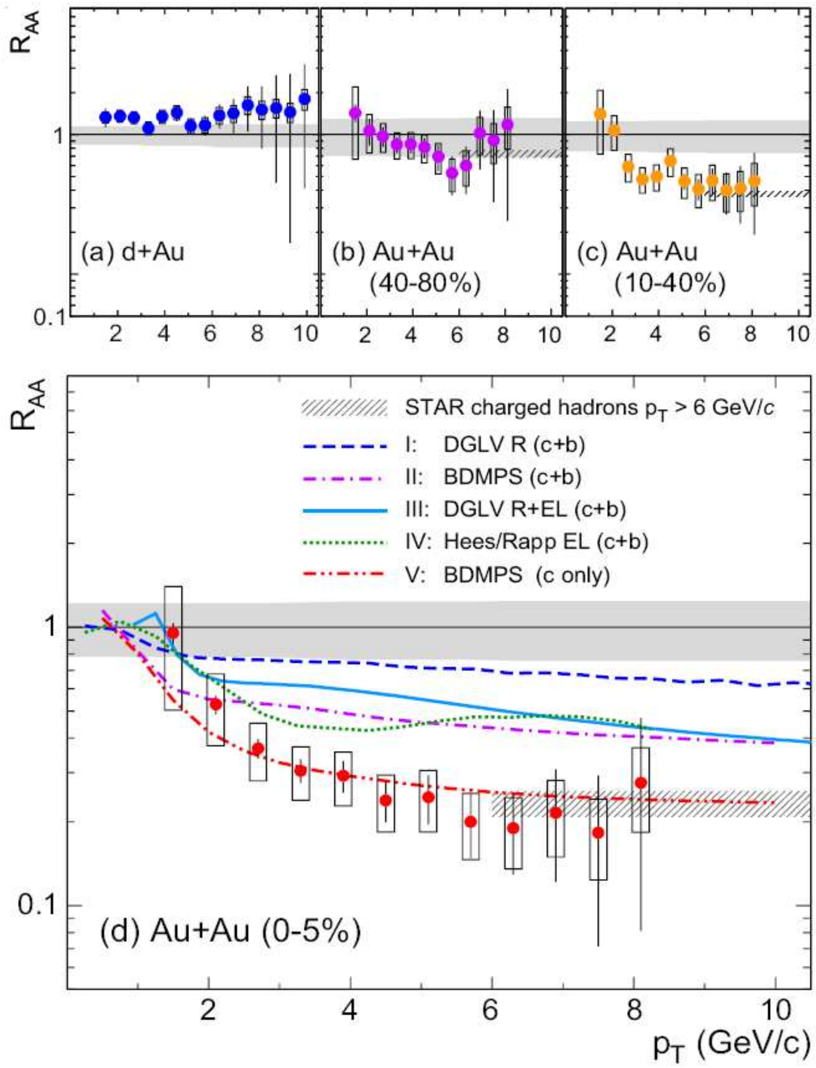

Figure 13. Measurement of non-photonic electron R_{AA} by STAR. [15]. The theory curves are discussed in the text.

both collisional and radiative energy loss [69]. The addition of collisional energy loss produces a substantial increase in suppression over the DGLV based radiative energy loss only calculation leading to curve I, but still underpredicts the suppression seen in the data. Calculation IV is a Langevin based heavy quark transport calculation that includes energy loss due to elastic scattering mediated by resonance excitation [72]. The resonance effects reduce the R_{AA} for charm decay electrons to 0.2, but have a smaller effect on the bottom quark energy loss, which causes the R_{AA} to increase again at higher p_T. Curve V is the same calculation as for curve II, except that only D meson decays are included.

The PHENIX R_{AA} and v_2 data are compared in Fig. 12 with models that calculate both quantities simultaneously. Curves I are from a perturbative QCD calculation with radiative energy loss [33]. It describes the R_{AA} data using a large transport coefficient of $\hat{q} = 14$ GeV/c, which also works well for light hadron suppression. However in this model the v_2 is due only to the path length dependence of energy loss, and the model clearly underpredicts the v_2 data. Curves II are from the Langevin based heavy quark transport calculation [72], including elastic scattering mediated by resonance excitation, that were compared with the STAR data. The best simultaneous description of the R_{AA} and v_2 data is achieved with a small heavy quark relaxation time. Curves III are also from a transport calculation [70] in which the diffusion and drag coefficients are calculated in perturbative QCD. The diffusion coefficients required by the data are small in both cases, implying a ratio of viscosity to entropy that is small enough to be at or near the conjectured quantum bound [16]. This is consistent with estimates obtained from elliptic flow and fluctuation analyses for light quark hadrons [79, 80].

There is considerable interest in the behavior of the non-photonic electron v_2 for $p_T > 2$ GeV/c where the bottom contribution is expected to become important [3]. The PHENIX v_2 results fall toward zero here, consistent with both a larger bottom contribution and a smaller degree of thermalization for higher p_T charm quarks. But, while the PHENIX data have small systematic errors at high p_T, their statistical precision is poor, keeping them from being definitive.

The fact that electrons from charm and bottom decays are not separated in the existing data is a serious limitation. It means that all model calculations must be made with assumptions about the magnitude and p_T dependence of the charm and bottom cross sections. In all of the models the bottom decay component raises the R_{AA} and lowers the v_2, the model results, and thus the conclusions, are sensitive to the accuracy of the charm and bottom distribution predictions. The ways in which this will be addressed in the future program at RHIC are discussed in the next section.

4.4. Proposed open heavy flavor experimental program at RHIC II

Here we focus on the new open heavy flavor physics that becomes available with the combination of the detector upgrades and the RHIC II luminosity upgrade.

With a displaced vertex measurement and RHIC II luminosity, the $B \rightarrow J/\psi$ decay channel can provide a very clean measurement of open bottom production by both PHENIX and STAR (see Tables 2 and 3). The displaced vertex distributions for prompt J/ψ and for $B \rightarrow J/\psi$ decays into the PHENIX muon arms are compared in the left panel of Fig. 14. The yields in Tables 2 and 3 assume a displaced vertex cut of 1 mm. A good measurement of the cross section and R_{AA} vs p_T and y for open bottom production will be possible using $B \rightarrow J/\psi$. Even at RHIC II luminosity, however, the yields are not expected to be large enough to permit a v_2 measurement.

With a displaced vertex measurement and the RHIC II luminosity, separation of the charm and bottom contributions to the semileptonic decay spectra can be done statistically using the different decay lengths for charm and bottom mesons (see the right-hand side of Fig. 14). By analyzing data samples with different decay length cuts,

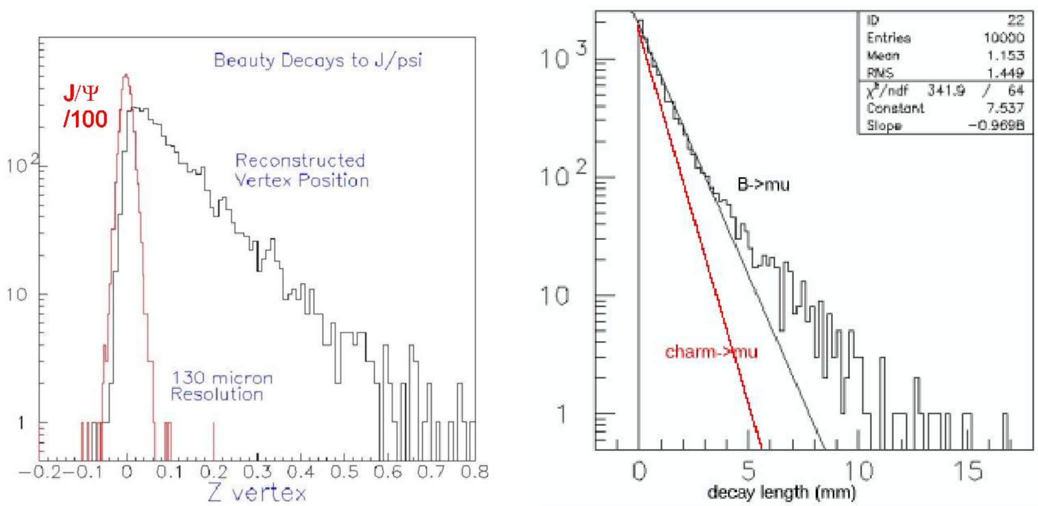

Figure 14. Left: Comparison of prompt J/ψ displaced vertex distribution (in cm) with that from $B \rightarrow J/\psi$ decays. Note that the prompt J/ψ distribution is scaled down by a factor of 100. Right: Decay length distributions (in mm) from simulations for open charm and bottom.

the fraction of the signal due to b quarks can be varied. The addition of a displaced vertex measurement will also reduce the single muon background in the heavy flavor measurement since a 1 cm displaced vertex cut reduces the muon yields from light hadron decays by about one order of magnitude. As a result, separate R_{AA} and v_2 measurements as a function of p_T and y should be possible for both open charm and bottom at RHIC II. Fig. 15 shows estimates [82] of the precision expected for semileptonic charm and bottom decay v_2 measurements at RHIC II in one year.

Tight displaced vertex cuts will also greatly reduce the background for the $D \rightarrow K\pi$ measurement of open charm yields by eliminating most of the prompt hadron tracks from the combinatorial background. The background reduction will result in much improved cross sections and $R_{AA}(p_T)$. Without a trigger for $D \rightarrow K\pi$ decays, however, this measurement will not greatly benefit from the increased luminosity at RHIC II. Therefore it is not clear if a useful v_2 measurement can be expected. The situation will be similar at the LHC.

5. Hidden heavy flavor: quarkonium

In this section we present a more detailed discussion of the theoretical motivation for studying heavy quarkonia in heavy ion collisions. We also summarize the present experimental and theoretical status and describe the proposed RHIC II experimental quarkonia program.

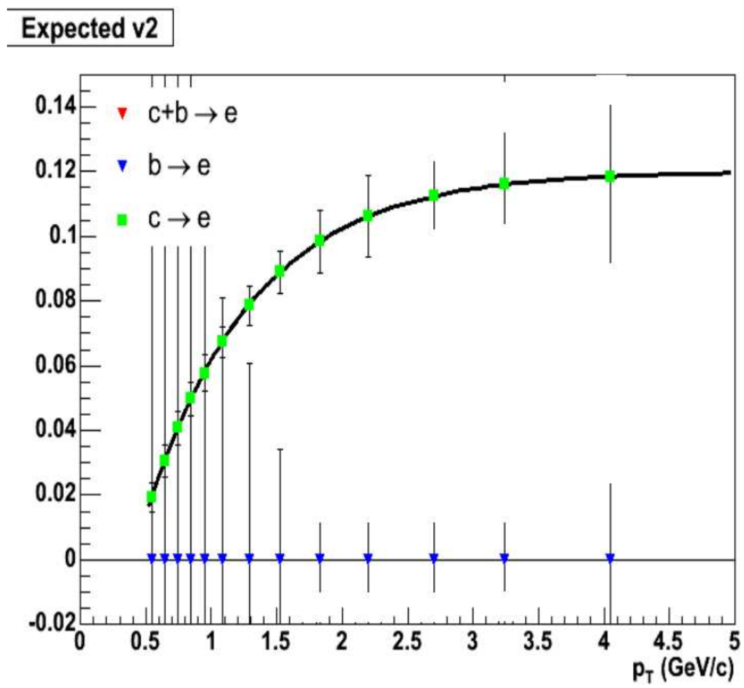

Figure 15. Estimmates [82] of the precision of v_2 measurements for electrons from open charm and bottom decay in one year of heavy ion running at RHIC II. The uncertainties at the lowest p_T for bottom decay are dominated by systematic errors.

5.1. Theoretical results

5.1.1. Cross sections in pp collisions We discuss quarkonium production in the color evaporation model (CEM) which can be used to calculate the total quarkonium cross sections. The CEM was first discussed some time ago [83, 84] and has enjoyed considerable phenomenological success. In the CEM, the quarkonium production cross section is some fraction F_C of all $Q\overline{Q}$ pairs below the $H\overline{H}$ threshold where H is the lowest mass heavy flavor hadron. Thus the CEM cross section is simply the $Q\overline{Q}$ production cross section with a cut on the pair mass but without any constraints on the color or spin of the final state. The produced $Q\overline{Q}$ pair then neutralizes its color by interaction with the collision-induced color field—"color evaporation". The Q and the $\overline{Q}$ either combine with light quarks to produce heavy-flavored hadrons or bind with each other to form quarkonium. The additional energy needed to produce heavy-flavored hadrons when the partonic center of mass energy, $\sqrt{\hat{s}}$, is less than $2m_H$, the heavy hadron threshold, is obtained nonperturbatively from the color field in the interaction region. Thus the yield of all quarkonium states may be only a small fraction of the total $Q\overline{Q}$ cross section below $2m_H$. At leading order, the production cross section of quarkonium state C in an AB collision is

$$\sigma_C^{\rm CEM} = F_C \sum_{i,j} \int_{4m^2}^{4m_H^2} d\hat{s} \int dx_1 dx_2 \; f_i^A(x_1,\mu^2) \; f_j^B(x_2,\mu^2) \; \hat{\sigma}_{ij}(\hat{s}) \; \delta(\hat{s} - x_1 x_2 s) \quad (2)$$

where $\hat{s}$ is the square of the parton-parton center of mass energy, $ij = q\overline{q}$ or gg and $\hat{\sigma}_{ij}(\hat{s})$ is the $ij \to Q\overline{Q}$ subprocess cross section. The total $Q\overline{Q}$ cross section takes $\hat{s} \to s$ in the upper limit of the integral over $\hat{s}$ in Eq. (2).

The fraction F_C must be universal so that, once it is fixed by data, the quarkonium production ratios should be constant as a function of $\sqrt{s}$, y and p_T. The actual value of F_C depends on the heavy quark mass, m, the scale, μ^2, the parton densities, $f_i^A(x, \mu^2)$ and the order of the calculation. It was shown in Ref. [46] that the quarkonium production ratios were indeed constant, as expected by the model.

Of course the leading order calculation in Eq. (2) is insufficient to describe high p_T quarkonium production since the $Q\overline{Q}$ pair p_T is zero at LO. Therefore, the CEM was taken to NLO [46, 85] using the exclusive $Q\overline{Q}$ hadroproduction code of Ref. [86]. At NLO in the CEM, the process $gg \to gQ\overline{Q}$ is included, providing a good description of the quarkonium p_T distributions at the Tevatron [85]. In the exclusive NLO calculation [86], both the Q and $\overline{Q}$ variables are integrated to obtain the pair distributions. Thus, although $\mu \propto m$ in analytic LO calculations, at NLO, $\mu^2 \propto m_T^2 = m_Q^2 + p_T^2$ where p_T is that of the $Q\overline{Q}$ pair, $p_T^2 = 0.5(p_{T_Q}^2 + p_{T_{\overline{Q}}}^2)$.

We use the same parton densities and parameters that agree with the $Q\overline{Q}$ total cross section data, given in Table 6, to determine F_C for J/ψ and Υ production. The fit parameters [87, 88] for the parton densities [89, 90, 91], quark masses and scales are given in Table 6 while the $Q\overline{Q}$ cross sections calculated with these parameters are compared to $pp \to Q\overline{Q}$ and $\pi^- p \to Q\overline{Q}$ data in Fig. 16.

Table 6. Parameters used to obtain the 'best' agreement to the $Q\overline{Q}$ cross sections. The quark mass is given in GeV/c^2. The inclusive J/ψ production fraction, $F_{J/\psi}$, and the inclusive Υ production fraction, F_Υ, obtained from the data are also given.

$c\overline{c}$					$b\overline{b}$				
Label	PDF	m	μ/m_T	$F_{J/\psi}$	Label	PDF	m	μ/m_T	F_Υ
$\psi1$	MRST HO	1.2	2	0.0144	$\Upsilon1$	MRST HO	4.75	1	0.0276
$\psi2$	MRST HO	1.4	1	0.0248	$\Upsilon2$	MRST HO	4.5	2	0.0201
$\psi3$	CTEQ 5M	1.2	2	0.0155	$\Upsilon3$	MRST HO	5.0	0.5	0.0508
$\psi4$	GRV 98 HO	1.3	1	0.0229	$\Upsilon4$	GRV 98 HO	4.75	1	0.0225

We now describe the extraction of F_C for the individual quarkonium states. The J/ψ has been measured in pp and $p + A$ interactions up to $\sqrt{s} = 63$ GeV. The data are of two types: the forward cross section, $\sigma(x_F > 0)$, and the cross section at zero rapidity, $d\sigma/dy|_{y=0}$. All the cross sections are inclusive with feed down from χ_c and ψ' decays. To obtain $F_{J/\psi}$ for inclusive J/ψ production, the normalization of Eq. (2) is obtained from a fit using the $c\overline{c}$ parameters in Table 6. The comparison of $\sigma_{J/\psi}^{\rm CEM}$ to the $x_F > 0$ data for all four fits is shown on the left-hand side of Fig. 17. The ratios of the direct production cross sections to the inclusive J/ψ cross section can be determined from data on inclusive cross section ratios and branching fractions. These direct ratios,

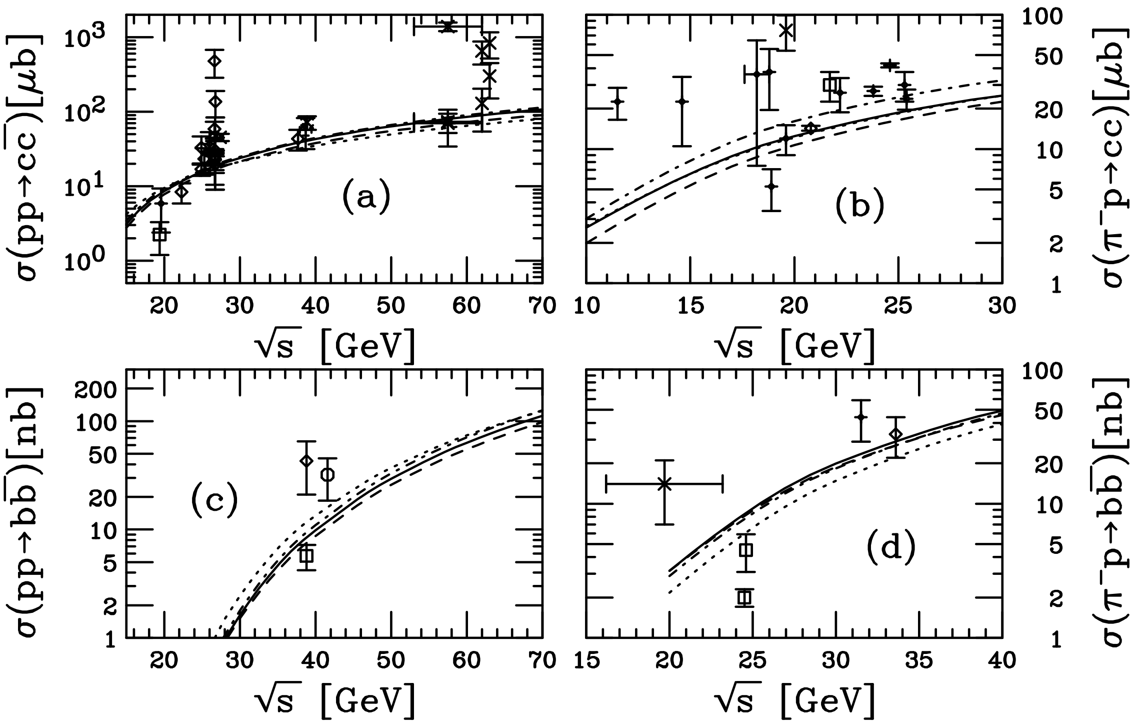

Figure 16. The $c\overline{c}$, (a) and (b), and $b\overline{b}$, (c) and (d), total cross section data in pp and $\pi^- p$ interactions compared to NLO calculations. In (a) and (b), we show $\psi1$ (solid), $\psi2$ (dashed), $\psi3$ (dot-dashed) and $\psi4$ (dotted). In (c) and (d), we show $\Upsilon1$ (solid), $\Upsilon2$ (dashed), $\Upsilon3$ (dot-dashed) and $\Upsilon4$ (dotted).

R_C, given in Table 7, are multiplied by the inclusive fitted $F_{J/\psi}$, also shown in Table 6 to obtain the direct production fractions, $F_C^{\rm dir} = F_{J/\psi} R_C$.

Table 7. Direct quarkonium production ratios, $R_C = \sigma_C^{\rm dir}/\sigma_{C'}^{\rm inc}$ where $C' = J/\psi$ and Υ. From Ref. [92].

	J/ψ	ψ'	χ_{c1}	χ_{c2}	Υ	Υ'	Υ''	$\chi_b(1P)$	$\chi_b(2P)$
R_C	0.62	0.14	0.60	0.99	0.52	0.33	0.20	1.08	0.84

The same procedure, albeit somewhat more complicated due to the larger number of bottomonium states below the $B\overline{B}$ threshold, is followed for bottomonium. For most data below $\sqrt{s} = 100$ GeV, the three bottomonium S states were either not separated or their sum was reported. No x_F-integrated cross sections were available so that the CEM Υ cross section were fittted to the effective lepton pair cross section at $y = 0$ for the three $\Upsilon(nS)$ states. The extracted fit fraction, $F_{\sum\Upsilon}$, combined with $\sigma_\Upsilon^{\rm CEM}$ and compared to the data for all parameter sets in Table 6, is shown on the right-hand side of Fig. 17. Using the individual branching ratios of the Υ, Υ' and Υ'' to lepton pairs and the total cross sections reported by CDF [93], it is possible to extract the inclusive Υ fit fraction, F_Υ, given in Table 6. The direct production ratios obtained in Ref. [31] have been updated in Ref. [92] using recent CDF χ_b data. The resulting direct

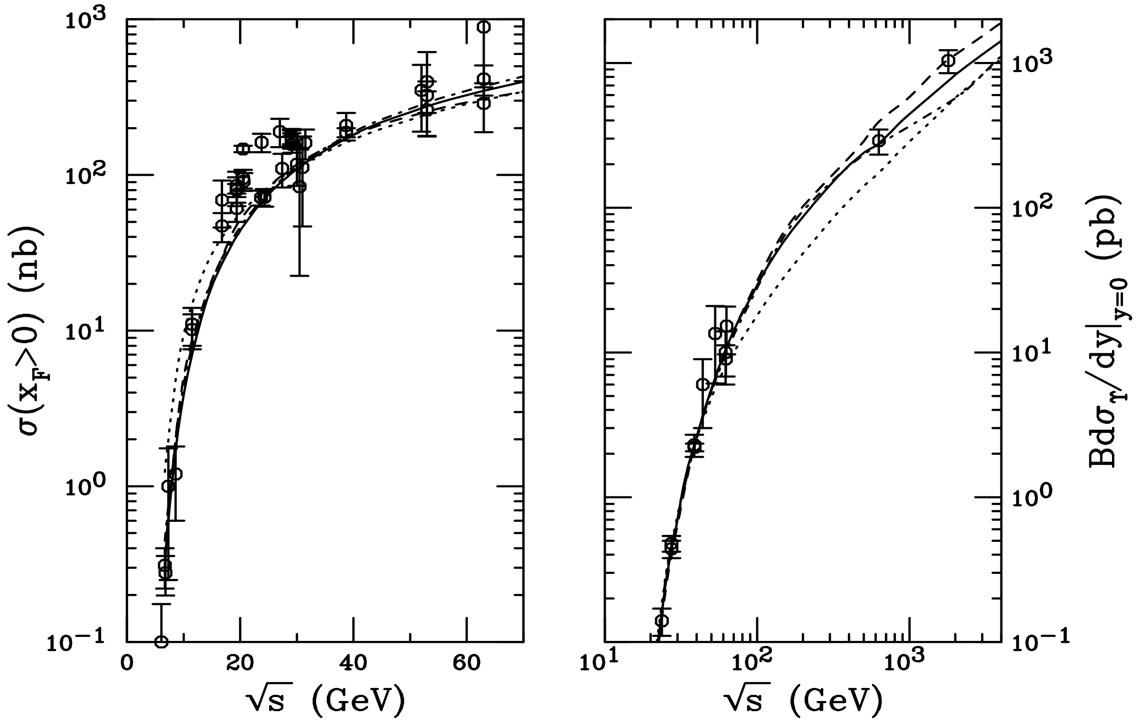

Figure 17. Forward J/ψ (left) and combined $\Upsilon + \Upsilon' + \Upsilon''$ inclusive (right) cross sections calculated to NLO in the CEM. On the left-hand side, we show $\psi1$ (solid), $\psi2$ (dashed), $\psi3$ (dot-dashed) and $\psi4$ (dotted). On the right-hand side, we show $\Upsilon1$ (solid), $\Upsilon2$ (dashed), $\Upsilon3$ (dot-dashed) and $\Upsilon4$ (dotted).

to inclusive Υ ratios, R_C, are also given in Table 7. The sub-threshold $b\overline{b}$ cross section is then multiplied by $F_C^{\rm dir} = F_\Upsilon R_C$ to obtain the direct bottomonium cross sections.

The total cross sections for the charmonium and bottomonium states in pp collisions at $\sqrt{s} = 200$ GeV are shown in Tables 8 and 9 respectively.

Table 8. The charmonium cross sections (in μb) for 200 GeV pp collisions. The inclusive and direct J/ψ cross sections are both given.

Case	$\sigma_{J/\psi}^{\rm inc}$	$\sigma_{J/\psi}^{\rm dir}$	$\sigma_{\chi_{c1}}$	$\sigma_{\chi_{c2}}$	$\sigma_{\psi'}$
$\psi1$	2.35	1.46	1.41	2.33	0.33
$\psi2$	1.76	1.09	1.06	1.74	0.25
$\psi3$	2.84	1.76	1.70	2.81	0.40
$\psi4$	2.10	1.31	1.26	2.08	0.29

The energy dependence shown in Fig. 17 for both states is well reproduced by the NLO CEM. All the fits are equivalent for $\sqrt{s} = 100$ GeV but differ by up to a factor of two at 2 TeV. The high energy Υ data seem to agree best with the energy dependence of $\Upsilon1$ and $\Upsilon2$ although $\Upsilon1$ underestimates the Tevatron result by a factor of ≈ 1.4. A similar check cannot be made for the J/ψ because the high lepton p_T cut excludes J/ψ acceptance for $p_T = 0$ at the Tevatron in Run I.

Table 9. The direct bottomonium cross sections (in nb) for pp collisions at 200 GeV. The production fractions for the total Υ are multiplied by the appropriate ratios determined from data.

Case	$\sigma_{\Upsilon}^{\rm inc}$	$\sigma_{\Upsilon}^{\rm dir}$	$\sigma_{\Upsilon'}$	$\sigma_{\Upsilon''}$	$\sigma_{\chi_b(1P)}$	$\sigma_{\chi_b(2P)}$
Υ1	6.60	3.43	2.18	1.32	7.13	5.54
Υ2	7.54	3.92	2.49	1.51	8.15	6.34
Υ3	5.75	2.99	1.90	1.15	6.21	4.83
Υ4	4.31	2.24	1.42	0.86	4.66	3.62

5.1.2. Cold nuclear matter effects on quarkonium production at RHIC It is essential that the A dependence be understood in cold nuclear matter to set a proper baseline for quarkonium suppression in $A+A$ collisions. The NA50 collaboration has studied the J/ψ A dependence and attributed its behavior to break up by nucleons in the final state, referred to as nuclear absorption. However, the parton distributions are modified in the nucleus relative to free protons. This modification, referred to here as shadowing, is increasingly important at higher energies, as emphasized in Ref. [94]. We now discuss the interplay of shadowing and absorption in d+Au and $A+A$ collisions at RHIC.

Shadowing, the modification of the parton densities in the nucleus with respect to the free nucleon, is taken into account by replacing f_j^p in Eq. (2) by $F_j^A(x,\mu^2,\vec{b},z) = \rho_A(\vec{b},z)S^j(A,x,\mu^2,\vec{b},z)f_j^p(x,\mu^2)$ and adding integrals over the spatial coordinates. Here S^j is the shadowing parameterization. The density distribution of the deuteron is also included in these calculations but the small effects of shadowing in deuterium are ignored. The PHENIX J/ψ d+Au data as a function of rapidity show a dependence consistent with nuclear shadowing plus a small absorption cross section of 1-3 mb. The J/ψ production cross section is calculated in the CEM using Eq. (2) with the same mass and scale as in $c\overline{c}$ production. The calculations of the d+Au/pp and $A+A/pp$ ratios are done at LO to simplify the calculations since the LO and NLO ratios are equivalent [4].

To implement nuclear absorption of the J/ψ in d+Au collisions, the d+N production cross section is weighted by the survival probability, $S^{\rm abs}$ [95]:

$$S^{\rm abs}(\vec{b},z) = \exp\left\{-\int_z^\infty dz' \rho_A(\vec{b},z')\sigma_{\rm abs}(z'-z)\right\} \tag{3}$$

where z is the longitudinal production point and z' is the point at which the state is absorbed. The nucleon absorption cross section, $\sigma_{\rm abs}$, typically depends on where the state is produced in the medium and how far it travels through nuclear matter. If absorption alone is active, *i.e.* no shadowing so that $S^j \equiv 1$, then an effective minimum bias A dependence is obtained after integrating $S^{\rm abs}$ over the spatial coordinates. If $S^{\rm abs} = 1$ also, $\sigma_{{\rm d}A} = 2A\sigma_{pN}$. When $S^{\rm abs} \neq 1$, $\sigma_{{\rm d}A} = 2A^\alpha\sigma_{pN}$ where, if $\sigma_{\rm abs}$ is a constant, independent of the production mechanism for a nucleus of $\rho_A = \rho_0\theta(R_A - b)$, $\alpha = 1 - 9\sigma_{\rm abs}/(16\pi r_0^2)$, where $r_0 = 1.2$ fm. The contribution to the full A dependence of α from absorption alone is only constant if $\sigma_{\rm abs}$ is constant and independent of the production mechanism [95]. The observed J/ψ yield includes feed down from χ_c and ψ' decays, giving

$$S^{\rm abs}_{J/\psi}(b,z) = 0.58 S^{\rm abs}_{J/\psi,\,{\rm dir}}(b,z) + 0.3 S^{\rm abs}_{\chi_c}(b,z) + 0.12 S^{\rm abs}_{\psi'}(b,z) \ . \tag{4}$$

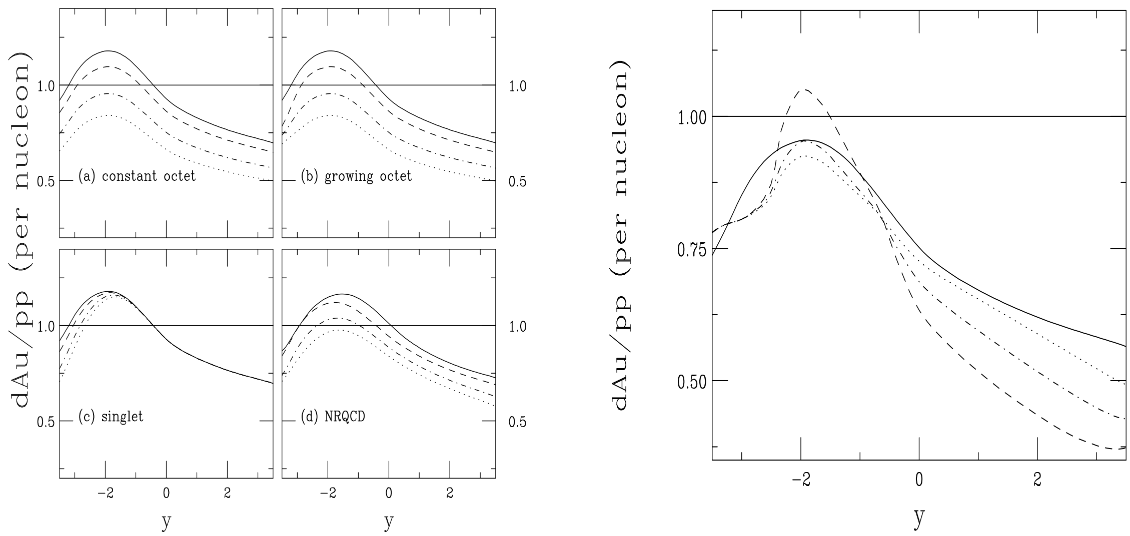

Figure 18. Left-hand side: The J/ψ d+Au/pp ratio with EKS98 at 200 GeV as a function of rapidity for (a) constant octet, (b) growing octet, (c) singlet, all calculated in the CEM and (d) NRQCD. For (a)-(c), the curves are no absorption (solid), $\sigma_{\rm abs} = 1$ (dashed), 3 (dot-dashed) and 5 mb (dotted). For (d), we show no absorption (solid), 1 mb octet/1 mb singlet (dashed), 3 mb octet/3 mb singlet (dot-dashed), and 5 mb octet/3 mb singlet (dotted). Right-hand side: The J/ψ d+Au/pp ratio at 200 GeV for a growing octet with $\sigma_{\rm abs} = 3$ mb is compared for four shadowing parameterizations. We show the EKS98 (solid), FGSo (dashed), FGSh (dot-dashed) and FGSl (dotted) results as a function of rapidity.

The J/ψ may be produced as a color singlet, a color octet or in a combination of the two. In color singlet production, the final state absorption cross section depends on the size of the $c\overline{c}$ pair as it traverses the nucleus, allowing absorption to be effective only while the cross section is growing toward its asymptotic size inside the target. On the other hand, if the $c\overline{c}$ is only produced as a color octet, hadronization will occur only after the pair has traversed the target except at very backward rapidity. We have considered a constant octet cross section, as well as one that reverts to a color singlet at backward rapidities. For singlets, $S^{\rm abs}_{J/\psi,\,{\rm dir}} \neq S^{\rm abs}_{\chi_c} \neq S^{\rm abs}_{\psi'}$ but, with octets, one assumes that $S^{\rm abs}_{J/\psi,\,{\rm dir}} = S^{\rm abs}_{\chi_c} = S^{\rm abs}_{\psi'}$. As can be seen in Fig. 18, the difference between the constant and growing octet assumptions is quite small at large $\sqrt{s_{_{NN}}}$ with only a small singlet effect at $y < -2$. Singlet absorption is also important only at similar rapidities and is otherwise not different from shadowing alone. Finally, we have also considered a combination of octet and singlet absorption in the context of the NRQCD approach, see Ref. [95] for more details. The combination of nonperturbative singlet and octet parameters changes the shape of the shadowing ratio slightly. Including the singlet

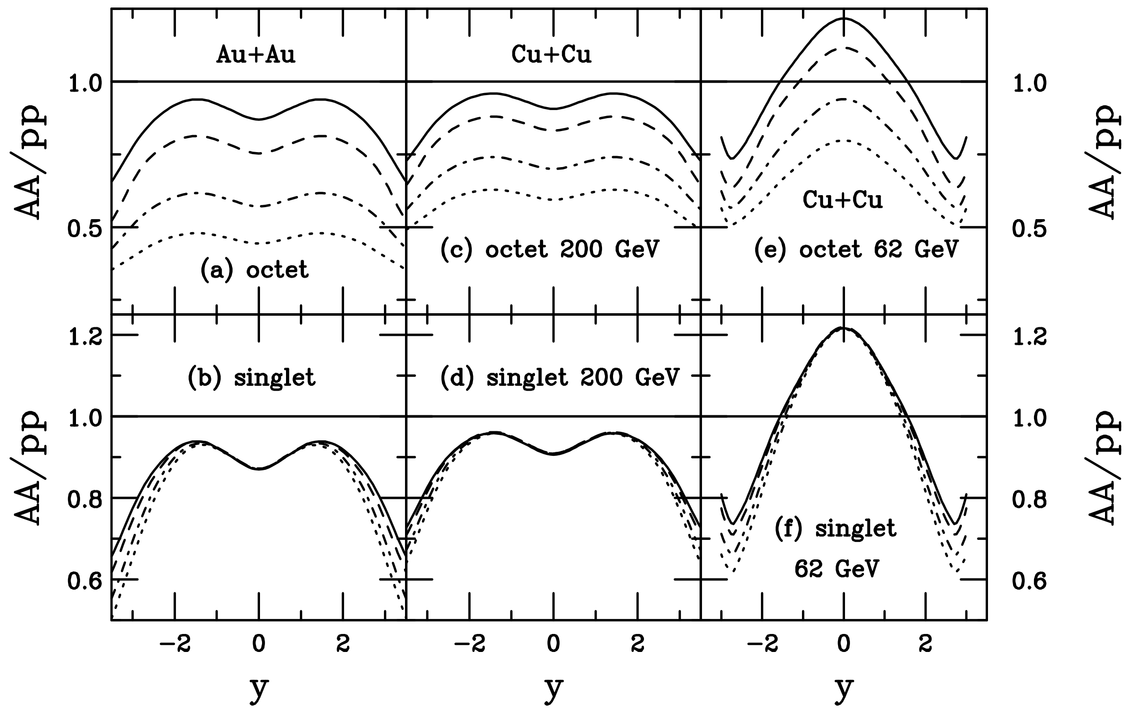

Figure 19. The AA/pp ratio with the EKS98 parameterization as a function of y for octet (upper) and singlet (lower) absorption. In (a) and (b) we show the Au+Au results at 200 GeV while the Cu+Cu results are shown at 200 GeV (c) and (d) as well as at 62 GeV (e) and (f). The curves are $\sigma_{\rm abs} = 0$ (solid), 1 (dashed), 3 (dot-dashed) and 5 mb (dotted).

contribution weakens the effective absorption. The results are shown integrated over impact parameter. The calculations use the EKS98 shadowing parameterization [96] since it gives good agreement with the trend of the PHENIX data. For results with other shadowing parameterizations, see Refs. [4, 5].

Several values of the asymptotic absorption cross section, $\sigma_{\rm abs} = 1$, 3 and 5 mb, corresponding to $\alpha = 0.98$, 0.95 and 0.92 respectively using Eqs. (3) and (4), are shown in Figs. 18 and 19 for d+Au and $A + A$ collisions respectively. These values of $\sigma_{\rm abs}$ are somewhat smaller than those obtained for the sharp sphere approximation. The diffuse surface of a real nucleus and the longer range of the density distribution result in a smaller value of $\sigma_{\rm abs}$ than a spherical nucleus. As will be seen later, there is good agreement with the trend of the PHENIX data [97] for $\sigma_{\rm abs} = 0 - 3$ mb. Work is in progress to quantify the shadowing parameterization and absorption cross section more precisely [98].

The current RHIC data are not sufficiently precise to distinguish between J/ψ production and absorption in the CEM relative to that in the NRQCD approach. However, a measurement of the χ_c A dependence may be able to clarify the situation [95]. In the CEM, the J/ψ and χ_c distributions differ only in the value of F_C. In the NRQCD approach, the J/ψ is produced primarily in a color octet state while the χ_c is produced as a color singlet state. Thus while the production of both states would exhibit the same shadowing effect, a difference in the J/ψ and χ_c d+Au/pp ratios due to octet relative to singlet absorption may be measurable.

We now turn to the centrality dependence of J/ψ production in d+Au and $A+A$ collisions. In central collisions, inhomogeneous (spatially dependent) shadowing is stronger than the homogeneous (minimum bias) result. The stronger the homogeneous shadowing, the larger the inhomogeneity. In peripheral collisions, inhomogeneous effects are weaker than the homogeneous results but some shadowing is still present. Shadowing persists in peripheral collisions in part because the density in a heavy nucleus is large and approximately constant except close to the surface and because the deuteron wave function has a long tail. Absorption is also expected to be stronger in central collisions.

To study the centrality dependence of shadowing and absorption, the d+Au/pp and $A+A/pp$ ratios are presented as a function of $N_{\rm coll}$,

$$N_{\rm coll}(b) = \sigma_{NN}^{\rm in} \int d^2s T_A(s) T_B(|\vec{b} - \vec{s}|) \ ,$$

where T_A and T_B are the nuclear thickness functions and the inelastic nucleon-nucleon cross section, $\sigma_{NN}^{\rm in}$, is 42 mb at 200 GeV. In Figs. 20 and 21, the $N_{\rm coll}$ dependence is shown for several representative rapidities, $y = -2$, 0 and 2 for RHIC. The inhomogeneous shadowing parameterization is chosen to be proportional to the path length of the parton through the nucleus [94]. For more results, see Refs. [4, 5].

The dependence of the RHIC ratios on $N_{\rm coll}$ is almost linear, as seen in Figs. 20 and 21. The results are not shown for $N_{\rm coll} < 1$. The weakest $N_{\rm coll}$ dependence occurs in the antishadowing region, illustrated by the $y = -2$ result (dot-dashed curve). The overall dependence on $N_{\rm coll}$ is stronger than that obtained from shadowing alone, described in Ref. [94], where inhomogeneous shadowing effects depend strongly on the amount of homogeneous shadowing. Relatively large effects at low x are accompanied by the strongest impact parameter, b, dependence. In the transition region around mid rapidity at RHIC, the b dependence of the ratio d+Au/pp due to shadowing is nearly negligible and almost all of the $N_{\rm coll}$ dependence at $y \sim 0$ can be attributed to absorption. The $y = -2$ results for color singlet production and absorption, in the antishadowing region, are fairly independent of $N_{\rm coll}$.

5.1.3. Models of quarkonium production in heavy ion collisions *In-medium properties of quarkonium from lattice QCD:*

Properties of heavy quarks have been used to characterize "thermal properties of the QCD vacuum" ever since the first lattice calculations at non-zero temperature [99]. Modifications of the interactions between heavy, static quarks in a thermal heat bath are clearly reflected by changes of the free energy which, in the zero temperature limit, reduces to the heavy quark potential [100]. To use this information to analyze thermal modifications of quarkonia requires an intermediate, phenomenological step: the construction of a temperature dependent effective potential which then can be used in a nonrelativistic Schrödinger equation [101, 102, 103] or a more refined coupled-channel analysis [104, 105]. Quite generically, the potential model analyses suggest a sequential

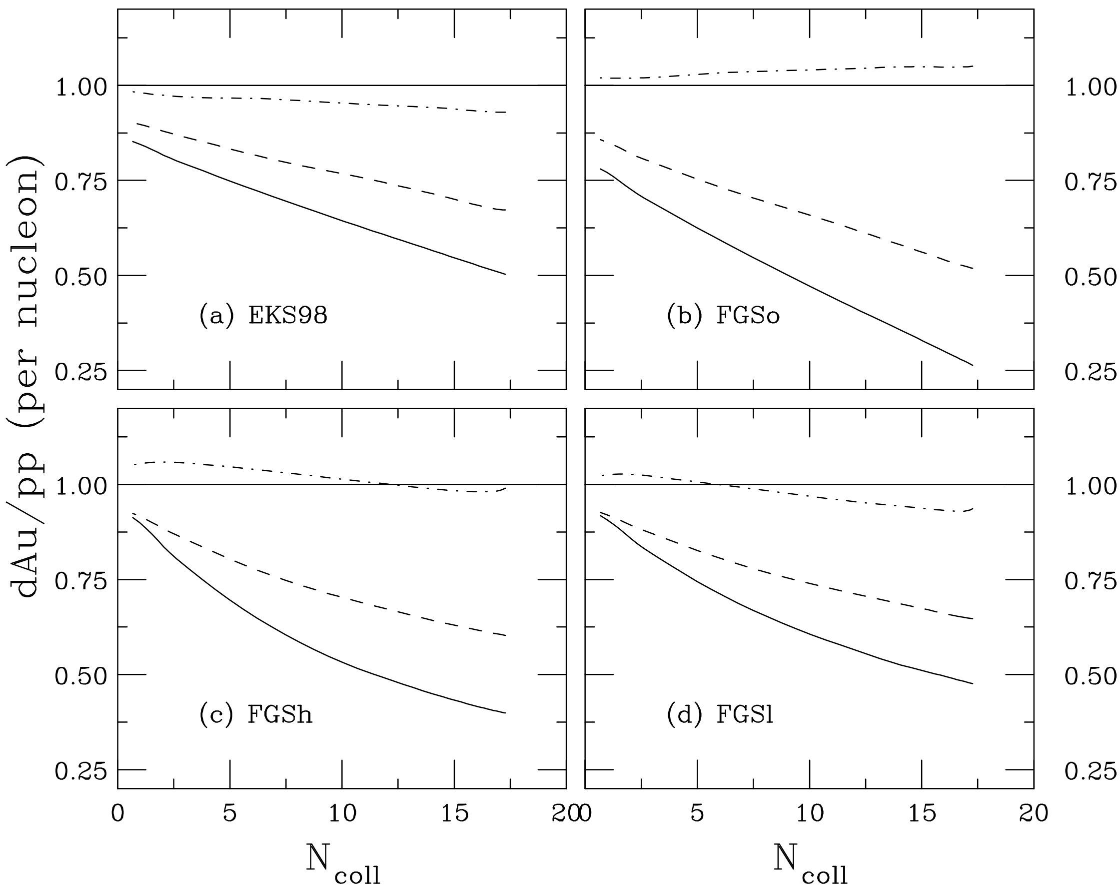

Figure 20. The ratio d+Au/pp as a function of $N_{\rm coll}$ for the EKS98 (a), FGSo (b), FGSh (c) and FGSl (d) shadowing parameterizations. The calculations with EKS98 and FGSo use the inhomogeneous path length parameterization while that obtained by FGS is used with FGSh and FGSl. Results are given for $y = -2$ (dot-dashed), $y = 0$ (dashed) and $y = 2$ (solid) at 200 GeV for a growing octet with $\sigma_{\rm abs} = 3$ mb.

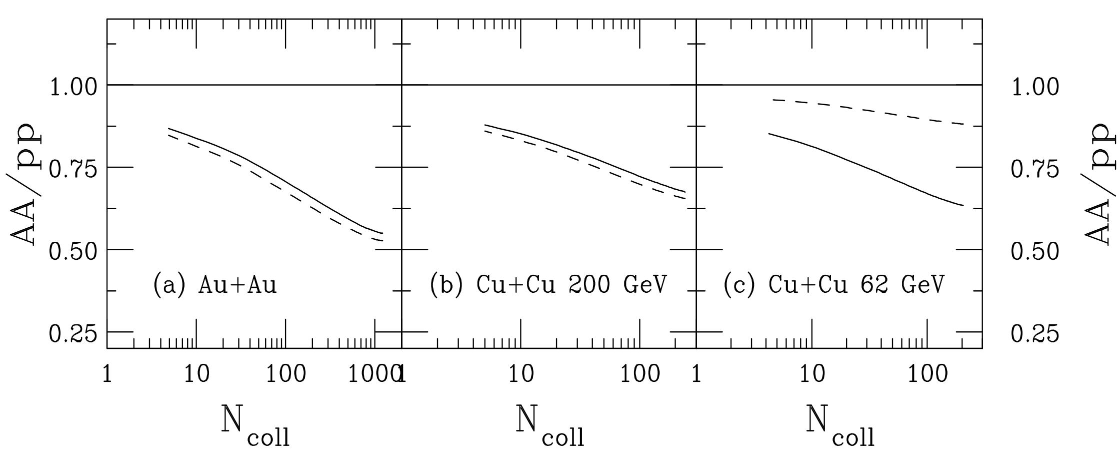

Figure 21. The ratio AA/pp as a function of $N_{\rm coll}$ for a 3 mb octet absorption cross section and the EKS98 parameterization at $y = 0$ (dashed) and $y = 2$ (solid) for Au+Au at 200 GeV (a) and Cu+Cu at 200 GeV (b) and 62 GeV (c).

suppression pattern where heavy quark bound states dissociate at temperatures at which their bound state radii become comparable to the Debye screening radius, illustrated in Fig. 22. Table 10 shows quarkonium dissociation temperatures from Ref. [106].

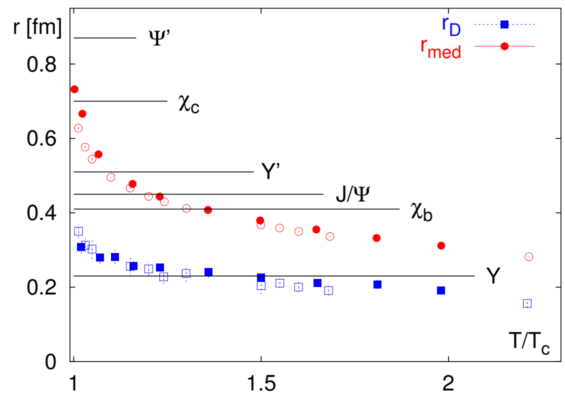

Figure 22. Mean squared charge radii of some charmonium and bottomonium states compared to the Debye screening radius, $r_D \equiv 1/m_D$ and a related scale, $r_{\rm med}$, an estimate of the distance beyond which the force between a static $Q\overline{Q}$ pair is strongly modified by temperature effects [107]. Open (closed) symbols correspond to SU(3) (2-flavor QCD) calculations [100].

Table 10. Quarkonium dissociation temperatures [106], illustrating the effects of binding energy on the dissociation temperature.

State	$J/\psi(1S)$	$\chi_c(1P)$	$\psi'(2S)$	$\Upsilon(1S)$	$\chi_b(1P)$	$\Upsilon(2S)$	$\chi_b(2P)$	$\Upsilon(3S)$
T_d/T_c	2.10	1.16	1.12	> 4.10	< 1.76	1.60	1.19	1.17

More recently, the calculation of thermal hadron correlation functions and their spectral analysis [108] eliminated some of the ambiguities inherent in the potential model approach. The spectral analysis, at least in principle, provides an ab-initio approach to the calculation of in-medium properties of heavy quark bound states. Its predictive power is reduced only by the application of statistical tools like the Maximum Entropy Method (MEM) which, however, can be steadily improved with further improvement of the available computing resources and numerical techniques. Predictions based on potential model calculations as well as the spectral analysis have been reviewed in recent studies that have been performed to analyze prospects for quarkonium studies at the LHC [41, 109]. In the following, the analysis of thermal hadron correlation functions and the spectral functions extracted from them are discussed.

The finite temperature, Euclidean time correlation functions

$$G_H(\tau,\vec{r},T) = \langle J_H(\tau,\vec{r}) J_H^\dagger(0,\vec{0})\rangle \qquad (5)$$

of hadronic currents, $J_H = \bar{q}(\tau,\vec{r})\Gamma_H q(\tau,\vec{r})$, where Γ_H denotes a suitable product of gamma matrices that projects onto the appropriate quantum numbers H, are directly

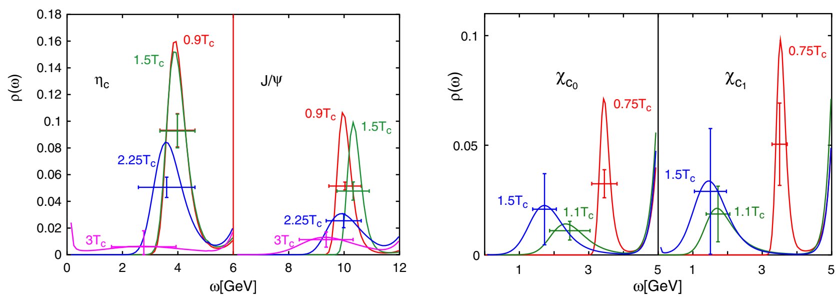

Figure 23. Spectral functions of η_c, J/ψ (left) and and χ_{c0}, χ_{c1} (right) at various temperatures below and above T_c. The vertical bars give the error on the average value of the spectral function in the bin indicated by the horizontal bars.

related to spectral functions, $\sigma_H(\omega, T)$. These spectral functions encompass all the information about thermal modifications of the hadron spectrum in channel H, so that

$$G_H(\tau,\vec{r},T) = \int_0^\infty d\omega \; \frac{d^3\vec{p}}{(2\pi)^3} \sigma_H(\omega,\vec{p},T) \; \mathrm{e}^{i\vec{p}\cdot\vec{r}} \frac{\cosh(\omega(\tau-1/2T))}{\sinh(\omega/2T)} \quad , \tag{6}$$

are directly related to experimental observables. In particular, the spectral function in the vector channel, $\sigma_V(\omega,\vec{p},T)$, is directly related to the differential cross section for thermal dilepton production,

$$\frac{dW}{d\omega d^3p} = \frac{5\alpha^2}{27\pi^2} \frac{\sigma_V(\omega,\vec{p},T)}{\omega^2(\mathrm{e}^{\omega/T}-1)} \quad . \tag{7}$$

Note that the rates obtained using this method do not include any contributions arising from the feed down of other channels into the vector channel [92, 110].

Some generic aspects of the influence of a thermal medium on states with different quantum numbers can already be deduced from the temperature dependence of the thermal correlation functions themselves and does not require the additional step of applying the MEM analysis which, after all, is based on probabilistic assumptions. Such comparisons show that zero-momentum, thermal hadron correlation functions in the ground state channels, *i.e.* the vector (J/ψ, Υ) and pseudoscalar (η_c, η_b) channels show only little modification in a thermal medium up to temperatures $T \gtrsim 1.5\ T_c$. Correlation functions corresponding to radially excited charmonium states (χ_c), however, are modified strongly already close to or at T_c.

These generic features are reflected by the spectral functions. Although results from different groups currently still differ in details, there are some general trends. The J/ψ and η_c remain unaffected by the thermal medium up to $T = 1.5\ T_c$, shown on the left-hand side of Fig. 23. At higher temperatures it is unclear whether the J/ψ already disappears at $\simeq 1.9\ T_c$ [111] or persists as a strongly modified resonance up to $2.25\ T_c$ [24]. The χ_{c0} and χ_{c1} both disappear at $T \lesssim 1.1\ T_c$, see the right-hand side of Fig. 23. Finite momentum J/ψ states show statistically significant but still small modifications for $T \lesssim 1.5\ T_c$ [112] due to collisional broadening by higher momentum gluons seen by bound states moving relative to the heat bath, see Fig. 24 [113]. Strong

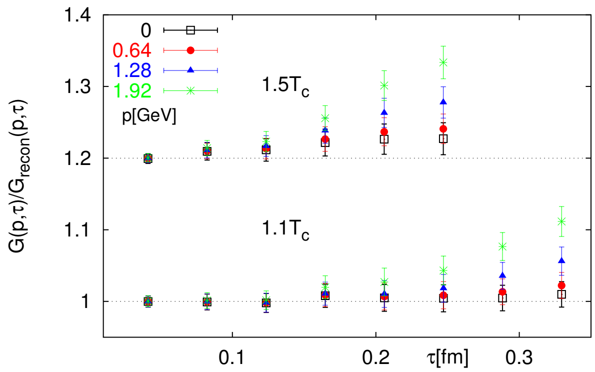

Figure 24. The ratio of pseudoscalar correlation functions at non-zero momentum above and below T_c [112]. Deviations from the horizontal dotted lines for increasing p indicate stronger temperature-dependent modifications of the spectral functions.

J/ψ binding above T_c also is supported by the analysis of spatial correlations [114] and the observed insensitivity of the thermal vector and pseudoscalar correlation functions to spatial boundary conditions [115].

Bottomonium studies are considerably more difficult since a larger lattice cut off is required to properly resolve these states, particularly for temperatures well above 2 T_c where the Υ states are expected to be dissolved. First exploratory finite temperature results on bottomonium have been reported for temperatures up to $\sim 1.5\ T_c$. At this temperature, no thermal modifications of the Υ and η_b have been observed, as expected. The χ_b correlation functions are, however, modified at $T \sim 1.5\ T_c$, similar to the scalar charmonium case at $T \simeq 1.1\ T_c$. To firmly establish the onset of medium modifications in bottomonium states, however, requires further refined studies of the bottomonium system at lower and higher temperatures.

Dynamical Coalescence:

The production of multiple $c\overline{c}$ pairs in a single collision introduces a new charmonium formation mechanism [18]. In-medium charmonium formation utilizes a c and a $\overline{c}$ quark from independently produced $c\overline{c}$ pairs to form a J/ψ.

In the plasma phase, there are two basic approaches: statistical and dynamical coalescence. Both these approaches depend on being able to measure the quarkonium rate relative to total $Q\overline{Q}$ production. The first calculations in the statistical approach assumed an equilibrated fireball in a grand canonical ensemble [26, 27]. This approach could be reasonable at the high energies of the LHC, where the number of produced $c\overline{c}$ pairs is large. But, at lower energies, charm conservation is required since a $c\overline{c}$ pair is not produced in every event. More recent calculations assumed a canonical ensemble only for charm production [116, 117, 118]. Dynamical coalescence models assume that some of the produced $Q\overline{Q}$ pairs can also form quarkonium which would not otherwise do so. This coalescence can take place in the QGP [18, 38] or at hadronization [28].

The model includes the rapidity differences, $|\Delta y|$, between the Q and $\overline{Q}$ and shows that the larger the rapidity difference, the smaller the enhancement. The impact parameter dependence of the statistical and dynamical coalescence models is quite different. Statistical coalescence gives the largest enhancement in peripheral collisions where the volume of the plasma is small, giving only a minor enhancement in central collisions. Dynamical coalescence produces a larger enhancement in central collisions where the number of $Q\overline{Q}$ pairs per event is greatest but still produces a significant effect in peripheral collisions [120].

Much smaller enhancements are predicted for secondary quarkonium production in the hadron gas, particularly for the J/ψ where the additional production is either small (20 - 60%) [29] or about a factor of two [30] at LHC energies and smaller still for RHIC. Larger enhancements may be expected for the ψ' [29]. The predictions depend strongly on the $J/\psi + \pi(\rho)$ cross sections, typically not more than 1-2 mb [121].

Secondary production will be at lower center of mass energies than the initial nucleon-nucleon collisions. Thus the production kinematics will be different, leading to narrower rapidity and p_T distributions. Secondary quarkonium may be separated from primary quarkonium, subject to suppression, by appropriate kinematic cuts. Such cuts are also useful for separating initial J/ψ's from those produced in B meson decays.

These secondary production models are already testable at RHIC where enhancements of factors of 2-3 are expected from coalescence [18, 118]. Hard scatterings of produced particles is related to the idea of crosstalk between unrelated interactions [122]. Important crosstalk effects were predicted in e^+e^- collisions at LEP [122] but were not observed. If secondary quarkonium production is found, it would indicate the relevance of such effects.

Predictions of J/ψ production by this dynamical coalescence suffer from substantial uncertainties due to the dependence on the charm quark distributions in the medium. In fact, it possible to turn this uncertainty into an advantage and probe the medium properties using the observed J/ψ momentum distributions. Two extremes can be considered [17]. If the charm quark distributions in the medium are identical to those of the initial production process, the interactions of charm quarks with the medium would be very weak. In this case, both the J/ψ rapidity and p_T distributions will be narrower than if no plasma is formed simply because the center of mass energy of secondary J/ψ production is lower than that of the initial nucleon-nucleon interactions. The lower energy results in a reduced $\langle p_T^2 \rangle$ and a narrower rapidity distribution. Thus, instead of the transverse momentum broadening expected from initial-state multiple scattering going from pp to $p + A$ to $A + A$, the average p_T^2 in $A + A$ would no longer exhibit the monotonic increase seen in pp and $p + A$ interactions for increasing A. On the other hand, if the charm quarks are assumed to be in thermal equilibrium with the surrounding medium, the charm interaction with the medium would be very strong. Any J/ψ's produced from thermalized charm quarks flowing with the medium would have a p_T distribution with a slope characteristic of the temperature of the system at the time they were formed, resulting in considerably narrower rapidity and p_T distributions.

In either case, the effect would be largest in central collisions, reverting to "normal" broadening in peripheral collisions where on the order of one or fewer $c\overline{c}$ pairs will be produced since the number of $c\overline{c}$ pairs scales approximately with the number of collisions.

In order to extract the medium properties from secondary J/ψ production, systematic studies of J/ψ production in pp, $p+A$ and $A+A$ interactions are necessary. The pp data set the intrinsic transverse momentum scale for a particular energy while the $p+A$ results determine the level of broadening due to cold nuclear matter effects which would then apply to $A+A$ interactions.

Models of regeneration, of course, also include J/ψ suppression. In addition to the screening effects discussed previously, the J/ψ can scatter with quarks and gluons in the plasma which may break it up more effectively than screening effects alone, especially if temperatures significantly above T_c are needed for screening to dissociate the directly produced J/ψ, as discussed in Ref. [28]. At low temperatures, relevant for SPS energies, $gJ/\psi \to c\overline{c}$ is effective for J/ψ breakup by a thermal gluon. However, at higher temperatures where the J/ψ should be more loosely bound, inelastic parton scattering, $g(q,\overline{q})J/\psi \to g(q,\overline{q})c\overline{c}$, calculated using the leading order matrix elements for gc and gq scattering, is more effective.

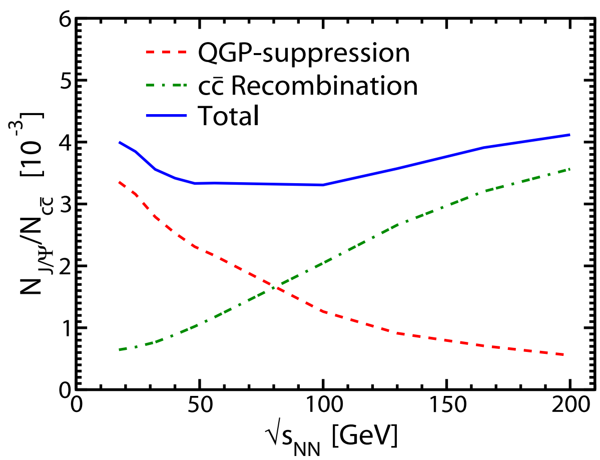

Figure 25. Excitation function of the ratio of produced J/ψ to the number of $c\overline{c}$ pairs in central heavy-ion collisions for $N_{\rm part} = 360$ [123].

The relative importance of J/ψ suppression and regeneration will change as a function of energy, as shown in Fig. 25 for central collisions of heavy nuclei, $N_{\rm part} = 360$, from Ref. [123]. The J/ψ yield is dominated by primordial production at SPS energy, and dominated by regeneration at RHIC full energy.

5.2. Status of Quarkonium Physics at the CERN/SPS

The prospects of a "clean" QGP signature, destruction of the J/ψ by color screening, was discussed in the landmark paper by Matsui and Satz in 1986 [22]. This triggered an extensive experimental program at the CERN/SPS. HELIOS-III [124] and NA38 [125] (subsequently NA50 [126] and currently NA60 [127]) conducted detailed measurements of the dimuon invariant mass spectrum around mid rapidity. Despite early enthusiasm and enormous statistics (see Fig. 26) the picture that evolved is still rather ambiguous. The SPS measurements must also be understood in light of the many results on quarkonium production in $p + A$ collisions from fixed target experiments. The status of the SPS program is summarized in this section.

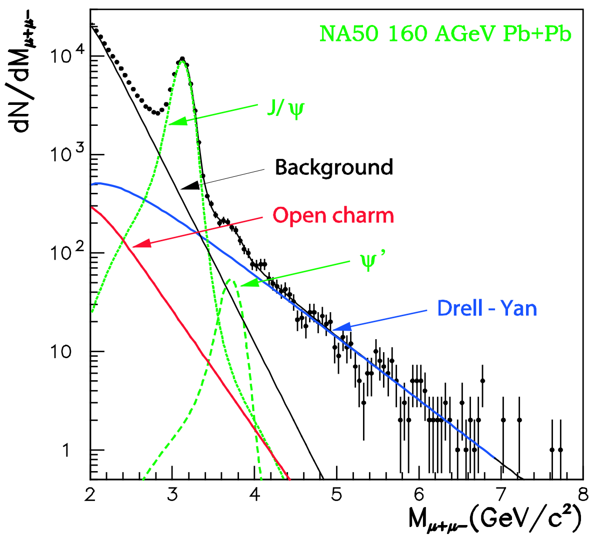

Figure 26. Dimuon invariant mass spectrum from 158 AGeV Pb+Pb collisions at NA50 [126].

Feed down contributions (see Fig. 27) from higher charmonium states, $\chi_c \rightarrow J/\psi\gamma$ ($\sim$ 30%) and $\psi' \rightarrow J/\psi\pi\pi$ ($\sim$ 10%), are important [128, 129]. The χ_c has not yet been measured by the heavy ion detectors at the SPS, although it has been seen in other experiments there. These measurements are extremely difficult and the large scatter of available data depicted in Fig. 28 indicates that better measurements are desperately needed. The NA60 experiment is planning to conduct this analysis, although the feasibility with the present data sets still has to be verified.

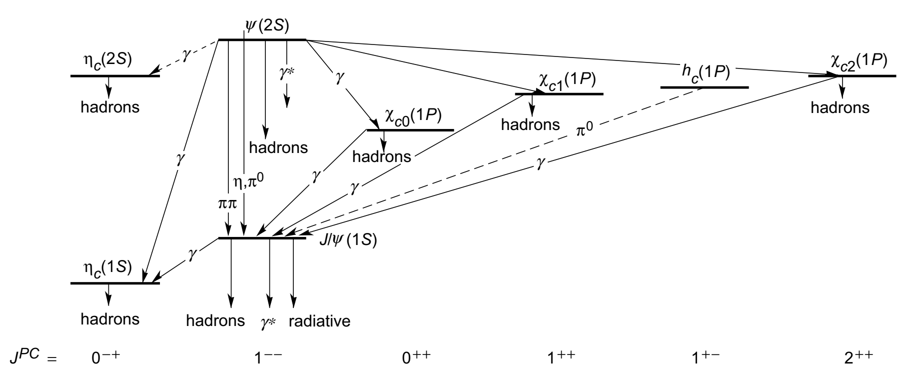

Figure 27. Charmonium mass levels and spin states. Common feed down channels are indicated.

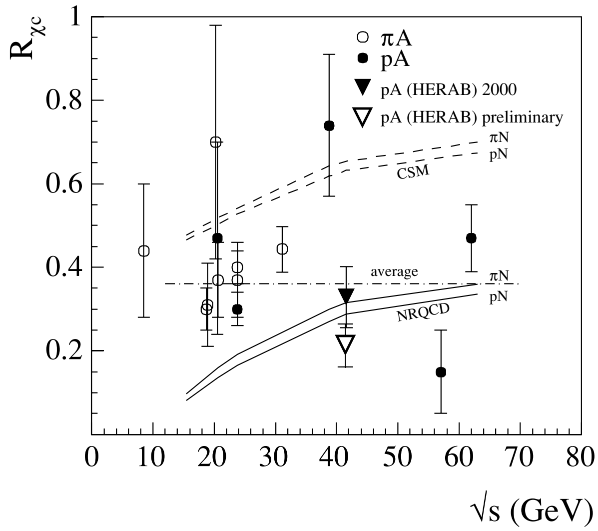

Figure 28. The fraction, R_{χ_c}, of observed J/ψ's originating from radiative $\chi_{c1,2} \rightarrow J/\psi\gamma$ decays as a function of energy for proton and pion beams [128].

The J/ψ and ψ' have substantial absorption cross sections in normal nuclear matter, 4.2 and 9.6 mb respectively at midrapidity, determined from fits to $p + A$ data (see Fig. 29) [130]. Studies of the A dependence were made at Fermilab over a large x_F range, but with higher $\sqrt{s}$ [131]. A very strong x_F dependence was observed for $x_F > 0.2$, as depicted in Fig. 30. Effects like shadowing, absorption and energy loss play varying roles at different x_F, resulting in the observed dependence [4].

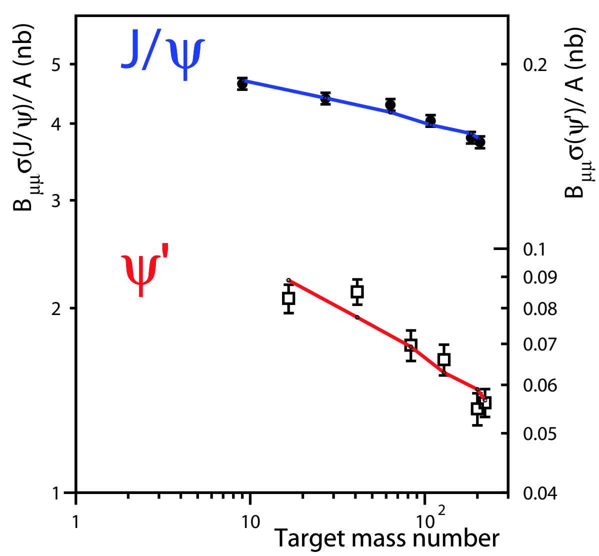

Figure 29. NA50 midrapidity ($x_F \sim 0$) measurements of J/ψ and ψ' absorption in 450 AGeV fixed-target $p + A$ collisions [130]. The respective absorption cross sections are $\sigma_{\rm abs}(J/\psi) = 4.2 \pm 0.5$ mb and $\sigma_{\rm abs}(\psi') = 9.6 \pm 1.6$ mb.

The J/ψ is suppressed in semi-central and central Pb+Pb collisions [126] beyond absorption by nucleons alone, as shown in Fig. 31. Shadowing has not yet been included

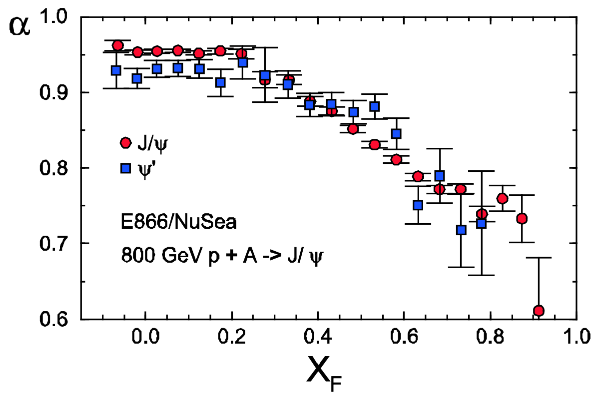

Figure 30. Measurement of J/ψ and ψ' absorption in 800 GeV $p + A$ collisions as a function of x_F at the Tevatron [131].

in the SPS analysis. The suppression observed in $A + A$ interactions at the SPS can, for the most part, be accounted for by the assumption that the more loosely bound ψ' and χ_c states are both suppressed by plasma production, eliminating their contribution to the inclusive J/ψ measurement. The direct J/ψ contribution is assumed to not be suppressed at the SPS [132, 133].

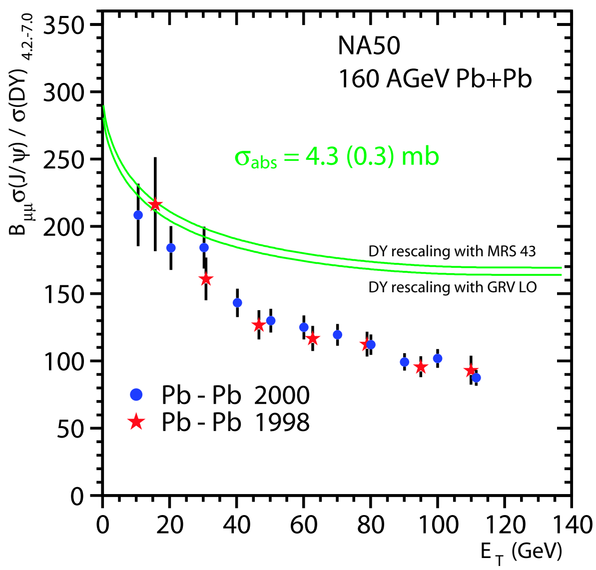

Figure 31. J/ψ absorption in 158 AGeV Pb+Pb collisions from NA50 [130]. The curves depict predictions assuming nuclear absorption alone. Suppression beyond cold nuclear matter effects is seen starting from $E_T \sim 30$ GeV, increasing to a factor of ~ 1.7 at the highest E_T [130].

Alternatives to the QGP models are able to describe the observed J/ψ suppression by assuming breakup of the bound state by comoving matter [37]. Although these approaches make some unrealistic assumptions about the hadron density, it is possible that a fraction of the observed suppression is due to comover absorption.

The ψ', lying 50 MeV below the $D\overline{D}$ threshold, can be more easily be broken up by interactions in the medium. The strong ψ' suppression measured by NA50 has been interpreted as both total suppression of the ψ' by color screening [133] and a larger interaction cross section for comovers [134].

Charm production was not measured in heavy ion experiments at the SPS until very recently. Figure 26 shows that the open charm contribution to the dilepton continuum in the J/ψ mass region is negligible at the SPS. Open charm measurements are, however, key to understanding the intermediate mass dilepton region. The NA60 experiment has used displaced vertices to separate charm decays from prompt dileptons. They have presented preliminary In+In results which show that while the enhancement in the intermediate mass region is confirmed, it is inconsistent with enhanced open charm. Instead, the enhancement is consistent with a prompt dilepton source [135].

The picture emerging from SPS studies is still somewhat inconclusive. The missing pieces of vital information have made quarkonium suppression seem to be an interesting but inconclusive study. Measurements from NA60 might provide some of the missing pieces although the future of the SPS program is currently rather uncertain. On the other hand, the vast experience gained at the SPS can and should be taken into account at RHIC. The main lesson learned is that a simple J/ψ measurement in $A+A$ collisions as a function of centrality is insufficient to draw unique conclusions. Rather, a systematic and detailed study of all related aspects, *i.e.*, a systematic study of open charm, J/ψ, ψ', and χ_c production in pp, $p+A$, and $A+A$ collisions is required. Centrality, rapidity, and A dependence studies are mandatory.

5.3. Quarkonium measurements to date at RHIC

All of the published J/ψ results from RHIC to date are from PHENIX. However some proof-of-principle J/ψ STAR results [136] indicate that STAR will have J/ψ results from RHIC Runs 4 and 5, as well as from future RHIC runs. PHENIX measures quarkonium yields by reconstructing their invariant mass from decays to dileptons. Dielectrons are used in the central arms ($|\eta| < 0.35$) and dimuons are used in the muon arms ($1.2 < |\eta| < 2.2$). STAR uses dielectrons within the TPC acceptance ($|\eta| < 1$).

PHENIX has reported J/ψ results at 200 GeV from pp [137, 97, 138], d+Au [97], Au+Au [34] and preliminary results from Cu+Cu collisions [35]. There are also J/ψ preliminary measurements from Cu+Cu collisions at 62 GeV [35].

PHENIX reported an observation of $\Upsilon \to \mu^+\mu^-$ in 200 GeV pp collisions from RHIC Run 5 at Quark Matter 2005 [139]. This was a very low statistics measurement (27 counts in both muon arms) that was used to make a preliminary cross section estimate $d\sigma/dy = 2.05 \pm$??(stat) $\pm$??(sys) for $1.2 < |y| < 2.2$. STAR reported observation of about 50 Υ for $|y| < 1$, leading to a preliminary cross section measurement of $d\sigma/dy$ $= 2.6 \pm 0.8$(stat) $\pm$ 0.63(sys) nb^{-1} [140]. In both cases, the cross section is for the lowest three Υ states combined. It will be difficult to make definitive Υ measurements at RHIC I luminosities, but a crude measurement of the Υ nuclear modification factor from both PHENIX and STAR may be possible at RHIC I with about 10 times the existing integrated luminosity.

5.3.1. Baseline quarkonium measurements at RHIC PHENIX has measured J/ψ cross sections in *pp* [138] and d+Au collisions [97] at 200 GeV. The rapidity dependence is summarized in Fig. 32. The left side shows the invariant J/ψ yields in *pp* collisions while the right side shows the nuclear modification factor, R_{dAu}, for minimum bias d+Au collisions.

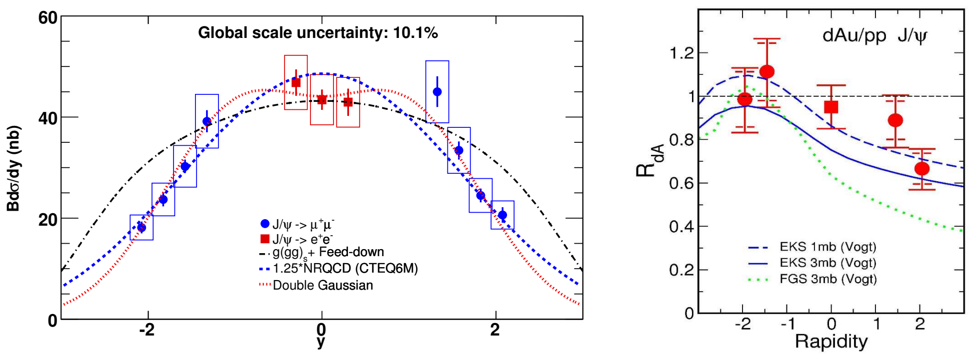

Figure 32. The rapidity dependence of the *pp* J/ψ invariant yield at 200 GeV [138] (left panel) and the nuclear modification factor for minimum bias d+Au collisions [97] (right panel). The curves on the left side are various fits used to extract the total cross section and estimate the systematic error. The curves on the right side are theory calculations discussed in the text. The deuteron is defined to be moving toward positive rapidity.

The curves on the right-hand side of Fig. 32 show the results of several calculations for d+Au that include absorption and shadowing [4, 94, 141]. These have been discussed in the previous section. The data favor the relatively modest shadowing of the EKS98 parameterization with moderate nuclear absorption.

The J/ψ nuclear modification factor for d+Au is shown as a function of centrality in Fig. 33 for the forward, mid and backward rapidity regions covered by the three PHENIX arms. The curves are calculated with the EKS98 (solid) and FGSh (dashed) shadowing parameterizations with a 3 mb absorption cross section.

5.3.2. Quarkonium measurements in heavy ion collisions at RHIC Measurements with the statistical precision needed to provide a strong test of models of J/ψ production in heavy ion collisions now exist from RHIC. These PHENIX measurements were from the Run 4 Au+Au and the Run 5 Cu+Cu data sets. The main features are summarized here.

Fig. 34 shows the J/ψ nuclear modification factor, R_{AA}, measured in 200 GeV Au+Au and Cu+Cu collisions at both mid- and forward/backward-rapidities [34, 35].

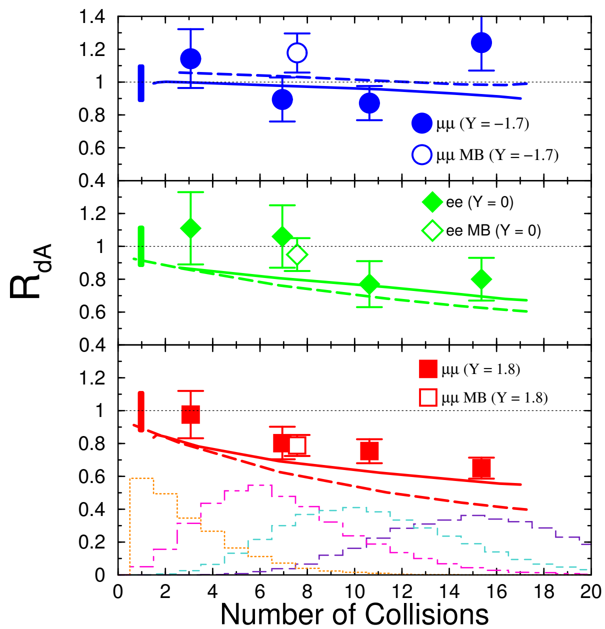

Figure 33. Nuclear modification factor as a function of centrality for d+Au collisions measured at forward (bottom), mid (center) and backward (top) rapidity. The deuteron is moving toward forward rapidity. The theoretical curves, including both shadowing and nuclear absorption, are discussed in the text.

The lower left panel of Fig. 34 shows that when the number of participants is above 150 the Au+Au nuclear modification factor at forward rapidity is only about 60% of that at mid rapidity. The Cu+Cu nuclear modification factors in Fig. 34 do not show a clear difference in suppression between forward and mid rapidity, This is consistent with the behavior of the Au+Au data in the $N_{\rm part}$ range covered by Cu+Cu collisions. The Au+Au data show that the J/ψ suppression is weaker at the maximum of the transverse energy density. This could be due to either entrance channel effects (shadowing) or to final state effects such as J/ψ formation due to coalescence of uncorrelated charm quarks.

In Fig. 35 [39] the PHENIX Au+Au data are compared on the left to a model [142] containing shadowing and comover effects - final state interactions of the J/ψ with the medium produced in the collision - in which the suppression is predicted to be larger at $y = 0$ than at $y = 1.7$, in disagreement with the data. In the same figure, on the right, the $y = 0$ Au+Au data are compared with calculations containing dissociation by thermal gluons with no recombination [119, 40]. All of these calculations overestimate J/ψ suppression at mid rapidity. Fig. 36 [39] shows the mid rapidity data compared to model calculations [119, 40, 17, 143, 144] that include J/ψ formation by coalescence. These models generally do a better job of describing the suppression. However they rely heavily on the rapidity density of charm production as input to the coalescence calculations, and charm distributions are poorly defined by the data so far at RHIC.

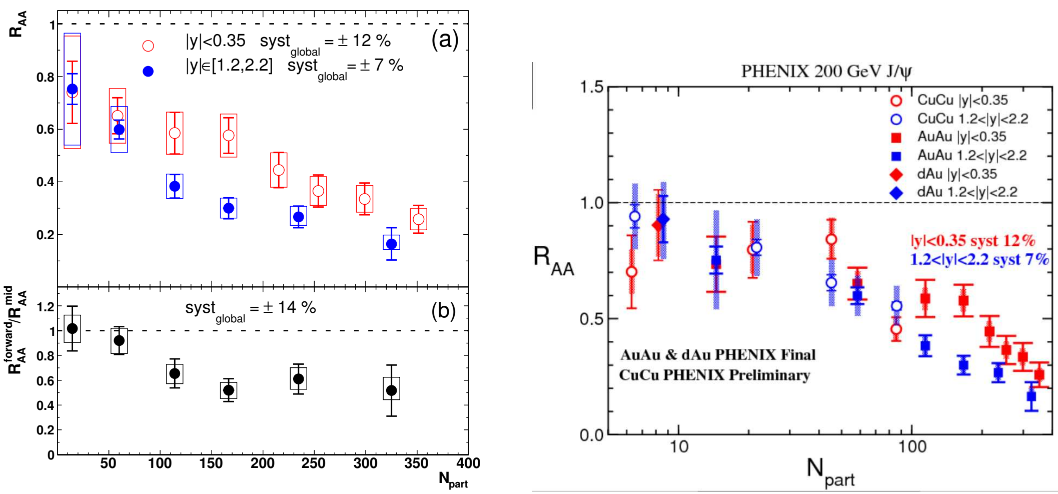

Figure 34. Left top: The nuclear modification factor as a function of centrality for 200 GeV Au+Au collisions measured at forward, mid and backward rapidity. Left bottom: The ratio of nuclear modification factors at forward and mid rapidity. Right: Nuclear modification factor for Cu+Cu (preliminary data) compared with that for Au+Au.

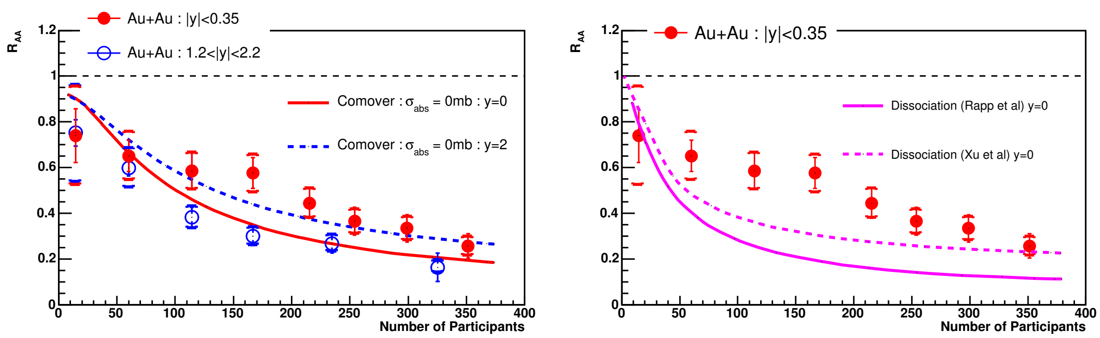

Figure 35. Left: Nuclear modification factor compared with a calculation from a comover model at mid- and forward/backward rapidity. Note that the model predicts maximum suppression at $y = 0$. Right: Comparison with two calculations showing the predicted effect of gluon dissociation..

PHENIX also showed a measurement of the nuclear modification factor for 62 GeV Cu+Cu collisions at Quark Matter 2005. While this measurement has relatively low statistics, the 62 GeV data exhibit similar, and perhaps slightly stronger, suppression in the most central collisions to that seen in 200 GeV Cu+Cu collisions, consistent with predictions of a model with color screening and coalescence [123].

Recently there have been theoretical efforts to predict the effects of $c\bar{c}$ coalescence on the rapidity and p_T dependence of the J/ψ yield [145, 40]. Figure 37 shows experimental results on the average p_T^2 of the J/ψ, $\langle p_T^2 \rangle$ (below 5 GeV/c) as a function of $N_{\rm part}$ for

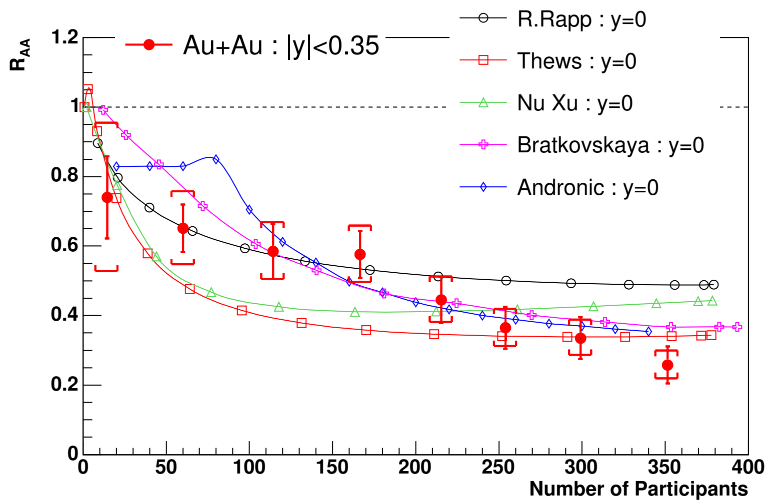

Figure 36. Nuclear modification factor compared with models that include J/ψ formation by coalescence. The calculations are for $y = 0$ only. See the text for details.

Au+Au and Cu+Cu collisions in the two rapidity regions covered by PHENIX. The Au+Au and Cu+Cu data are in very good agreement at the same $N_{\rm part}$ values and the same rapidity. Also shown are calculations from Thews [145] and Yan, Zhuang and Xu [40] that incorporate the effect of coalescence on the centrality dependence of $\langle p_T^2 \rangle$. In the Thews calculation, the $\langle p_T^2 \rangle$ of the primordial J/ψ yield is considerably larger and more steeply rising than in the Yan *et al.* calculation. However both calculations with regeneration of J/ψ agree fairly well with the $\langle p_T^2 \rangle$ data, even though the regeneration component is a smaller fraction of the J/ψ yield in the Yan *et al.* case.

No realistic calculations of the rapidity distribution from models including J/ψ coalescence are available for heavy ion collisions so far, but based on the assumption of an underlying open charm distribution that is peaked at $y = 0$, it is predicted [17] that a strong charm coalescence contribution to J/ψ production will lead to a narrowing of the rapidity distribution, just as for the p_T distribution. This has been investigated by PHENIX, who have extracted the RMS of the rapidity distribution in four centrality bins from their Au+Au data and from their *pp* data [34]. The extracted RMS values show a decrease of the RMS of the rapidity distribution of only 8% with increasing centrality, but with uncertainties almost as large as the difference. Thus the data show that any narrowing of the rapidity distribution is small, a change in the RMS of roughly 10% or less.

The evidence for a strong coalescence component in the J/ψ yield in central collisions seems to be mixed. The suppression as a function of centrality at midrapidity shown in Fig. 36 is reasonably consistent with models that include coalescence, as is the $\langle p_T^2 \rangle$ in Fig. 37, and the stronger suppression at forward rapidity is qualitatively consistent with expectations from a coalescence picture.. However, very little narrowing

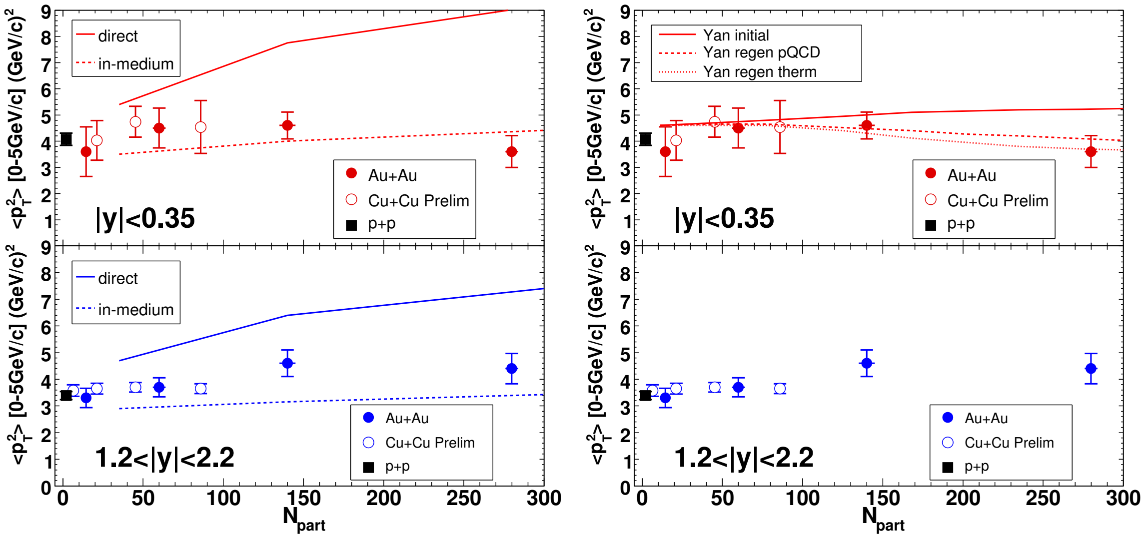

Figure 37. The $\langle p_T^2 \rangle$ for 200 GeV Au+Au and Cu+Cu collisions measured by PHENIX at mid rapidity (upper panels) and forward/backward rapidity (lower panels). The integrals are restricted to less than 5 GeV/c because extrapolating to infinity adds significant systematic errors. Left: Comparison with calculations by Thews [145]. Right: Comparison with calculations by Yan, Zhuang and Xu [40], showing the behavior if the regenerated J/ψ are formed from thermalized charm quarks or from the pQCD momentum distribution . The calculations are discussed further in the text.

of the rapidity distribution is observed, while this is predicted as a general feature of J/ψ formation by coalescence, based on the assumption of an underlying charm distribution peaked near midrapidity. But the open charm rapidity distribution has not yet been very well determined experimentally, and it should be kept in mind that shadowing is predicted to modify the underlying charm rapidity distribution in central collisions. The prediction of p_T narrowing, on the other hand, is based on a steeply falling charm p_T distribution, well established by the existing data.

There has been considerable interest in what might be learrned about the J/ψ production mechanism from the R_{AA} as a function of p_T, since there is a general expectation that the importance of coalescence should decrease at high p_T. PHENIX has recently published data on the p_T dependence of R_{AA} for Au+Au [34]. The measured R_{AA} for central collisions is flat within errors over the range of the data, which extend only to 5 GeV/c. A recent ADS/CFT calculation of screening length in hot N = 4 supersymmetric Yang Mills theory [146] suggests that there might be a marked decrease in J/ψ dissociation temperature at p_T values in excess of 5 GeV/c, beyond the range of the existing data. Extending the R_{AA} measurement with good precision to much higher p_T will require RHIC II luminosity, as will be discussed later.

There have been attempts in PHENIX to extract the J/ψ v_2, but the limited statistics of the existing heavy ion data sets preclude a meaningful result. Similarly, a statistically meaningful J/ψ polarization measurement is not feasible from the present data sets. Again, precise measurements will need RHIC II luminosity.

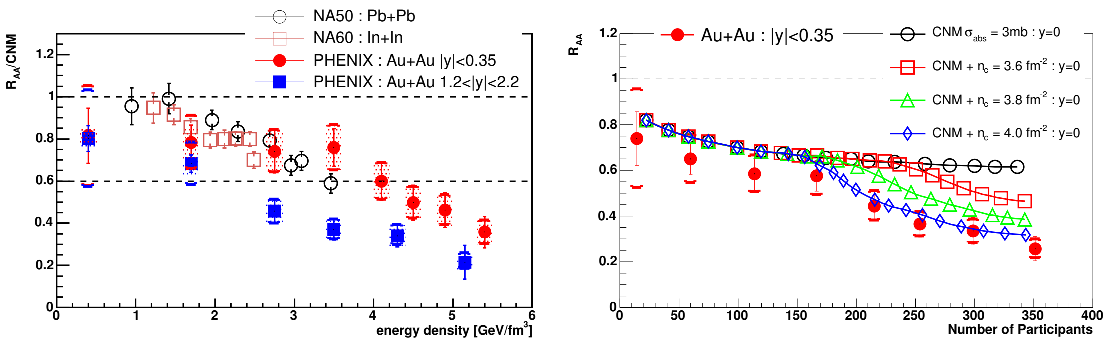

Figure 38. Left: PHENIX and SPS R_{AA} data compared with the sequential charmonium suppression model. Right: PHENIX mid rapidity data compared with the threshold density model. See the text for discussion.

Recently, a model of sequential charmonium suppression has been applied to the preliminiary PHENIX data and to the SPS data [147]. The model assumes that the ψ' and χ_c are suppressed completely above a critical energy density, while the J/ψ survival probability due to color screening is equal to unity at RHIC. Normal nuclear absorption is parameterized by an effective absorption cross section that accounts for all cold nuclear matter effects. Gluon dissociation of J/ψ in the final state is assumed to be negligible. The SPS pA data give a larger effective J/ψ absorption cross section than the RHIC d+Au data, as also implied by the results in Ref. [98]. Three values of $\sigma_{\rm abs}$ are extracted from the d+Au data, one for each rapidity bin. These values are used to obtain the survival probability in AA collisions. When $N_{\rm part}$ is converted to energy density, ϵ, and the survival probabilities for color screening and cold nuclear matter are included, the SPS and RHIC data were found to lie on a common suppression curve as a function of energy density. However the more precise final PHENIX data, which show that the forward rapidity J/ψ yield is significantly more strongly suppressed than the mid rapidity yield, are inconsistent with such a picture, as can be seen on the left side of Fig. 38 [39]. The fact that the observed $\langle p_T^2 \rangle$ is flat or decreasing with centrality is also inconsistent with the picture. A model with different, but also very simple, assumptions is the threshold energy density model [148]. Aside from normal nuclear absorption, the J/ψ yield is completely suppressed when the energy density exceeds a threshold. Gluon dissociation and the effects of feed down from the ψ' and χ_c are neglected. Calculations from the threshold model are compared with PHENIX mid rapidity data on the right of Fig. 38. The model produces behavior quite similar to that of the measured Au+Au R_{AA} at mid rapidity. However it does not describe the much stronger suppression for Au+Au at forward/backward rapidity, or the centrality dependence of the suppression for Cu+Cu.

5.4. Proposed RHIC II quarkonia measurements

Unlike other probes, quarkonia measurements are guided by predictions from lattice QCD calculations. Color screening modifies the linear rise of the QCD potential at large distances. The quarkonia spectral functions quantify the temperature dependence of the potential. Since quarkonia suppression is determined by the plasma temperature and the binding energy (equivalently the quarkonium size and the Debye screening length), measuring the sequential disappearance of these states acts as a QCD thermometer.

Thus the importance of a comprehensive study of **all** experimentally accessible quarkonium states cannot be overstated. A systematic study of heavy quarkonium spectroscopy, with a complete determination of the suppression pattern of the quarkonium states, remains the most **direct probe of deconfinement**. It is also the signature that most closely resembles a thermometer of the hot initial state which, with future improved lattice calculations, can be directly compared to QCD.

While J/ψ physics is as compelling as it was in 1986 when first proposed by Matsui and Satz [22], the systematic study of all quarkonia states, and especially bottomonium, feasible at RHIC II, provides a more complete QGP probe than heretofore possible.

Table 11 relates the main physics topics to the relevant probes and subsequent detector requirements. The ability of a program at RHIC II to make these measurements can be judged from the yields given in Tables 2, 3, and 4. The measurements that are possible at RHIC without the luminosity upgrade are the J/ψ rapidity and p_T distributions at full energy. The measurements that are newly possible at RHIC II are those for the excited charmonium states (ψ' and χ_c) and the bottomonium states ($\Upsilon(1S)$, $\Upsilon(2S)$ and $\Upsilon(3S)$). High p_T J/ψ measurements, precise measurements of the J/ψ v_2 and polarization, and excitation functions of heavy flavor distributions will be possible only at RHIC II. This is illustrated in Fig. 39, which shows the statistical significance of the J/ψ nuclear modification measurement in Au+Au at high p_T, and in Fig. 40, showing the expected precision of the J/ψ v_2 measurement in Au+Au at RHIC II. It is evident that a comprehensive program to use quarkonium as a QCD thermometer to provide direct evidence of deconfinement is possible only with RHIC II luminosity.

The measurements needed to study the excited charmonium states, χ_c and ψ', have quite different problems. The ψ' measurement technique is the same as that for the J/ψ, namely reconstruction of dilepton decays, but requires ~ 100 times as much integrated luminosity for the same yield. In addition, the ψ' measurement is made more difficult by the existence of a significant background under the peak in the invariant mass spectrum, increasing the integrated luminosity needed for measurements of a given precision. The presence of the SVTX detector in PHENIX will lead to significantly better mass resolution at the J/ψ mass, as shown in Fig. 41. A ψ' measurement is certainly feasible at RHIC II. The χ_c measurement can be done with the $\chi_c \rightarrow J/\psi\ \gamma$ channel, where the J/ψ is reconstructed from dilepton decays and the photon is detected

Table 11. The main physics goals of the RHIC II quarkonium program with corresponding probes, studies, and requirements.

Physics Motivation	Probes	Measurements	Requirements
Baseline measurements	J/ψ, ψ', χ_c, $\Upsilon(1S)$, $\Upsilon(2S)$, and $\Upsilon(3S)$ decays to dileptons	Rapidity and p_T spectra in $p+A$and pp as a function of $\sqrt{s}$	High luminosity and acceptance for sufficient statistics, especially for the Υ family. Good mass resolution to resolve ψ and Υ states.
Deconfinement, Initial Temperature	J/ψ, ψ', χ_c, $\Upsilon(1S)$, $\Upsilon(2S)$, and $\Upsilon(3S)$ decays to dileptons	Suppression patterns in $A+A$ as a function of $\sqrt{s}$ and A	High luminosity, acceptance and mass resolution for quarkonium, and triggers that work in Au+Au collisions.
Thermalization and Transport	J/ψ	J/ψ v_2 as function of $\sqrt{s}$ and A.	High luminosity for good statistics in short runs for $\sqrt{s}$ and A scans

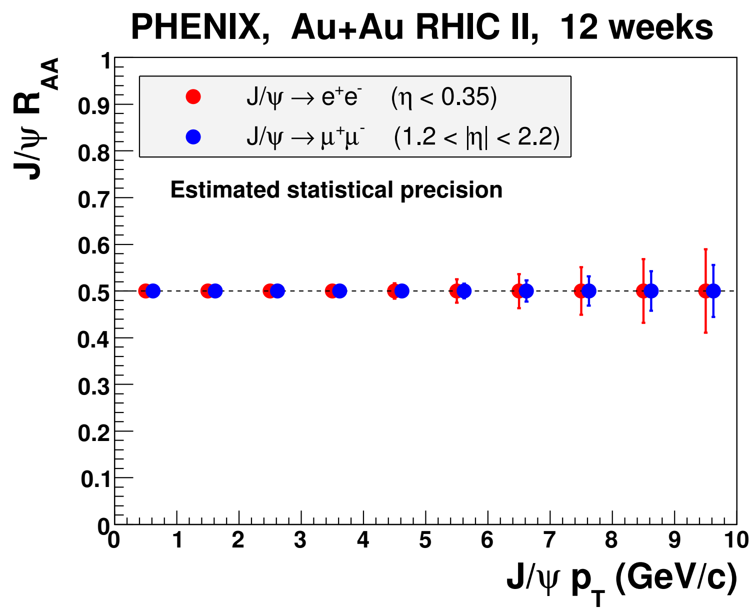

Figure 39. The statistical significance after background subtraction of the J/ψ nuclear modification factor as a function of p_T in PHENIX at mid rapidity and forward rapidity with RHIC II luminosity. Values above 5 GeV/c are from an extrapolation in p_T of existing PHENIX data.

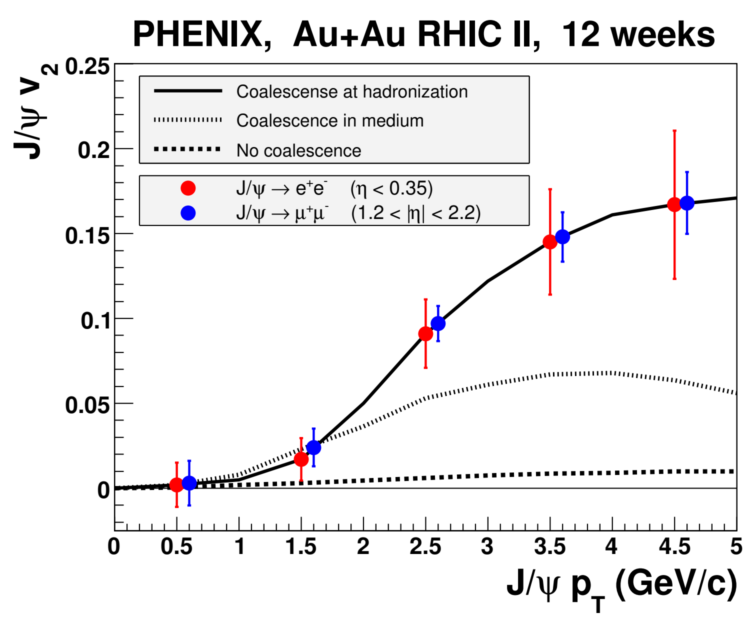

Figure 40. The absolute precision of the J/ψ v_2 measurement in PHENIX at mid rapidity and forward rapidity with RHIC II luminosity. The precision is compared with values calculated theoretically in several different scenarios [13, 40].

in an electromagnetic calorimeter. This has already been demonstrated by PHENIX in the central arms for pp collisions [149]. But while the yields are larger than for the ψ', the need to form the χ_c invariant mass by combining each J/ψ candidate with a large number of photons means that combinatorial backgrounds will be quite large in Au+AuThus the χ_c measurement will be difficult for central heavy ion collisions. There are ongoing simulation studies by PHENIX and STAR to determine how difficult it will be.

Figure 42 shows the results of a PHENIX simulation for the muon arms and the Nose Cone Calorimeter where simulated $\chi_c \rightarrow J/\psi\ \gamma$ decays are embedded in the 10% most central Au+Au events from HIJING. After rejecting all events where the pre-shower and shower-max detectors show multiple hits in a Nose Cone Calorimeter module, a clean χ_c mass peak is seen. While this simulation shows that the χ_c decay can be cleanly reconstructed, it remains to be demonstrated that the signal to combinatorial background ratio is acceptable in central Au+Au collisions.

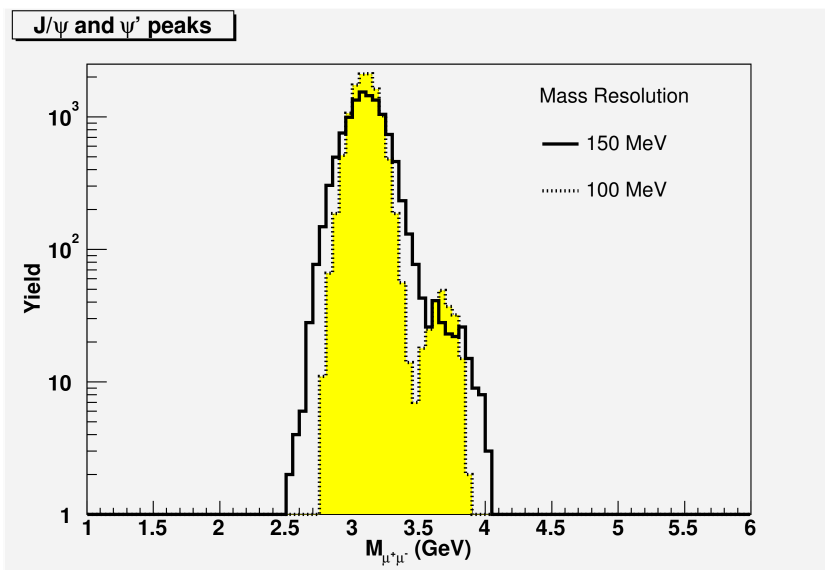

Figure 41. The J/ψ and ψ' invariant mass spectrum in the muon arms with (dashed histogram) and without (solid histogram) the improvement in mass resolution from the SVTX detector. The yields are as expected from a 25 pb^{-1} pp run.

Like the J/ψ, bottomonium states are studied using their dilepton decays. The bottomonium measurements require very large integrated luminosity and good invariant mass resolution. PHENIX expects to be able to resolve the $\Upsilon(1S)$, $\Upsilon(2S)$ and $\Upsilon(3S)$ states (see Fig. 43). Because of its larger acceptance, STAR will have $\sim$ 10 times greater Υ yields than PHENIX but the states will not be cleanly resolved and fitting will be required to extract individual yields. (See Fig. 44 for a STAR simulation of the Υ mass spectrum.) Although the yields are small relative to the J/ψ, bottomonium measurements are quite clean. The states are massive ($\sim$ 10 GeV/c^2) so that their

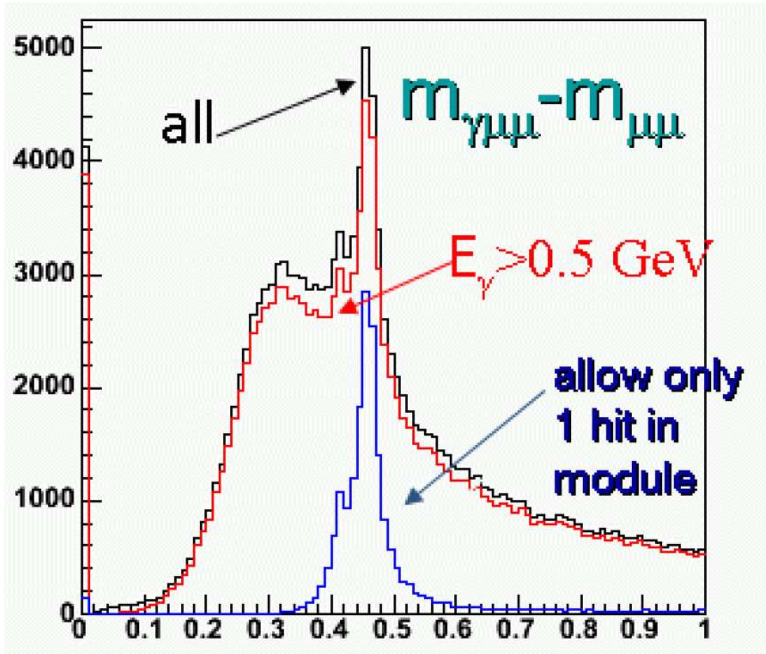

Figure 42. The invariant mass spectrum in the PHENIX muon arms and Nose Cone Calorimeter from a simulation where $\chi_c \rightarrow J/\psi\ \gamma$ decays are embedded in the 10% most central Au+Au events from HIJING. The muons and photon are required to come from the χ_c so there is no combinatorial background included in this plot.

decay leptons have relatively large momenta and are thus easily distinguished from background leptons. The combinatorial background is small and multiple scattering is of less concern. While the interpretation of charmonium suppression is made more difficult by the rather large cross section for nucleon and comover absorption, the situation for bottomonium is considerably better. Absorption of directly produced bottomonium by hadronic comovers was shown to be negligible [150].

The $\sqrt{s}$ dependence of produced J/ψ's relative to the number of $c\bar{c}$ pairs, depicted in Fig. 25 [123], is striking. An excitation function measurement of this ratio for $30 < \sqrt{s_{NN}} < 200$ GeV could help to disentangle suppression from enhancement mechanisms such as recombination/coalescence. Such measurements, however, are extremely statistically demanding since both heavy quarks and quarkonia will need to be measured with good statistics over a wide range of beam energies.

A measurement of the quarkonium nuclear modification factor at high p_T can provide a unique experimental probe for studying energy loss and color diffusion [151]. At relatively large transverse momentum, suppression due to color screening and coalescence are predicted to become negligible. Instead, the quarkonium state is a hard probe that interacts with the medium. In particular, any color octet can suffer energy loss. The relative abundance of charmonium resonances can provide an experimental handle on studying such phenomena as each resonance may have a different octet

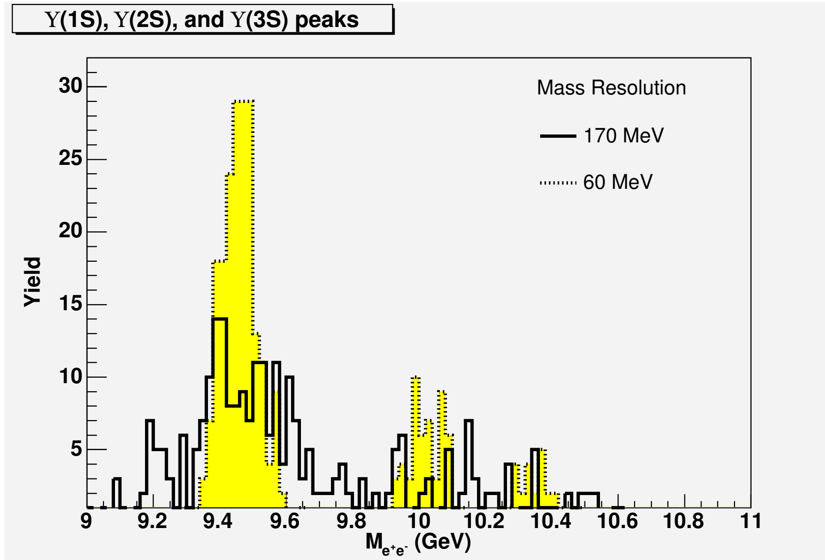

Figure 43. The Υ family dielectron mass spectrum from a PHENIX simulation for the central arms, showing the expected improvement in Υ mass resolution provided by the initial direction measurement in the SVTX barrel. The number of events shown correspond to about half of a 12 week Au+Au run at RHIC II.

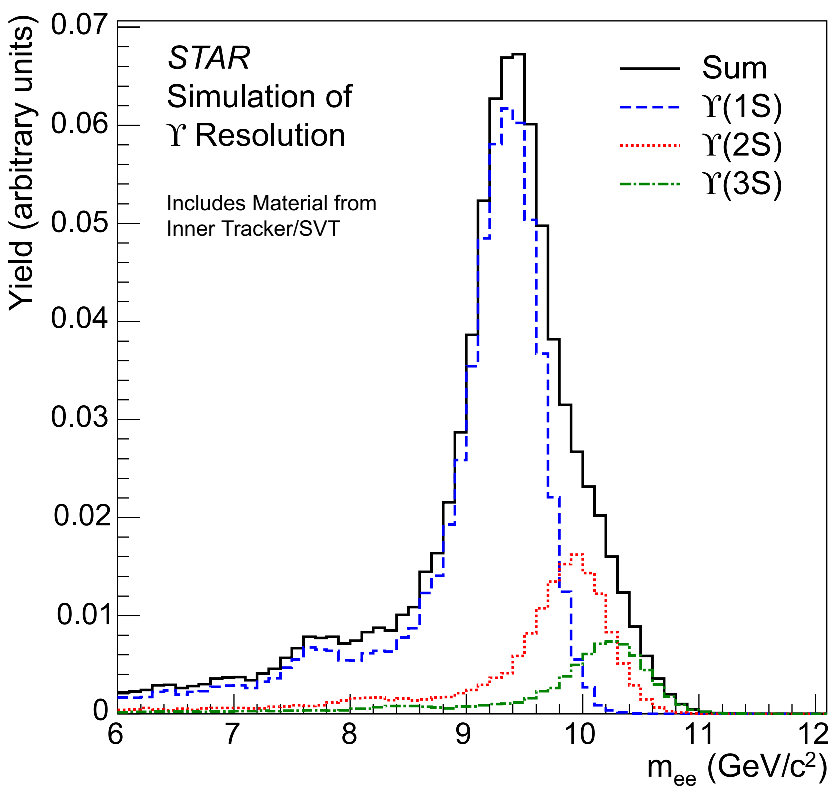

Figure 44. The Υ family dielectron mass spectrum from a STAR simulation.

contribution. We must exercise caution, however, as competing charmonium production models exist. In parallel with any nucleus-nucleus studies, it is therefore important to investigate and compare production mechanisms in pp and $p + A$ interactions, at both central and forward rapidities [152, 153, 154].

In addition to the baseline quarkonium measurements in pp and $p + A$ collisions listed in Table 11, other measurements are required as input to the models that attempt to explain the quarkonium results. The most prominent of these are listed in Table 12.

Table 12. Baseline measurements (beyond Au+Au) required in order to address the main physics questions.

Topic	Measurements	Requirements
Cold Nuclear Effects	In pp and $p + A$ collisions: • $x_{1,2}$, x_F and y dependence of quarkonia production • A dependence	Large y acceptance, including forward coverage
Suppression vs. Recombination	In pp $p + A$ and $A + A$ collisions • Charm $d\sigma/dp_T dy$ • J/ψ v_2 • p_T dependence of suppression	High resolution vertex detectors (charm)
Feed down contribution	χ_c, at least in pp and $p+A$	Photon detection capabilities over wide rapidity range. High rates, good energy and momentum resolution to enhance χ_c S/B ratio
Production mechanism	χ_c, polarization at least in pp and $p + A$	Large acceptance for $\cos\theta^*$ measurement

The importance of measuring the underlying charm distributions as input to models of J/ψ coalescence is obvious, as is the importance of understanding cold nucleus effects on quarkonium production.

It is crucial for the interpretation of the $A + A$ quarkonia yields to understand the feed down contributions from the χ_c states (see Fig. 27). The best feed down measurement will be made in 500 GeV pp collisions because the increased luminosity and increased charmonium production cross sections lead to ~ 10 times larger charmonium yields than in 200 GeV pp collisions. Since the χ_c contribution to the J/ψ yield will not change significantly between 200 and 500 GeV, the increased yield at 500 GeV will provide a definitive baseline measurement of χ_c feed down in pp collisions.

Recently, quarkonium polarization measurements were suggested as signatures of QGP formation [155]. The quarkonium yields at RHIC II will be large enough to permit a J/ψ polarization measurement at low p_T by both PHENIX and STAR.

6. Relationship to the LHC program

The major differences between quarkonium studies at RHIC II and at the LHC will be the temperature and lifetime of the medium, the relative production cross sections, luminosities and run times.

The initial temperature in 5.5A TeV central Pb+Pb collisions at the LHC is expected to be $\sim 4\ T_c$, while it is $\sim 2\ T_c$ in 200A GeV central Au+Au collisions at RHIC [156]. The QGP lifetime in 5.5A TeV central Pb+Pb collisions at the LHC is expected to be two to three times longer than in 200A GeV central Au+Au collisions at RHIC [156].

Heavy flavor production cross sections are much larger at the LHC. The open charm and bottom production cross sections are $\sim$ 15 and $\sim$ 100 times higher respectively [11]. The charmonium and bottomonium cross sections are ~ 13 and ~ 55 times higher than RHIC respectively [41]. The higher LHC open heavy flavor cross sections increase the number of $c\bar{c}$ and $b\bar{b}$ pairs produced in central $A + A$ collisions. There are ~ 10 and ~ 0.05 pairs, respectively, in Au+Au collisions at RHIC, while there should be ~ 115 and ~ 5, respectively, in central Pb+Pb collisions at the LHC [11].

The RHIC II Au+Au luminosity is projected to be 14 times larger than the LHC Pb+Pb luminosity (7×10^{27} cm^{-2} s^{-1} relative to 5×10^{26} cm^{-2} s^{-1}). The yearly heavy ion runs at RHIC II are also expected to be considerably longer than at the LHC. Taking the polarized pp program at RHIC II into account, the heavy ion program is expected to get ~ 12 week long physics runs on average per year while the LHC heavy ion program will be allocated 1 month long physics runs per year. Thus the annual integrated luminosity at RHIC II is expected to be about 42 times larger for heavy ions.

The larger heavy flavor cross sections at the LHC are approximately balanced by the increased luminosity and running times at RHIC II, making the heavy flavor yields per year similar. Thus the types of measurements that can be made at the two facilities will also be similar as well as of similar quality (see Tables 2, 3 and 5). However, there will be important differences in the physics environments prevailing at the two facilities which will make the two programs complementary.

The higher initial energy density at the LHC means that the QGP will be created at a significantly higher temperature with a correspondingly strong potential for new physics effects at the LHC. In addition, the factor of ten increase in $c\bar{c}$ pairs and the factor of 100 increase in $b\bar{b}$ pairs per central collision at the LHC will have a major impact on the interpretation of heavy flavor measurements. We will discuss some of those differences here.

Lattice calculations suggest that the J/ψ may remain bound at the highest RHIC temperatures, while the excited charmonium states are predicted to be unbound. At the LHC, all the charmonium states should be unbound at the highest temperatures, implying that almost all charmonium production in central Pb+Pb collisions at the LHC will be due to coalescence of $c\bar{c}$ pairs. Thus the prompt charmonium yields at the LHC should reflect only the coalescence mechanism with no contribution from the primordial J/ψ production (except in very peripheral collisions). The measurements at RHIC and the LHC will thus provide very different windows on charmonium suppression in the QGP that will help resolve the ambiguities in interpreting data due to the balance between destruction and coalescence formation of charmonium at RHIC.

Because of its higher binding energy, the characteristics of bottomonium production at the LHC should be similar to those of charmonium at RHIC. The bottomonium states are shown in Fig. 45 The $\Upsilon(1S)$ may remain bound at the highest temperatures at the LHC while the other bottomonium states will be dissociated. Given ~ 5 $b\bar{b}$ pairs in central Pb+Pb collisions (relative to ~ 10 $c\bar{c}$ pairs at RHIC), the Υ yield at the LHC is predicted [157] to reflect a balance between dissociation and coalescence reminiscent of the RHIC J/ψ production models. However, at RHIC, the bottomonium dissociation rates will be significantly different. While the $\Upsilon(1S)$ is predicted to be bound, the $\Upsilon(2S)$ may also remain bound. Only the $\Upsilon(3S)$ is likely to dissociate at RHIC. Also, since the $b\bar{b}$ pair yield at RHIC is $\sim$ 0.05 per Au+Au central collision, no significant bottomonium production by coalescence is expected. Thus the bottomonium yields at RHIC II should reflect only QGP suppression. Measurements at RHIC II and the LHC will thus provide very different windows on bottomonium suppression in the QGP that will help to resolve the ambiguities in interpretation due to the balance of bottomonium destruction and coalescence at the LHC.

The open heavy flavor programs at RHIC II and the LHC will consist of similar measurements with similar goals. They will study energy loss, thermalization and flow of heavy quarks in systems with very different energy densities, interaction cross sections and lifetimes. However, not all challenges in the measurements are similar. At $\sqrt{s} = 200$ GeV, bottom decays to leptons begin to dominate the single electron spectrum at $p_T \sim 4$ GeV/c. As the collision energy increases, the lepton spectra from B and D decays move closer together rather than further apart. Thus, the large increase in the $b\bar{b}$ cross section relative to $c\bar{c}$ does not make single leptons from B and D decays easier to separate. Preliminary calculations show that the $B \to e$ decay does become larger than that of $D \to e$ but at higher p_T, $p_T > 10$ GeV/c. The two lepton sources differ by less than a factor of two to $p_T \sim 50$ GeV/c in the range $|y| \leq 1$. Separating single leptons from charm and bottom decays will require statistical separation using differences in the displaced vertex distributions at all p_T at the LHC. Thus interpretation of single lepton data from heavy flavor decays will be more difficult at the LHC.

ALICE can reconstruct D^0 decays from $p_T \sim 0$ to $p_T \sim 25$ GeV/c [42]. Like STAR, ALICE will be unable to trigger on D decays and will have to obtain these events from

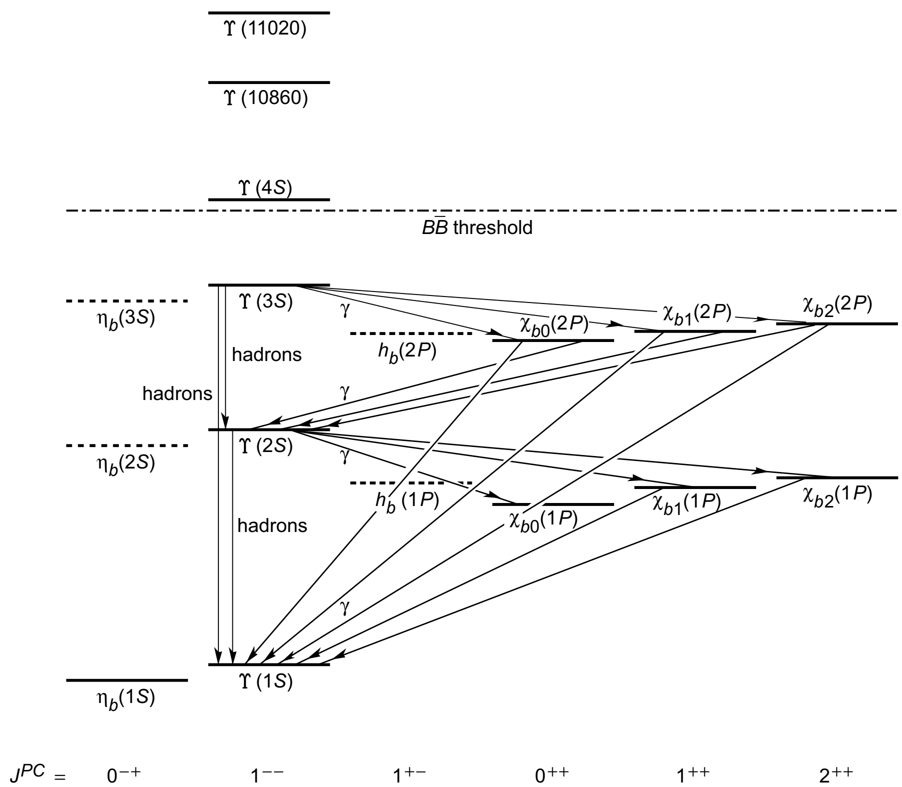

Figure 45. Bottomonium mass levels and spin states. The common feed down channels are indicated.

the minimum bias sample. Thus the longer running times at RHIC are an advantage since more minimum bias data can be taken (see Tables 3 and 5). While it is not yet clear what CMS and ATLAS will do to reconstruct charm, they should be able to do b jets well, similar to the Tevatron measurements. As at RHIC, B mesons can be measured cleanly at the LHC through their decays to J/ψ, although triggering on low p_T J/ψ at LHC is difficult.

It has also been suggested that the $B\overline{B}$ contribution to the dimuon continuum, the dominant contribution above the Υ mass, can be used to measure energy loss [43]. That channel would be fairly clean at the LHC but more difficult at RHIC.

7. Conclusions

We have shown that, so far, the RHIC heavy flavor physics program is very rich and stimulating, with many provocative and challenging results. To fully realize the potential of this compelling program, however, both detector upgrades and a luminosity upgrade are mandatory. Detector upgrades will improve reconstruction of charm hadron decays into hadronic channels and allow detection of $B \to J/\psi X$ decays using secondary vertex measurements. Upgrades will also make χ_c detection possible and, in the case of STAR, lead to significant quarkonium yields. However only increased luminosities will allow high statistics measurements of all of these yields as well as increase the p_T reach of J/ψ

and heavy flavor R_{AA} and v_2.

We have also shown that the RHIC II and LHC heavy flavor physics programs are complementary. Both are required for a complete understanding of heavy flavor production as a function of energy and temperature. We have also demonstrated that, despite lower heavy flavor cross sections at RHIC, the longer running times and higher luminosity of RHIC II make the recorded yields similar at the two facilities.

Acknowledgments

We thank F. Karsch for the lattice contribution. The work of R. Vogt was supported in part by the U. S. Department of Energy under Contract No. DE-AC02-05CH11231 and by the National Science Foundation Grant NSF PHY-0555660. The work of T. Ullrich was supported in part by the U. S. Department of Energy under Contract No. DE-AC02-98CH10886. The work of A. D. Frawley was supported by National Science Foundation grant PHY-04-56463.

References

[1] The RHIC experiment white papers, Nucl. Phys.**A757**, Issues 1-2, 1-283 (2005).
[2] M. Gyulassy and L. McLerran, Nucl. Phys. A 750, 30 (2005).
[3] Cacciari M, Nason P and Vogt R 2005 *Phys. Rev. Lett.* **95** 122001 (*Preprint* hep-ph/0502203)
[4] Vogt R 2005 *Phys. Rev.* C **71** 054902 (*Preprint* hep-ph/0411378)
[5] Vogt R 2006 *Acta Phys. Hung. New Ser. Heavy Ion Phys.* **25** 97 (*Preprint* nucl-th/0507027)
[6] Djordjevic M, Gyulassy M, Vogt R and Wicks S, *Phys. Lett.* B **632** 81 (*Preprint* nucl-th/0507019)
[7] Djordjevic M, Gyulassy M and Wicks S 2005 *Phys. Rev. Lett.* **94** 112301 (*Preprint* hep-ph/0410372)
[8] Armesto N, Salgado C A and Wiedemann U A 2004 *Phys. Rev.* D **69** 114003 (*Preprint* hep-ph/0312106)
[9] Dokshitzer Y L and Kharzeev D E 2001 *Phys. Lett.* B **519** 199 (*Preprint* hep-ph/0106202)
[10] Lin Z w, Vogt R and Wang X-N 1998 *Phys. Rev.* C **57** 899 (*Preprint* nucl-th/9705006); Lin Z w and Vogt R 1999 *Nucl. Phys.* B **544** 339 (*Preprint* hep-ph/9808214)
[11] Vogt R [Hard Probe Collaboration] 2003 *Int. J. Mod. Phys.* E **12** 211 (*Preprint* hep-ph/0111271)
[12] Svetitsky B and Uziel A 1997 *Phys. Rev.* D **55** 2616 (*Preprint* hep-ph/9606284)
[13] Greco V, Ko C M and Rapp R 2004 *Phys. Lett.* B **595** 202 (*Preprint* nucl-th/0312100)
[14] Lin Z w and Molnar D 2003 *Phys. Rev.* C **68** 044901 (*Preprint* nucl-th/0304045)
[15] Adams J *et al.* [STAR Collaboration] (*Preprint* nucl-ex/0607012)
[16] A. Adare *et al.* [PHENIX Collaboration] (*Preprint* nucl-ex/0611018)
[17] Thews R L and Mangano M L 2006 *Phys. Rev.* C **73** 014904 (*Preprint* nucl-th/0505055)
[18] Thews R L, Schroedter M and Rafelski J 2001 *Phys. Rev.* C **63** 054905 (*Preprint* hep-ph/0007323)
[19] Andronic A, Braun-Munzinger P, Redlich K and Stachel J 2003 *Phys. Lett.* B **571** 36 (*Preprint* nucl-th/0303036)
[20] Kostyuk A P, Gorenstein M I, Stöcker H and Greiner W 2003 *Phys. Rev.* C **68** 041902 (*Preprint* hep-ph/0305277)
[21] Abreu M C *et al.* [NA50 Collaboration] 1997 *Phys. Lett.* **410** 327; 337
[22] Matsui T and Satz H 1986 *Phys. Lett.* B **178** 416
[23] Karsch F, Mehr M T and Satz H 1988 *Z. Phys.* C **37** 617
[24] Datta S, Karsch F, Petreczky P and Wetzorke I 2004 *J. Phys. G: Nucl. Part. Phys.* **30** S1347 (*Preprint* hep-lat/0403017)

[25] Kharzeev D and H Satz 1994 *Phys. Lett.* B **334** 155 (*Preprint* hep-ph/9405414)
[26] Braun-Munzinger P and J Stachel 2000 *Phys. Lett.* B **490** 196 (*Preprint* nucl-th/0007059)
[27] Braun-Munzinger P and J Stachel 2001 *Nucl. Phys.* A **690** 119 (*Preprint* nucl-th/0012064)
[28] Grandchamp L and R Rapp 2001 *Phys. Lett.* B **523** 60 (*Preprint* hep-ph/0103124)
[29] Braun-Munzinger P and K Redlich 2000 *Eur. Phys. J.* C **16** 519 (*Preprint* hep-ph/0001008)
[30] Ko C M, B Zhang, X-N Wang and X F Zhang 1998 *Phys. Lett.* B **444** 237 (*Preprint* nucl-th/9808032)
[31] Gunion J F and R Vogt 1997 *Nucl. Phys.* B **492** 301 (*Preprint* hep-ph/9610420)
[32] Adler S S *et al.* [PHENIX Collaboration] 2005 *Phys. Rev. Lett.* **94** 082301 (*Preprint* nucl-ex/0409028)
[33] Armesto N *et al.;* 2006 *Nucl. Phys.* A **774** 589 (*Preprint* hep-ph/0510284); 2006 *Phys. Lett.* B **637** 362 (*Preprint* hep-ph/0511257)
[34] A. Adare *et al.* [PHENIX Collaboration] (*Preprint* nucl-ex/0611020)
[35] Periera H [PHENIX Collaboration] 2006 *Nucl. Phys.* A **774** 747
[36] Bratkovskaya E L, Kostyuk A P, Cassing W and Stöcker H 2004 *Phys. Rev.* C **69** 054903 (*Preprint* nucl-th/0402042)
[37] Capella A and E G Ferreiro 2005 *Eur. Phys. J.* C **42** 419 (*Preprint* hep-ph/0505032)
[38] Grandchamp L, R Rapp and G E Brown 2004 *Phys. Rev. Lett.* **92** 212301 (*Preprint* hep-ph/0306077)
[39] T. Gunji [PHENIX Collaboration] QM2006 Proceedings.
[40] Li Yan, Pengfei Zhuang and Nu Xu; *Preprint* nucl-th/0608010.
[41] M Bedjidian *et al.* 2003 ed R Vogt and S Frixione *Preprint* hep-ph/0311048.
[42] Dainese A, R Vogt, M Bondila, K J Eskola and V J Kolhinen 2004 *J. Phys. G: Nucl. Part. Phys.* **30** 1787 (*Preprint* hep-ph/0403098)
[43] Lokhtin I P and A M Snigirev 2001 *Eur. Phys. J.* C **21** 155 (*Preprint* hep-ph/0105244)
[44] Kodolova O 2003 CMS Internal Note 2003-002.
[45] Ackermann K H *et al.* 2003 *Nucl. Instrum. Methods* A **499** 624
[46] Gavai R V, D Kharzeev, H Satz, G A Schuler, K Sridhar and R Vogt 1995 *Int. J. Mod. Phys.* A **10** 3043 (*Preprint* hep-ph/9502270)
[47] Crochet P [ALICE Collaboration] 2005 EPJdirect A **1** 1; private communication
[48] Wyslouch B [CMS Collaboration]; private communication.
[49] Takai H [ATLAS Collaboration] 2005 PANIC LHC Satellite workshop [http://indico.cern.ch/conferenceDisplay.py?confId=a054585]
[50] Arneodo M 1994 *Phys. Rept.* **240** 301
[51] Cacciari M, Greco M and Nason P 1998 *J. High Energy Phys.* JHEP9805(1998)007 (*Preprint* hep-ph/9803400); Cacciari M, Frixione S and Nason P 2001 *J. High Energy Phys.* JHEP0103(2001)006 (*Preprint* hep-ph/0102134)
[52] Nason P, Dawson S and Ellis R K 1988 *Nucl. Phys.* B **303** 607; 1989 *Nucl. Phys.* B **327** 49 [*Erratum* 1990 *Nucl. Phys.* B **335** 260]
[53] Beenakker W, van Neerven W L, Meng R, Schuler G A and Smith J *Nucl. Phys.* B **351** 507
[54] Adams J *et al.* [STAR Collaboration] 2005 *Phys. Rev. Lett.* **94** 062301 (*Preprint* nucl-ex/0407006)
[55] Tai A [STAR Collaboration] 2004 *J. Phys. G: Nucl. Part. Phys.* **30** S809 (*Preprint* nucl-ex/0404029)
[56] Cacciari M and Greco M 1994 *Nucl. Phys.* B **421** 530 (*Preprint* hep-ph/9311260)
[57] Cacciari M and Nason P 2002 *Phys. Rev. Lett.* **89** 122003 (*Preprint* hep-ph/0204025)
[58] Eidelman S *et al.* [Particle Data Group Collaboration] 2004 *Phys. Lett.* B **592** 1
[59] Adler S S *et al.* [PHENIX Collaboration] 2006 *Phys. Rev. Lett.* **96** 032001 (*Preprint* hep-ex/0508034)
[60] Bjorken J D 1982 *Preprint* FERMILAB-PUB-82-059-THY
[61] Thoma M H and Gyulassy M 1991 *Nucl. Phys.* B **351** 491
[62] Thoma M H 1991 *Phys. Lett.* B **273** 128

[63] Mrowczynski S 1991 *Phys. Lett.* B **269** 383
[64] Braaten E and Thoma M H 1991 *Phys. Rev.* D **44** 2625
[65] Svetitsky B 1988 *Phys. Rev.* D **37** 2484
[66] Koike Y and Matsui T 1991 *Phys. Rev.* D **45** 3237
[67] Mustafa M G, Pal D, Srivastava D K and Thoma M H 1998 *Phys. Lett.* B **428** 234 (*Preprint* nucl-th/9711059)
[68] Shuryak E 1997 *Phys. Rev.* C **55** 961 (*Preprint* nucl-th/9605011)
[69] Wicks S, Horowitz W, Djordjevic M and Gyulassy M 2005 *Preprint* nucl-th/0512076
[70] Moore G D and Teaney D 2005 *Phys. Rev.* C **71** 064904 (*Preprint* hep-ph/0412346)
[71] van Hees H and Rapp R 2005 *Phys. Rev.* C **71** 034907 (*Preprint* nucl-th/0412015)
[72] van Hees H, Greco V and Rapp R 2006 *Phys. Rev.* C **73** 034913 (*Preprint* nucl-th/0508055)
[73] A. Adare *et al.* [PHENIX Collaboration] Phys. Rev. Lett.. 97, 252002 (2006).
[74] S.S. Adler *et al.* [PHENIX Collaboration] (*Preprint* nucl-ex/0609032)
[75] Kelly S [PHENIX Collaboration] 2004 *J. Phys. G: Nucl. Part. Phys.* **30** S1189
[76] Dong X 2006 *Nucl. Phys.* A **774** 343 (*Preprint* nucl-ex/0509038)
[77] M. Cacciari *et. al Phys. Rev. Lett.* 95 122001 (2005).
[78] Adcox K *et al.* [PHENIX Collaboration] 2005 *Nucl. Phys.* A **757** 184 (*Preprint* nucl-ex/0410003)
[79] R. A. Lacey *et al.,* nucl-ex/0609025.
[80] S. Gavin, M. Abdel-Aziz, nucl-th/0606061.
[81] Zhang B, Chen L W and Ko C M 2005 *Phys. Rev.* C **72** 024906 (*Preprint* nucl-th/0502056)
[82] ????
[83] Barger V D, Keung W Y and Phillips R J 1980 *Phys. Lett.* B **91** 253
[84] Barger V D, Keung W Y and Phillips R J *Z. Phys.* C **6** 169
[85] Schuler G A and Vogt R 1996 *Phys. Lett.* B **387** 181 (*Preprint* hep-ph/9606410)
[86] Mangano M L, Nason P and Ridolfi G 1993 *Nucl. Phys.* B **405** 507
[87] Vogt R 2002 *Preprint* hep-ph/0203151
[88] Vogt R 2003 *Acta Phys. Hung. New Ser. Heavy Ion Phys.* **18** 11 (*Preprint* hep-ph/0205330)
[89] Martin A D, Roberts R G, Stirling W G and Thorne R S 1998 *Eur. Phys. J.* C **4** 463 (*Preprint* hep-ph/9803445)
[90] Lai H L *et al.* [CTEQ Collaboration] 2000 *Eur. Phys. J.* C **12** 375 (*Preprint* hep-ph/9903282)
[91] Gluck M, Reya E and Vogt A 1998 *Eur. Phys. J.* C **5** 461 (*Preprint* hep-ph/9806404)
[92] Digal S, Petreczky P and Satz H 2001 *Phys. Rev.* D **64** 094015 (*Preprint* hep-ph/0106017)
[93] Affolder T *et al.* [CDF Collaboration] 2000 *Phys. Rev. Lett.* **84** 2094 (*Preprint* hep-ex/9910025)
[94] Klein S R and Vogt R 2003 *Phys. Rev. Lett.* **91** 142301 (*Preprint* nucl-th/0305046)
[95] Vogt R 2002 *Nucl. Phys.* A **700** 539 (*Preprint* hep-ph/0107045)
[96] Eskola K J, Kolhinen V J and Ruuskanen P V 1998 *Nucl. Phys.* B **535** 351 (*Preprint* hep-ph/9802350); Eskola K J, Kolhinen V J and Salgado C A 1999 *Eur. Phys. J.* C **9** 61 (*Preprint* hep-ph/9807297)
[97] Adler S S *et al.* [PHENIX Collaboration] 2006 *Phys. Rev. Lett.* **96** 012304 (*Preprint* nucl-ex/0507032)
[98] Leitch M and Vogt R, in progress
[99] McLerran L D and Svetitsky B 1981 *Phys. Lett.* B **98** 195; Kuti J, Polonyi J and Szlachanyi K 1981 *Phys. Lett.* B **98** 199
[100] Kaczmarek O and Zantow F 2005 *Eur. Phys. J.* C **43** 63 (*Preprint* hep-lat/0502011)
[101] Digal S, Petreczky P and Satz H 2001 *Phys. Lett.* B **514** 57 (*Preprint* hep-ph/0105234)
[102] Wong C Y 2005 *Phys. Rev.* C **72** 034906 (*Preprint* hep-ph/0408020)
[103] Alberico W M, Beraudo A, De Pace A and Molinari A 2005 *Phys. Rev.* D **72** 114011 (*Preprint* hep-ph/0507084)
[104] Shuryak E V and Zahed I 2004 *Phys. Rev.* D **70** 054507 (*Preprint* hep-ph/0403127)
[105] Blaschke D, Kaczmarek O, Laermann E and Yudichev V 2005 *Eur. Phys. J.* C **43** 81 (*Preprint* hep-ph/0505053)

[106] Satz H 2005 *J. Phys. G: Nucl. Part. Phys.* **32** R25 (*Preprint* hep-ph/0512217)
[107] Karsch F 2005 *Eur. Phys. J.* C **43** 35 (*Preprint* hep-lat/0502014)
[108] Nakahara Y, Asakawa M and Hatsuda T 1999 *Phys. Rev.* D **60** 091503 (*Preprint* hep-lat/9905034)
[109] Brambilla N *et al.* [Quarkonium Working Group] 2004 *Preprint* hep-ph/0412158
[110] Karsch F and Petronzio R 1988 *Z. Phys.* C **37** 627
[111] Asakawa M and Hatsuda T 2004 *Phys. Rev. Lett.* **92** 012001 (*Preprint* hep-lat/0308034)
[112] Datta S, Karsch F, Wissel S, Petreczky P and Wetzorke I 2004 *Preprint* hep-lat/0409147
[113] Haglin K L and Gale C 2001 *Phys. Rev.* C **63** 065201 (*Preprint* nucl-th/0010017)
[114] Umeda T, Katayama R, Miyamura O and Matsufuru H 2001 *Int. J. Mod. Phys.* A **16** 2215 (*Preprint* hep-lat/0011085)
[115] Iida H, Doi T, Ishii N and Suganuma H 2006 PoS **LAT2005** 184 (*Preprint* hep-lat/0509129)
[116] Gorenstein M I, Kostyuk A P, Stöcker H and Greiner W 2001 *Phys. Lett.* B **509** 277
[117] Gorenstein M I, Kostyuk A P, Stöcker H and Greiner W 2001 *J. Phys. G: Nucl. Part. Phys.* **27** L47
[118] Gorenstein M I, Kostyuk A P, Stöcker H and Greiner W 2000 *Preprint* hep-ph/0012292
[119] R. Rapp Eur. Phys. J. C **43** (2005) 91, hep-ph/0502208.
[120] Thews R L 2001 *Preprint* hep-ph/0111015
[121] Martins K, Blaschke D, and Quack E 1995 *Phys. Rev.* C **51** 2723; Matinyan S G and Müller B 1998 *Phys. Rev.* C **58** 2994; Haglin K 2000 *Phys. Rev.* C **61** 031902R; Lin Z w and Ko C M 2000 *Phys. Rev.* C **62** 034903
[122] Geiger K and Ellis J R 1995 *Phys. Rev.* D **52** 1500; *Phys. Rev.* D **54** 1967
[123] Grandchamp L and Rapp R 2003 *Nucl. Phys.* A **715** 545 (*Preprint* hep-ph/0209141)
[124] Angelis A L S *et al.* [HELIOS-3 Collaboration] 1998 *Eur. Phys. J.* C **5** 63
[125] Abreu M C *et al.* [NA50 Collaboration] 1999 *Phys. Lett.* B **466** 408
[126] Abreu M C *et al.* [NA50 Collaboration] 2000 *Phys. Lett.* B **477** 28
[127] Baldit A *et al.* [NA60 Collaboration] 2000 *Preprint* CERN-SPSC-2000-010
[128] Kolanoski H [HERA-B Collaboration] 2005 *J. Phys. G: Nucl. Part. Phys.* **31** S799
[129] Abt I *et al.* [HERA-B Collaboration] 2003 *Phys. Lett.* B **561** 61 (*Preprint* hep-ex/0211033)
[130] Borges G [NA50 Collaboration] 2004 *J. Phys. G: Nucl. Part. Phys.* **30** S1351
[131] Leitch M J *et al.* [FNAL E866/NuSea collaboration] 2000 *Phys. Rev. Lett.* **84** 3256 (*Preprint* nucl-ex/9909007)
[132] Blaizot J-P, Dinh M and Ollitrault J-Y 2000 *Phys. Rev. Lett.* **85** 4012 (*Preprint* nucl-th/0007020)
[133] Nardi M and Satz H 1998 *Phys. Lett.* B **442** 14 (*Preprint* hep-ph/9805247)
[134] Kharzeev D, Lourenco C, Nardi M and Satz H 1997 *Z. Phys.* C **74** 307 (*Preprint* hep-ph/9612217)
[135] Shahoyan R [NA60 Collaboration] 2005 *Eur. Phys. J.* C **43** 209
[136] Calderon de la Barca Sanchez M [STAR Collaboration] 2006 *Preprint* nucl-ex/0606009
[137] Adler S S *et al.* [PHENIX Collaboration] 2004 *Phys. Rev. Lett.* **92** 051802 (*Preprint* hep-ex/0307019)
[138] A. Adare *et al.,* hep-ex/0611020.
[139] Leitch M J [PHENIX collaboration] 2005, poster at Quark Matter '05, Budapest, Hungary, August 2005.
[140] Pibero Djawotho [STAR Collaboration, talk at Quark Matter '06, Shanghai, China, November, 2006.
[141] Kopeliovich B, Tarasov A, and Huffner J 2001 *Nucl. Phys.* A **696** 669
[142] A. Capella and E. G. Ferriero *Preprint* hep-ph/0610313.
[143] A. Andronic, P. Braun-Munzinger, K. Redlich and J. Stachel nucl-th/0611023.
[144] W. Cassing, E. L. Bratkovskaya, S. Juchem 2000 *Nucl. Phys.* A **674** 249.
[145] Thews R L 2006 *Eur. Phys. J.* A **29** 15 (*Preprint* hep-ph/0511292)
[146] Hong Liu, Krishna Rajagopal and Urs Achim Weidemann *Preprint* hep-ph/0607062.
[147] Karsch F, Kharzeev D and Satz H 2006 *Phys. Lett.* B **637** 75 (*Preprint* hep-ph/0512239)
[148] A. K. Chaudhuri *Preprint* nucl-th/0610031.

[149] PHENIX χ_c data ?????????
[150] Lin Z w and Ko C M 2001 *Phys. Lett.* B **503** 104 (*Preprint* nucl-th/0007027)
[151] Baier R, Schiff D and Zakharov B G 2000 *Ann. Rev. Nucl. Part. Sci.* **50** 37
[152] Gavin S and Milana J 1992 *Phys. Rev. Lett.* **68** 1834
[153] Johnson M B *et al.* 2002 *Phys. Rev.* C **65**, 025203 (*Preprint* hep-ph/0105195)
[154] Vogt R 2000 *Phys. Rev.* C **61** 035203 (*Preprint* hep-ph/9907317)
[155] Ioffe B L and Kharzeev D E 2003 *Phys. Rev.* C **68** 061902 (*Preprint* hep-ph/0306176)
[156] Vitev I 2004 *J. Phys. G: Nucl. Part. Phys.* **30** S791 (*Preprint* hep-ph/0403089)
[157] Grandchamp L, Lumpkins S, Sun D, van Hees H and Rapp R 2006 *Phys. Rev.* C **73** 064906 (*Preprint* hep-ph/0507314)